Space Internet of Things (Space-IoT)

Narayana, S.

DOI
10.4233/uuid:07fade0a-fd62-4732-93fa-92cbb0dac538

Publication date
2023

Document Version
Final published version

Citation (APA)
Narayana, S. (2023). *Space Internet of Things (Space-IoT)*. [Dissertation (TU Delft), Delft University of Technology]. https://doi.org/10.4233/uuid:07fade0a-fd62-4732-93fa-92cbb0dac538

SPACE INTERNET OF THINGS (SPACE-IOT)

SPACE INTERNET OF THINGS (SPACE-IOT)

Dissertation

for the purpose of obtaining the degree of doctor
at Delft University of Technology
by the authority of the Rector Magnificus, prof.dr.ir. T.H.J.J. van der Hagen,
chair of the Board for Doctorates,
to be defended publicly on
Monday 1 May 2023 at 15:00 hours

by

Sujay NARAYANA

Master of Science in Embedded Systems,
Delft University of Technology, The Netherlands
born in Puttur, India.

This dissertation has been approved by the promotors

Prof. dr. K.G. Langendoen
Dr. R.R. Venkatesha Prasad

Composition of the doctoral committee:

Rector Magnificus,	Chairman
Prof. dr. K.G. Langendoen	Delft University of Technology, promotor
Dr. R.R. Venkatesha Prasad	Delft University of Technology, promotor

Independent members:

Prof.dr. K. Chowdhury	Northeastern University, USA
Prof.dr. A. Bharadwaj	Indian Institute of Science, India
Prof.dr. T. Voigt	Uppsala University, Sweden
Prof.dr.ir. A. Bozzon	Delft University of Technology
Dr.ir. E.J.O. Schrama	Delft University of Technology

Reserve member:

Prof.dr. A. van Deursen	Delft University of Technology

This work was carried out at Delft University of technology, The Netherlands.

During the course of this PhD, internships were done at Indian Institute of Science, India, and Indian Space Research Organization.

ISBN 978-94-6366-690-9

An electronic version of this dissertation is available at
http://repository.tudelft.nl/

CONTENTS

1

INTRODUCTION

With the advent of low-power miniaturized electronics enabling high-end computations and breakthroughs in wireless technologies, the Internet of Things (IoT) has become one of the key technology enablers for smart-* systems. IoT is making a great impact on our lifestyle and changing the way we interact with others, the environment, and even machines. IoT has profoundly become a disruptive technology connecting billions of devices and has created applications such as intelligent spaces, connected vehicles, and smart healthcare. From basic use cases such as ambient temperature monitoring to extremely real-time applications such as remote surgery, IoT has demonstrated its utmost capabilities and the entire world is embracing it.

IoT comprises a network of embedded devices with sensing, communication capabilities and actuation capabilities. It leverages the existing wired and wireless infrastructures for communication and control of the physical environment through electronic systems. With the emergence of new requirements and mass deployment of such systems, several new devices and services need to be introduced around the globe. With the growth of IoT, the number of devices deployed is increasing. It is predicted that the number of connected (IoT) devices will rise from 25 billion in 2020 to about 38.6 billion by 2025, and 50 billion by 2030 [1, 2]. With this tremendous growth, one needs to fulfil the hunger for scalability, ubiquitous global coverage, and real-time connectivity in the IoT ecosystem. This is not only challenging but also demands cost-viable installations, especially when connecting IoT devices to the internet in remote and underserved regions of the world. Moreover, it is not feasible to setup cables or mobile towers in many remote areas or places with difficult terrain. Currently, there is no single communication technology that can reach all possible regions and devices in the world; there is no single satellite constellation that can create a network of existing IoT sensors on earth. Moreover, the present IoT systems cannot handle the multitude of connections required, and the desired high data rates and staggering

1

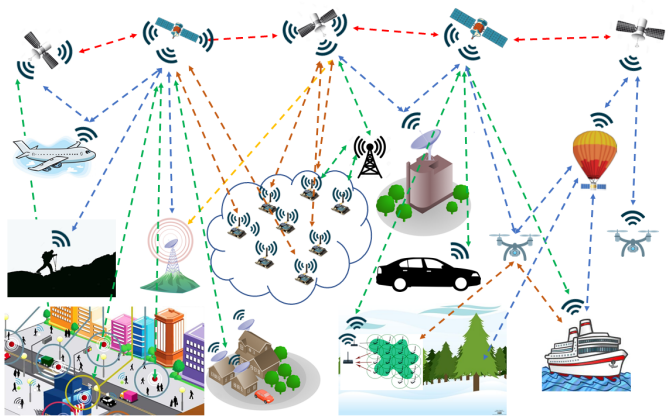

Figure 1.1: The concept of Space-IoT

bandwidth entailed for future IoT applications as the number of devices deployed increases by billions. These aspects have led to recent investments in the space-based Internet of Things. Space can be a suitable platform to solve the majority of existing/upcoming problems in the IoT domain, and the possible solutions are yet to be explored in depth in the space environment.

1.1. SPACE INTERNET OF THINGS (SPACE-IOT)

Space is the next frontier for innovations in IoT. Space is becoming enthralling day by day, for example, companies such as Virgin Galactic and Blue Origin have opened up space tourism, promising "space" to all in Space [3, 4], and many space enthusiasts will be able to launch their satellites soon [5]. The next step, which is just around the corner, is to employ space technologies for IoT applications. Space Internet of Things (Space-IoT), as we call it, is a concept that involves a network of satellites to address the main challenges in terrestrial IoT deployments – *global coverage, scalability, and connectivity*. Figure 1.1 demonstrates the concept of Space-IoT, wherein varieties of terrestrial IoT devices are connected to the internet using a network of satellites. Here, a single satellite or a swarm of them in specific orbits can communicate with the IoT sensor and actuator nodes on earth directly, or via a communication gateway. Space-IoT is a game-changer for the future of IoT, and it opens a world of new possibilities by providing global network coverage.

In Space-IoT, a single or a group of satellites can communicate with aircraft, high-altitude platform systems such as blimps, drones, cellular towers, millions of terrestrial IoT nodes, gateways, vehicles, directly anywhere on earth –cities/villages, mountains, oceans, forests– at the same time. A single satellite in space can communicate with many sensor nodes and gateways over a vast area (thus solving *coverage* issues) on earth simultaneously (thus *scalable*) compared to a single gateway on the ground. Further, multiple such satellites in space can seamlessly interconnect devices in unconnected and distinct areas on earth such as the Arctic and Antarctic regions, mountains, oceans and places that have little or no infras-

tructure (thus resolving *connectivity* issues). Further, it is possible to achieve global data collection and high throughput data transfer that can reduce traffic on the ground. Space-IoT is not just limited to satellite-to-satellite or satellite-to-earth networks; the notion also includes connecting one device to another irrespective of their location on earth, within a satellite, on a Moon rover, or any other space object.

While space technologies are decades old, Space-IoT brings in a new dimension, making it a hotbed for innovation. It is an interdisciplinary technology that brings in different domains: structural, mechanical, electrical, communication and importantly, embedded systems and software engineering. As obviously evident, this field is vast, and we do not intend to discuss all the domains in this dissertation. Our focus is on the embedded and networked systems within the realm of Space-IoT, specifically, tackling a few important challenges that can aid in revolutionizing Space-IoT. While satellites are the building blocks of Space-IoT, they need to be small and inexpensive to be launched in numbers with a short design, development, and launch cycle. When satellites are miniaturized, energy consumption is one of the main metrics that need to be focused on. In this dissertation, we mainly target energy minimization in different subsystems of a satellite. This work is one of the first attempts in tackling issues in Space-IoT.

Before we delve into the contributions made through this thesis, we outline, in the following sections, the advantages and applications of Space-IoT, the broad challenges in realizing Space-IoT and the current race and developments in the market in this field.

1.2. ADVANTAGES AND APPLICATIONS OF SPACE-IOT

Satellite-based IoT has a plethora of benefits when compared to the existing terrestrial IoT infrastructure. The major ones are listed below.

1.2.1. ADVANTAGES

Global coverage. Currently, most IoT deployments rely on cellular networks, public and private long-range networks, and WiFi. All of these networks have a limited coverage range. Furthermore, cellular networks and public long-range networks, such as the Things Network, are prevalent in densely populated areas but scarce to none in rural areas. While installation of infrastructure to increase coverage is desired, the return on investments may not always be positive; moreover, installation may also be infeasible at certain locations.

A network of interconnected satellites, on the other hand, can cover thousands of square kilometers, which could span all kinds of terrains and waters on Earth. While just five or six satellites in geostationary orbits are sufficient to offer global communication, constellations of as low as 66 satellites can cover the entire earth from Low Earth Orbits [6]. A glimpse of the arrangement of satellites in the second generation Iridium NEXT constellation is shown in Figure 1.2. Satellite-based IoT can be employed to accomplish true ubiquitous global connectivity. 'Black spots' in connectivity can be avoided across the globe for better services and also prevent losing track of vehicles for example. A case in point is the disappearance of Malaysian flight MH370 [7].

Reliability. As more devices are being added to the IoT ecosystem, there should be a way to ensure that the services are reliable. Especially, in mission-critical IoT applications, that

Figure 1.2: A glimpse of arrangement of satellites in the second generation Iridium NEXT constellation [6]

include Machine to Machine (M2M) communications, high reliability is a must.

Terrestrial wireless communications are usually subject to complex RF propagation phenomena, even when a device is placed outdoors, as compared to a device communicating with a satellite. This is due to the lack of urban clutter and terrains not coming into the picture when communicating with a satellite.

Orbits for a constellation of satellites can be calculated such that they can provide 100% availability, i.e., more than one satellite is visible at any location and time, as well as high-reliability, which can be better than or equal to the services offered by terrestrial networks, including cellular networks [8, 9].

Scalability. IoT communication systems must be scalable and nimbly accommodate a fast-growing number of IoT devices. Its infrastructure should meet the changing needs in the future. Given the large field of view of a satellite, it is imperative that several thousands of nodes can communicate at once, which can be supported by a single satellite [10]. Regardless of changes in deployment on the ground, the same constellation of satellites can support IoT devices.

Connectivity. Continuous and steady availability of the communication system is crucial to many IoT applications, especially, in applications having mobile devices. Examples include connected cars, marine communication, logistics and asset tracking.

Data bandwidth. Satellite communication technologies are advancing swiftly. For example, the Starlink constellation is promising up to 10 Tbps of throughput [11]. Enabling direct sensor node – satellite communication or sensor nodes – gateway – satellite network paths can provide high throughput. Edge computing on each satellite can be useful for managing communication bandwidth for downlink on a satellite. In a network of satellites, each satellite acts as an edge of the network. By processing data at the edge, close to the source of the data, unnecessary data can be filtered out and only the relevant data can be transmitted to the satellite for downlink. This can reduce the amount of data that needs to be transmitted, thereby reducing bandwidth usage. This can also help to reduce latency and improve overall network performance. Further, with edge computing on a network of satellites, real-time data analysis can be performed, allowing for quick decision-making and response to changes in the network or data. This can help to improve overall network efficiency and

reduce the risk of congestion or other issues.

Space Exploration. Space-IoT paves a way for advanced space explorations that include space robots, planetary missions, satellite swarms forming radio telescopes, and space colonization. The strategy of execution of space systems, such as Moon habitat, includes hundreds of connected sensors and actuators, and a swarm of Artificial Intelligence (AI) based robots assisting the astronauts [12]. In such cases, the reliability and availability of these devices are crucial. Space-IoT can meet the requirements of such space explorations.

1.2.2. APPLICATIONS

As mentioned earlier, the major contributions of Space-IoT are global coverage, connectivity, and scalability. Space-IoT also has a major role in 5G communications. Hence, Space-IoT comes with a plethora of applications where the existing terrestrial IoT lacks performance in several aspects. While not all of them can be presented here, we cherry-pick the notable categories as follows.

Emergency services. Emergency services are mission-critical and the network must be available all the time. For example, emergency services can include disaster management, military data transmissions, and satellite phone systems. These applications cannot afford any interruptions in the network. Especially, during natural calamities, such as floods, and cyclones, the terrestrial communication infrastructures are directly affected. The networks go out of operation very often for days or weeks. However, satellites are immune to these problems. Hence, Space-IoT is preferred for emergency services when the terrestrial network is either inaccessible or reliable.

Maritime applications. Space-IoT offers thriving solutions when it comes to maritime applications. Satellites deliver uninterrupted and endless service even on seas and oceans that are far from the coverage of terrestrial networks. This is advantageous for services such as tracking fishermen and early warning systems, marine logistics and vessel tracking, emergency communication services for the navy, and satellite-based networking for offshore oil and gas industries. Inmarsat, with a constellation of 14 geostationary satellites, is already providing commercial services such as long-range ship tracking, real-time weather updates to sea passengers, and assisting fishermen with location-based fishing data [13].

Smart agriculture. Agriculture is a fundamental source of income for many people in developing countries. Modern smart agriculture includes numerous sensors to monitor crop health, temperature, soil, humidity, etc. to enhance crop quality and increased yield. The data from these sensors are collected by a gateway and then communicated to a cellular tower. In most countries, agricultural lands are far away from the cities due to the unavailability of vast land suitable for agriculture in densely populated locations [15]. Such areas may not be in proximity to cellular networks. For such areas, Space-IoT is a prominent asset. Satellites can communicate with numerous agricultural sensors directly or via a gateway and facilitate precision farming to make accurate data-driven decisions. Many companies are investigating the potential of Space-IoT in smart agriculture. Orbcomm is one such company that offers satellite-based IoT devices for smart agriculture using M2M technologies [16].

Figure 1.3: A satellite imagery of agricultural fields [14]

Satellite services such as imagery can be beneficial in connected farming to estimate crop yield, identify crop diseases, forest fires, and irrigation [17]. Figure 1.3 shows an image of agricultural fields captured by a spectral camera aboard a satellite. Monitoring systems such as cattle sensors, which track cows and their activities, health, and nutrition insights, have shown their competencies in smart agriculture hitherto [18]. Satellites can communicate with such sensors directly, track the cattle, and gather data even if they are out of the coverage area of terrestrial gateways. Considering the capabilities of satellite networks, there is no doubt that the synergy between satellites and terrestrial networks will take farming to the next level.

Healthcare. Healthcare is given the utmost importance in any country. The researches in this field are incessant and Space-IoT can contribute to healthcare in various aspects. Examples include (i) satellite communication-based IoT devices mounted beside streets that can detect accidents in isolated areas and call for emergency help, (ii) remote health monitoring of patients before they arrive at the hospitals under critical conditions, especially when terrestrial networks fall short. Satellites can navigate and track ambulance drones equipped with lifesaving technologies such as Automated External Defibrillator (AED), medication, and Cardio-Pulmonary Resuscitation (CPR) aids. Applications of these kinds need continuous communication over long distances and remote locations, and Space-IoT will be of paramount importance here.

5G and IoT. The mobile industry is ushering in the 5G communications era. New standards are being finalised in 5G to poptimize communication technology in many ways. Satellites are already a part of the 5G network for wireless communication. 5G is relying on satellite constellations to create a network of networks, including 4G LTE and other cellular technologies. As of now, satellites are mainly serving as backhaul in hard-to-reach geographical locations. However, it is speculated that in the near future, smart cities will utilize satellite networks in a 5G-interconnected world to manage connectivity to vehicles, houses, office

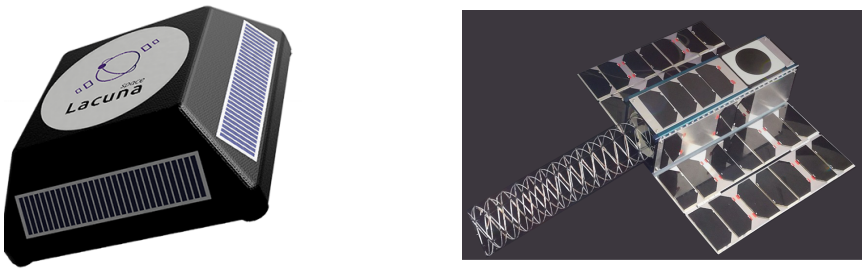

(a) IoT sensor unit that costs around 20 USD [10]

(b) One of the satellites used for Space-IoT by Lacuna [10]

Figure 1.4: Terrestrial IoT sensor and shoebox-sized satellite from Lacuna Space used for Space-IoT

spaces, hospitals, traffic signals, etc [19].

Furthermore, satellite networks have already demonstrated their exceptional abilities in Software-Defined Networking (SDN), Software Defined Radios (SDR), edge computing, and in various scenarios where a lot of bandwidth, optimal performance, and low latency are required. As a result of these advantages, Space-IoT is a boon for 5G communication. Overall, the combination of 5G and IoT in satellite communication has the potential to unlock a range of new applications and possibilities, making space exploration and research more efficient and accessible. As the technology continues to evolve, we can expect to see more innovative uses of 5G and IoT in space-based applications.

Connected vehicles. Connected vehicular technology is getting more popular. The future of mobility is automated and connected. To prove safety at high levels of automation, reliability is key. A robust and redundant connection from the vehicle to the digital infrastructure is required and must be available everywhere. Satellites and terrestrial services can integrate with 5G to provide this connectivity.

If we analyse all the above applications, three main factors place Space-IoT at the pinnacle – coverage, scalability, and continuous availability. Hence, Space-IoT is a solitary solution to the diverse problems encountered in terrestrial IoT.

1.3. THE RACE FOR SPACE-IOT

Space-IoT is an upcoming technology; the industry is working towards it by developing low-cost satellite constellations and IoT devices [9, 10, 20]. There is a commercial race for placing thousands of low-cost satellites around earth to accomplish Space-IoT.

A commercial venture named Hiber has developed a special battery-operated sensor node called *HiberBand* for their proposed system "Low-power Global Area Network". It can communicate directly with their satellite constellations in Low Earth Orbit (around 600 km altitude or less) [20]. Their major goals are to provide IoT services using satellites for fleet management and asset tracking, and remote pressure and temperature monitoring.

Lacuna space is another startup that is concentrating on the development of an ultra-low-cost tracking and detection service, wherein a fleet of satellites can receive data from terrestrial sensor nodes directly [10]. Figure 1.4a shows their battery-powered wireless sen-

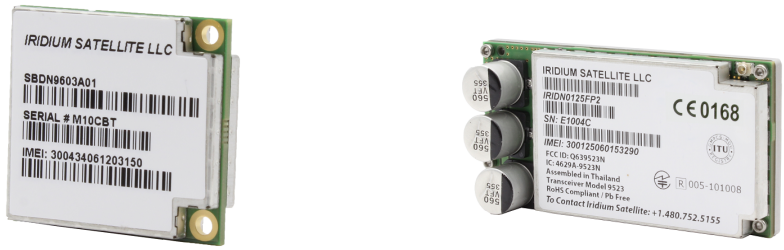

(a) Iridium 9603 module, weighing just 11.4g, used in monitoring, tracking and alarm systems

(b) Iridium 9523 module, a voice and data-based satellite transceiver module

Figure 1.5: Iridium modules [6]

sor unit that can communicate directly with their satellites (Figure 1.4b). The signals use a long-range wide area network protocol, such as Long Range Wide Area Network (LoRaWAN), and the satellites store the messages for a short period until they pass over their designated network of ground stations. The messages are then relayed automatically from the ground station to the cloud platform and relayed to the customer. The device targets multiple IoT applications: real-time wildlife tracking, asset tracking, smart agriculture, and remote monitoring.

A well-known satellite constellation, Iridium NEXT that was launched between 2017 and 2019 is being used for Space-IoT [6]. With just 66 cross-linked satellites in Low Earth Orbit(s) (LEO), the satellites communicate with their proprietary devices anywhere in the world, and at any time. Two of their satellite communication modules, Iridium 9603 and Iridium 9523, are shown in Figure 1.5a and Figure 1.5b respectively. Iridium also demonstrated LoRaWAN back-haul communications for IoT devices via satellite, enabling low-cost global IoT networking across the globe.

Similarly, Inmarsat and Vodafone have teamed up to provide satellite connectivity to Vodafone's IoT platform using Inmarsat constellation [21]. Inmarsat is the leading provider of global mobile satellite communication services for reliable voice and high-speed data across the globe [13]. Vodafone's Satellite IoT service uses Inmarsat's Broadband Global Area Network to address any terrestrial IoT connectivity challenge deriving from poor cellular coverage conditions. This is equivalent to Vodafone having a cellular tower in space. This is an example substantiating how an existing communication-based satellite constellation can be utilized in Space-IoT.

Swarm Space, with the ambition to provide continuous global coverage for IoT applications, is planning to launch 150 satellites with at least three satellites covering every point on the earth at all times. Applications include agriculture IoT, maritime, ground transportation, remote smart energy meters, disaster response, and air/water quality monitoring [22]. Swarm Technologies has integrated Semtech's Long Range (LoRa) devices into its connectivity solution to enable two-way communications to and from its satellites in Low Earth Orbits (LEO) [23]. LoRa is a wireless communication technology that has gained popularity in the Internet of Things (IoT) space due to its low-power consumption, long-range, and high interference immunity. In the context of space-IoT, LoRa can be used to enable com-

(a) IoT satellite communication device from Swarm Space [22]

(b) Astrocast's Astronode S module [24]

Figure 1.6: Space-IoT modules from Swarm Space and Astrocast

munication between ground-based IoT devices and satellites. One of the key advantages of LoRa in Space-IoT is its long-range capabilities. LoRa can transmit data over long distances with minimal power consumption, making it ideal for communication between remote IoT devices and satellites. This can be particularly useful in areas where traditional communication technologies such as cellular networks are not available or are unreliable. One of the IoT devices from Swarm Space is shown in Figure 1.6a.

Airbus is in collaboration with a Switzerland-based establishment called Astrocast to co-develop and deploy a unique data protocol for global satellite-based IoT communications [24]. Their IoT module, shown in Figure 1.6b, can be embedded on any product and used in ample applications such as maritime, mining, oil and gas, connected vehicles, agriculture and livestock, asset monitoring, and what not? The device exploits satellite communication to connect one IoT system to another.

There are more Tech-Ventures, such as Sateliot, Fleet, and Myriota, that are reinventing the future through transformative Space-IoT systems but they are just taking baby steps. Thus, there is an immense commercial interest to bring Space-IoT into existence. With this note, it is crucial to look into the aspects of Space-IoT from the research point of view. IoT in space has just started growing.

1.4. CHALLENGES FOR REALIZING SPACE-IOT

While it is factual that satellite technology is better than terrestrial networks, in some ways, and can act as an ideal complement to the terrestrial IoT networks, the past designs of satellites may not be suitable for Space-IoT. Most of the existing satellite constellations are designed to communicate with ground stations and not with cellular towers or sensor nodes/gateways. Hence, adopting such satellites for IoT may be impracticable. Space-IoT is an exciting field to work waiting for innovations to happen. Designing, implementing, and deploying satellites from the perspective of Space-IoT come with many challenges. In this section, we discuss primary challenges concerning embedded and networked systems to realize Space-IoT. In particular, the motivation for our work comes from these challenges, projected in Figure 1.7.

1. Miniaturization. Access to space has always been expensive as enormous efforts and resources are required to launch a satellite. It takes around $20,000 to place 1 kg of payload (satellite) in orbit at an altitude of around 500 km [25]. Extrapolating this cost linearly,

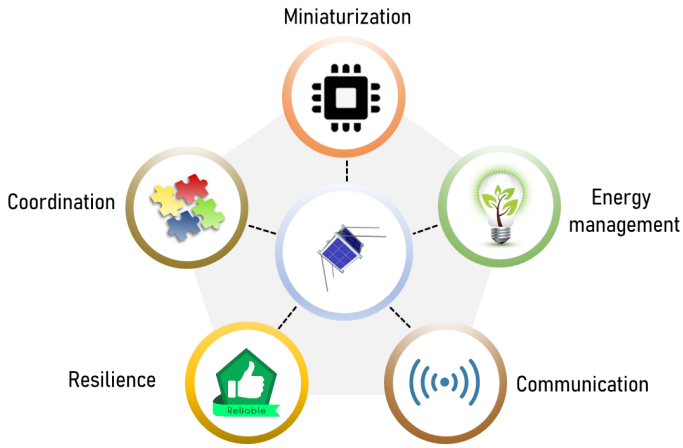

Figure 1.7: Major challenges in realizing small satellite constellations in the context of Space-IoT.

even a small satellite of 10 kg would cost $200,000 just for the launch. Considering these numbers, one can imagine the time and cost that would take to construct a mega constellation of hundreds or thousands of satellites orbiting the earth and working as one system. Therefore, the miniaturization of satellites takes prime importance to reduce space mission costs.

Miniaturization does not come without challenges. As the electronics and physical structures of the satellites become smaller, the size and number of solar cells used for harvesting energy are also reduced. This directly constrains the overall energy budget and affects the entire satellite operation. Additionally, the need for compacting equipment in small spaces leads to issues in mitigating radiation and controlling temperatures, which are generally expensive or difficult to address [26]. Further, the miniaturization of electronic components may lead to packing things into a much tighter volumetric package. This can lead to hot spots and thermal management challenges.

2. Energy management. As aforementioned, when a satellite is miniaturized, its solar cells may get reduced in size and count, thus causing a shortage in generated power. An interesting question that will arise is "should the power consumption of the satellite subsystems not reduce as they get smaller?". Let us consider the communication subsystem of a satellite as an example to answer this: regardless of the satellite size, transmission power settings may need to fulfil strict requirements to ensure range and bandwidth. For example, a CubeSat's transmission power is usually set to 1 W, whereas the maximum harvested power with its solar cells is approximately 2 W. If half of the energy budget is allotted just for communication, then other modules, including thermal control, onboard processing, attitude determination and control, and sensing equipment must work within the remaining 1 W without performance degradation. This imposes severe requirements on both the energy consump-

tion figures of individual modules and the run-time distribution of available power. Thus, while harvested energy reduces due to miniaturization, the power consumption of the different modules on a satellite may not reduce *proportionally*.

3. Communication. Relaying data to the ground and exchanging information among the satellites in a constellation are functional requirements of Space-IoT. Both these requirements expose sharply different requirements compounded by the different communication technologies used in small satellites, ranging from RF to optical communications [27]. Considering the Space-IoT applications, a large bandwidth is necessary to funnel data to the end users. This can only be achieved by allocating a large amount of energy, which is scarce as per the previous discussions. With advancements in RF technology, large antennas potentially ameliorate these issues but their sizes are limited by the physical structures of satellites. When exchanging data with other small satellites, on the other hand, optical communications, such as lasers [27], are also reported to be operational in space with the help of accurate attitude control to ensure precise beaming to the destination. This again requires energy. Further, primordial modulation techniques, such as Frequency Shift Keying (FSK), Binary Phase Shift Keying (BPSK), and Quadrature Phase Shift Keying (QPSK), may have to be revisited in the context of Space-IoT to comply with the existing earth-bound IoT nodes or sensor node - satellite communication.

Another critical challenge that needs to be considered in satellite communication is the Doppler effect. Most satellites move faster than a bullet. For example, a satellite in LEO may travel as fast as 7.8 km/s. This speed induces a Doppler shift in the received frequency of the signal either on the satellite or a sensor node on earth. While this is a well-studied rudimentary problem in satellite ground station communication, the low-power IoT nodes need a new outlook in this aspect. Increasing the RF receiver bandwidth on IoT nodes can tackle the Doppler issue but it has an adverse effect on the receiver sensitivity and communication range.

4. Resilience. Satellites are bound to operate in harsh space environments, with temperatures varying from -100° C to 150° C and cosmic radiations harming elementary data operations, such as memory read/write, causing transient faults [28]. Large satellites are designed to be highly dependable, using expensive thermal protections, radiation-hardened space-grade components, and highly reliable storage hardware, such as Error Coding and Correction memories. Small satellites are usually built using Commercial Off The Shelf (COTS) components to reduce costs. However, they provide nowhere near the same or similar dependability guarantees. Almost all the Space-IoT-based satellites that are already launched or under design employ COTS components [9, 10, 20, 22, 24]. Redundancy is the chosen design approach to ensure dependable operations in satellite systems. However, this inherently clashes with the aforementioned need for miniaturization and energy constraints. Therefore, resiliency in COTS-based satellite systems needs to be revisited.

5. Localization. Connected to coordination between the satellites, accurate positioning is essential for both the satellite's operation and for application-level tasks, e.g., when coordinating a constellation for high-resolution imagery and radio interferometry [17, 29]. Global Positioning Service (GPS) based localization is the most commonly used positioning technique in space. The existing GPS algorithms for such tasks require a high amount of com-

putation and are power-hungry. Thus, reducing energy consumption for localization while providing high position accuracy is non-trivial and extremely challenging in miniaturized energy-constrained satellites.

1.5. PROBLEM STATEMENT

In the previous section, we charted out the high-level challenges and provided a broader picture of the problems that need to be tackled for Space-IoT. Apart from these challenges, there are many unresolved problems such as time synchronization, multi-hop communication, and packet delivery improvements, to mention a few. Solving the above challenges, most often, entails striking proper trade-offs with solutions addressing different issues, or sacrificing performance on orthogonal system metrics.

Encompassing all the aforementioned challenges, this thesis addresses the following research question.

How to build innovative miniaturized COTS components-based space subsystems with reduced energy consumption in the context of Space-IoT?

While this thesis does not solve all the aforementioned issues, since there are too many, for an entire satellite, we cherry-pick a few subsystems of a satellite to demonstrate the necessity to address the issues and portray the ways to achieve them. To this end, we consider three subsystems of a satellite: communication, attitude determination, and health monitoring. Though this work concentrates on the problems in satellites, the proposed solutions can also be adapted for terrestrial counterparts wherever applicable.

1.6. THESIS CONTRIBUTIONS AND OUTLINE

This thesis contains four chapters that detail the way toward realizing Space-IoT. The rest of the chapters and their contributions are as follows.

SWANS: Sensor Wireless Actuator Network in Space - Chapter 2. In this chapter, we enumerate the innovations in space and the vision concerning embedded and wireless systems for space applications in the context of Space-IoT. In particular, we bring in the notion of *Sensor Wireless Actuator Networks in Space* (SWANS) wherein a satellite is treated as a collection of sensors and actuators. We discuss with examples what we envision for the next decade in the field of Space-IoT. We discuss three important broad themes, which have long-term research and innovation potential: (i) wireless sensor actuator networks in space for deep space and Low Earth Orbit (LEO) missions and applications. This is an exciting new frontier. The idea is to connect multiple modules within satellite systems to make them low-cost and mass deployable to ease Space-IoT; (ii) satellite swarms will be the order of the future. Swarms will be part of any future space missions since it allows the incremental build-up of large space missions using smaller, yet complete systems that are individually accomplishing some of the tasks; (iii) Space-IoT is not only limited to space-earth communication but also can be interplanetary. In this regard, space robotics is an important topic since it can be autonomous and is crucial for space explorations. We describe these topics

with initial studies and experiments while listing their umpteen challenges. As Space-IoT is revolutionary and visionary, this chapter provides a new outlook to the research community in the direction of Space-IoT.

Demodulation of Bandpass Sampled Noisy FSK Signals for Space-IoT - Chapter 3. In Space-IoT, the terrestrial sensor nodes are expected to communicate with satellites directly, over hundreds of kilometres. Almost all the existing IoT devices on earth are designed and tuned to communicate with gateways or cellular towers, that are only a few km away. Hence, when such IoT nodes communicate with a satellite, without any modification in the antenna and transmission power, the Signal to Noise Ratio (SNR) of the received signal will be very low. Using high transmission power or bigger antennas to maintain high SNR are the alternatives but they conflict with miniaturization and energy minimization demands. Additionally, the received signals on a satellite or a sensor node are affected by Doppler shifts. In such cases, obtaining reliable communication while being energy-efficient is very challenging.

In this chapter, we propose a new data recovery scheme, wherein bandpass-sampled FSK telemetry signals can be decoded successfully even in the presence of noise and Doppler shift. We propose an algorithm called Teager Energy Decoder (TED), which is based on Teager Energy Operator, to decode noisy FSK signals. TED does not need any Doppler correction mechanisms and can dynamically adapt to the changing frequency shifts. We comprehensively provide the evaluation results of TED using simulation as well as the signals received from two nanosatellites. We show that TED performs better than COTS transceivers and GNU-radio-based solutions. We show that TED can be easily adopted on satellites to decode signals for Space-IoT applications. We further made the algorithm more reliable and energy-efficient so that it can be used even in terrestrial low-power Wireless Sensor Nodes (WSN). This facilitates direct communication between a terrestrial IoT node and a satellite without demanding any increase in the module size.

Hummingbird: An Energy-efficient GPS Receiver for Small Satellites - Chapter 4. Accurate positioning is essential for both the satellite's operation and for application-level tasks, e.g., coordinating a constellation for Space-IoT. Especially, in satellite swarm-based use cases such as high-resolution imaging, and Electronic signals intelligence (ELINT), stitching the data from each satellite in a constellation to get a broader outline is highly imperative. GPS is one of the widely adopted techniques for localization in space. However, most of the small satellites are severely power-constrained (because of their restricted solar panel size), and GPS receivers are seen as one of the subsystems that consume a significant portion of the available energy [30, 31]. Minimizing energy consumption for localization with high accuracy is non-trivial and extremely challenging in miniaturized energy-constrained satellites. The reasons are, (i) as described earlier, a satellite in LEO may travel as fast as 7.8 km/s. GPS satellites, in turn, orbit at 3.8 km/s. The relative movement of small satellites compared to the GPS satellites magnifies Doppler effects. The search range due to Doppler effects increases up to ±80 KHz, as opposed to a mere ±10 KHz on Earth, prolonging the time taken to get the first position fix, (ii) in small satellites with no attitude control, rapid changes in GPS visibility due to tumbling further compound the problem. GPS receivers are normally duty-cycled to save energy but longer times to get the first GPS fix play against this, as the GPS receiver must stay on for a long time, eventually. The energy minimiza-

tion challenge is at the core of our work on 'μGPS': our space-proven GPS receiver for small satellites.

In this work, we elucidate the design of a low-cost, low-power GPS receiver μGPS for small satellite applications. We present our work that tackles energy minimization issues in the localization sub-system of small satellites without any trade-off with miniaturization. We propose an energy optimization algorithm called F^3 to improve the TTFF, which is the main reason for higher energy consumption during cold start. With simulations and in-orbit evaluations, we show that up to 96.16% of energy savings (consuming only $\sim \frac{1}{25}$th) can be achieved when compared to the state-of-the-art.

An Isolated Health Monitoring System for Small Satellites - Chapter 5. With the advent of Space-IoT, the rate of the launch of satellites is growing significantly. Alongside this, the failure rate of small satellites also surged tremendously [32]. Space systems are physically non-repairable in orbit or it is a very expensive process [33]), and the financial losses incurred when they fail before their expected mission time is substantial. However, if the source of failure can be identified, then the satellite may be saved by sending appropriate commands from the ground station. Satellites are generally equipped with onboard health monitoring systems. While most of these solutions are based on onboard software diagnostics, information needs to be transmitted to the ground station using the same hardware present onboard. However, if the communication system fails to operate, then the reasons for failure stay unexplained. Health monitoring systems in the existing satellites are tightly coupled in terms of hardware and software. Any fault in the subsystem may affect its onboard health monitoring modules as they are electrically connected.

In this chapter, we present a simple, miniaturized, independent satellite health monitoring system called Chirper. The Chirper provides a secondary channel for the health monitoring system for satellites. It is equipped with multiple modules such as an Inertial Motion Unit, isolated voltage and current measurement probes, and an onboard communication channel. With examples, we first explain how can a failed satellite be revived and how can Chirper aid to save a satellite. Further, we list the major causes of failures in satellites and the main challenges that need to be addressed while designing Chirper. To enable electrical isolation between Chirper and the satellite, we propose a novel methodology and a model to measure low DC voltage based on capacitive technology that does not need any electrical contact for measurement. We are the first to provide such an isolated voltage measurement solution, and this technique can be used not only in the space domain but also in terrestrial applications. Finally, we present the performance evaluation results of the Chirper in different scenarios: simulation, by mounting it on a test satellite system in a space laboratory, and by launching it on a helium balloon. This work mainly addresses the resilience and energy issues mentioned in Section 1.4.

The contributions listed in the aforementioned chapters have resulted in the following publications.

1. **S. Narayana**, and R. Venkatesha Prasad, *"Space, the Final "Communications" Frontier?"*, In ComSoc Technology News (CTN), November 2022, [Online Access - https://www.comsoc.org/publications/ctn/space-final-communications-frontier] **(Chapter-1)**.

2. **S. Narayana**, R. Venkatesha Prasad, V. Rao, and Chris Verhoeven, *"SWANS: Sensor Wireless Actuator Network in Space"*, In Proceedings of the 15th ACM Conference on Embedded Network Sensor Systems **(SenSys '17)**, art. 23, pp. 1-6, 2017. **(Chapter-2)**.

3. **S. Narayana**, R. Muralishankar, R. Venkatesha Prasad, and V. Rao, *"Recovering bits from thin air: demodulation of bandpass sampled noisy signals for Space-IoT"*, In Proceedings of the 18th International Conference on Information Processing in Sensor Networks **(IPSN '19)**, pp. 1–12, 2019. **(Chapter-3)**.

4. **S. Narayana**, R. Venkatesha Prasad, V. Rao, L. Mottola, and T. V. Prabhakar, *"Hummingbird: energy efficient GPS receiver for small satellites"*, In Proceedings of the 26th Annual International Conference on Mobile Computing and Networking **(MobiCom '20)**, art. 9, pp. 1–13, 2020, ***- best paper award***. **(Chapter-4)**.

5. **S. Narayana**, R. Venkatesha Prasad, V. Rao, L. Mottola, and T.V. Prabhakar, *"A Hummingbird in Space: An energy-efficient GPS receiver for small satellites"*, In ACM **GetMobile**: Mobile Comp. and Comm. 25, pp. 24–29, 2021. **(Chapter-4)**.

6. **S. Narayana**, R. Venkatesha Prasad, V. Rao, L. Mottola, and T.V. Prabhakar, *"Hummingbird: Energy Efficient GPS Receiver for Small Satellites"*, In Communications of the ACM **CACM**, Volume 65, Issue 11, November 2022. **(Chapter-4)**.

7. **S. Narayana**, R. Venkatesha Prasad, and T. V. Prabhakar, *"SOS: isolated health monitoring system to Save Our Satellites"*, In Proceedings of the 19th Annual International Conference on Mobile Systems, Applications, and Services **(MobiSys '21)**, pp. 283–295, 2021. **(Chapter-5)**.

2

SWANS: SENSOR WIRELESS ACTUATOR NETWORK IN SPACE

In the previous chapter, we presented the concept of Space-IoT, its advantages, applications, and the motivation for this work. In this chapter, we present the vision of a Sensor Wireless Actuator Network in Space (SWANS), a collection of sensors and actuators in space that can bring Space-IoT into reality. The scope of sensors and actuators in terrestrial IoT is well-studied in the literature. In Chapter 1, we portrayed Space-IoT as a network of sensors and actuators on Earth and in space, and they are strongly connected. This is one perspective of Space-IoT where satellites communicate with IoT devices on Earth. However, Space-IoT can also be seen from an alternate view: satellites communicating with each other (inter-satellite communication), satellites communicating with sensors–actuators nodes on the Moon, other planets, etc. Let us look at a satellite as a single, massive IoT device. A satellite is already a collection of different sensor and actuator systems such as gyroscopes, magnetometers, solar panels, antennas, star and sun sensors, reaction wheels, magnetorquers, and propulsion systems. These sensors and actuators are connected to form different subsystems that perform certain tasks in a satellite. This is nothing but an IoT inside a satellite itself.

The major subsystems of a satellite are ① OnBoard Computer (OBC), the brain of the satellite, that is responsible for the overall system processing, and sending commands to the rest of the subsystems; ② Electrical Power System (EPS), that is responsible for energy harvesting and power management; ③ Attitude Determination and Control (ADCS), that includes diverse sensors and actuators to determine and change the attitude of the satellite in orbit; ④ Communication subsystem, that addresses command and mission data handling, and satellite–ground station and inter-satellite communication; and ⑤ Mechanical subsystem, that incorporates structural and thermal mechanics of the satellite.

Besides these, a satellite may have a software or hardware-based health monitoring system residing on each of these subsystems. The subsystems are connected mostly by wires (also called *harness*) within a satellite, which adds to the weight and size of the satellite. Re-

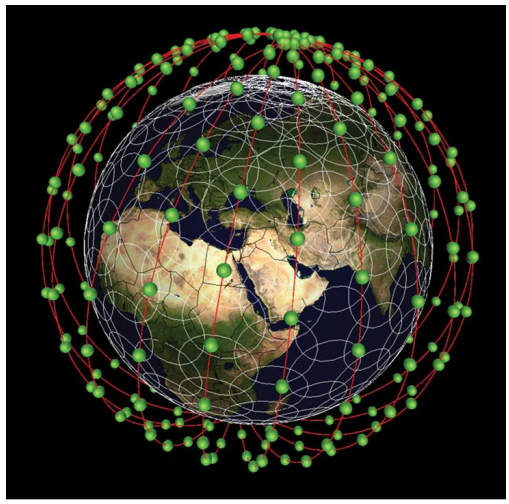

Figure 2.1: An example of a satellite constellation in LEO. Each green dot represents a satellite

placing wires with wireless technologies without sacrificing performance will make a satellite a Sensor Wireless Actuator Network in Space (SWANS) – a wireless IoT inside a satellite. Together with all the subsystems of a satellite, we extend SWANS to include a group of satellites to enable several applications including *swarms or constellations of satellites*. Therefore, we define SWANS as, "a collection of connected wireless sensors and actuators in space represented by a single satellite or a constellation of them, or any sensor and actuator in space". Using SWANS, we can connect ground from space globally, which is one of the visions of Space-IoT. We envision that SWANS will impact the space industry significantly including traditional space applications in the near future. The main driver for SWANS is the need for a miniaturized, inexpensive, low-power network of satellites:

(a) As explained in Chapter 1, a swarm of autonomous small satellites (or tiny wireless smart sensor-actuator networks) deployed around the earth can provide global coverage and connectivity to the terrestrial IoT. Furthermore, they can also collect more data with respect to deep space exploration than any observatory station on Earth. An example of such constellations in Low Earth Orbit is shown in Figure 2.1;

(b) IoT applications that include precise measurements of various particle concentrations in the atmosphere can be done more easily and more effectively using a swarm of tiny satellites orbiting in very Low Earth Orbits (LEO) than having bulky equipment on the earth;

(c) With a swarm of satellites, space robotics on the Moon, Mars, or other space objects can be improved significantly to control robots from the earth or the International Space Station with much lower latencies.

Though there have been advancements in building satellites and their launching technologies, access to space has been expensive, and many scientific challenges still exist [25].

An important question is how these existing sensor and actuator systems in satellites should be adapted to form SWANS so that the solution is inexpensive, reliable, and efficient. Since the beginning of the satellite era, there has always been a demand for mass production, miniaturization, low-cost solutions, innovative system designs, reliable inter-networking of satellites, etc., for space applications, but much exploration is yet to be done to meet these requirements. Compared to terrestrial applications, the implementation of SWANS in the form of wireless networked satellite systems requires innovation, optimization of space and weight, and higher levels of reliability. They should withstand harsh space environments such as extreme temperatures, high mobility, power constraints, and undesirable perturbations that influence their operation significantly. Further, the wireless communication between two satellites in a constellation will rely on an inter-satellite link or intra-satellite link, whose establishment and stability are impacted by the satellite orbit and attitude, antenna configuration, link range, mobility, and the layout of the spacecraft. If the communication range of each node (satellite) is limited, the nodes may use multi-hop communication to send their data to the destination. This requires complex control and should adopt an auto configuration [34, 35] and routing strategy [36] to ensure time and/or energy optimization as they are resource-constrained.

2.1. SMALL SATELLITES

Currently, most of the existing long-term mission-oriented satellites in space are bulky and expensive, but ultra-reliable. They are designed for a particular mission, and once the mission is complete, these satellites may become space debris. Even during mission time if there is a critical failure in the satellite's sub-system, then it may be difficult to fix it. Physical repair or upgrade after the launch is very tedious and expensive, and in some cases, it is next to impossible. Hubble telescope is the only space telescope that has been serviced in orbit to date. NASA dropped the plan of such missions as the upgrade cost is in the order of a new satellite itself [33]. Such problems in space missions have led to an insight into the space industry to develop space systems that are affordable, flexible, multipurpose, and reusable. Thus, making space objects as small as possible is inevitable when thousands of them need to be fabricated and deployed in space. A swarm of networked, small, and inexpensive satellites can form a wireless sensor-actuator network in a distributed way to achieve the same desired features of a big satellite [37]. These swarms can communicate with each other and also with ground stations to perform better than a single big satellite in most cases. Such swarms in space can provide advantages such as redundancy, fault tolerance, low-cost production and incremental deployment, and massive distribution. Moreover, if one satellite in a swarm is dead, then the mission is not affected much, except that there may be an impact on the global coverage. In this case, a new small satellite can be launched in no time and at a low cost to replace the faulty satellite. Hence, small satellite technology can be a key element to the future vision of Space-IoT.

Small satellites come in a variety of form factors, from femtosatellites (<0.1 Kg mass) to nanosatellites (1 Kg to 10 Kg mass). Table 2.1 lists a classification of satellites in terms of deployed mass that has been generally adopted in recent years [42]. A few examples of small satellites are shown in Figure 2.2. The evolution of small sensor and actuator systems with MEMS technology has made it possible to shrink the size of many satellite components

Category	Mass in kg	Approximate size in m
Large	> 1,000	50 x 10 x 10
Medium	500-1,000	15 x 10 x 5
Mini	100-500	10 x 5 x 3
Micro	10-100	3 x 3 x 3
Nano	1-10	0.3 x 0.2 x 0.1
Pico	0.1-1	0.1 x 0.05 x 0.05
Femto	< 0.1	0.03 x 0.03 x 0.02

Table 2.1: Classification of satellites by mass

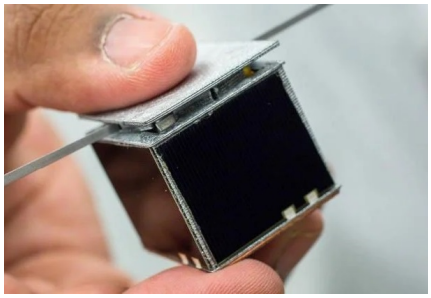

(a) SunCube, a femtosatellite (3cm x 3cm x 3cm) [38]

(b) PocketQube, a 3 unit picosatellite (50cm x 50cm x 17cm) [39]

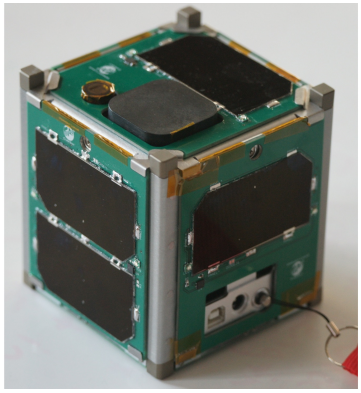

(c) Vermont, a CubeSat (10cm x 10cm x 10cm) [40]

(d) Delft-C3, a nanosatellite (10cm x 10cm x 30cm) [41]

Figure 2.2: Small satellites

and in turn, reduce the size of satellites dramatically from 1000 kg in the 1960s to 10 kg now. Small satellites are cost-effective due to the use of COTS components. Satellites such as Swiss Cube[43], STRaND-1[44], Delfi-C^3[41], etc., have proven that COTS components work

in space, thus providing inexpensive solutions and fast access to space. Moreover, it is easier to extradite such small satellites from space when compared to the bigger ones once they become debris [45]. Small satellites such as CubeSats started as an academic effort and eventually ended up providing a paradigmatic shift because of their features, advantages, and limitations [46]. CubeSat and nanosatellite initiatives are spreading globally, especially towards deploying massively distributed constellations of them able to achieve global coverage and ubiquitous Internet access through a coordinated operation [47]. The current trend in the space industry targets nanosatellites and CubeSats that have many advantages over large satellites such as,

(i) less production time and development cost because of reduced mass and COTS approach,

(ii) many satellite launch providers have demonstrated the possibility of launching multiple (even hundreds of) nanosatellites in a single launch [48], it is an era of small satellites now,

(iii) suitability for small, short-time missions of up to 5 years, and

(iv) tremendous potential for scientific research, and technology development and demonstration.

Thus, we envisage a large number of these small space systems that are agile being very low-cost alternatives to dominate the space. With this background, we next describe our vision of SWANS.

2.2. VISION OF SWANS

SWANS represent the next-generation space missions, which are agile, networked, and wireless communication-enabled closed-loop control systems to autonomously accomplish multiple tasks. The vision of SWANS is that it addresses not only smaller issues, for example, cable harnesses in satellites but also the future potential of Space-IoT in general. The idea is to automate and connect multiple modules within and between systems such as satellites, terrestrial networks, and rovers on different planets. We take a big leap into space covering many important aspects of SWANS and list three topics below. These topics invariably involve sensors, actuators, and wireless communications in space systems.

(i) *Satellite Swarms* will be the order of the day because of the widespread deployment of mobile systems on Earth and space in the future. Swarms of satellites will be part of any future space mission since it allows the incremental building up of a large space mission using smaller, yet complete systems that are individually accomplishing some of the tasks;

(ii) *Radio Interferometry (RI)* requires multiple, spatially separated low-frequency RF antennas to mimic optical telescopes on the ground. The size of the antennas in RI is expected to be very large compared to their mountings. RI can be used in deep space as well as Low Earth Orbit (LEO) missions. RI in space requires distributed computations, pointing and orientation (involving micro-thrusters), and synchronization to mention a few. This is an exciting new frontier;

(iii) *Space robotics* is an important topic since humans are not in a position to live in outer space yet without daily consumables; we need robotic limbs/extensions or a swarm of rovers to work on future outer planet explorations. We expand on these topics in the sections below.

2.2.1. SATELLITE SWARMS

Though space technology has advanced immensely, a small satellite may not replace large ones in terms of mission capacity. However, a constellation of small satellites can provide much higher functionality and flexibility for many important future missions, providing an equivalent performance of a bigger one or even better. For instance, a large satellite with huge antennas used in radio astronomy can be replaced by multiple small satellites providing the same performance but at very low cost and power. They form constellations of satellites ("satellite swarms") and are distributed and interconnected in space forming a specific orbital geometry. In general, these swarms are nothing but flexible distributed networked sensor-actuator systems in space that can maneuver, self-organize and execute specific tasks together. Such a swarm system can adopt star topology where small satellites are connected to a single gateway or a mesh with multiple gateways that can communicate directly with Earth. If the satellites in a swarm are bound to a specific control algorithm to maintain relative navigation with respect to each other by enabling communications amongst themselves or with a leader, it results in *formation flying*. Small satellites orbiting in close formations can target their mission at low-cost and low-power compared to multiple bigger satellites, with enhanced reliability compared to larger single-platform operations.

Most of the future missions planned by the space industry will include small satellites and formation flying [49–51], especially in LEO. LEO satellites are popular for Space-IoT applications. That is because LEO orbits have altitudes less than 2000 km and are nearer to the earth's surface as compared to the medium earth or geostationary orbits (35,786 km). Further, LEO provides flexibility in the launch, low-cost deployment, less cosmic radiation, and low communication latency. The advantages and use cases of the future satellite swarms are many: ① they can take remote sensing to the next level. Multiple interconnected small satellites can achieve remote sensing simultaneously, and get the complete three-dimensional mapping of the globe in less time; ② precise measurements at very low orbits around the earth (for instance at 250 km altitude) are very expensive and time-consuming with a single large satellite as the lifetime of objects in these orbits varies from several days to a few months. Small satellite swarms, being low-cost and providing quick results, are the sought-after solution in such situations. Examples include measurement of aerosol, smoke, and ozone concentration in the atmosphere, seismic activities, greenhouse effect, and dynamics of Ionosphere concerning radiation and communication; ③ they can provide reliable communication and broadband services to remote areas; ④ best services in military applications such as tracking soldiers and navy ships with shorter revisit times; ⑤ communication with a single larger satellite is possible only when it is visible to the ground station, whereas, in the case of a swarm, communication with non-visible satellite is possible because of inter-satellite links; ⑥ high expandability, autonomy, reliability, and redundancy are built-in. If one satellite fails others can work intelligently without

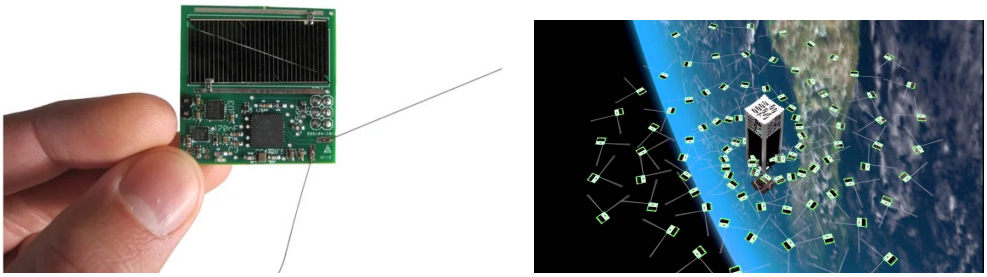

(a) Sprite, a femtosatellite of size 3.2cm x 3.2cm

(b) The concept of a nanosatellite, deploying hundreds of sprites

Figure 2.3: KickSat: A crowd-funded mission to demonstrate the world's smallest spacecraft [52]

breaking the formation, whereas, a failure of a single large satellite ends the entire expensive mission. Several satellites can be added to the swarm whenever necessary, and ⑦ small satellites also provide the opportunity to test new scientific experiments quickly because of swift development time and low-cost production.

Space organizations such as NASA have come up with a wealth of new ideas for the future, targeting small satellites. NASA's Cube Quest Challenge to design small satellites[49], Starlink's idea for global Internet service with small satellites in a few years [9], and the concept of PCBSat and Satellite on Chip from Surrey space centre[53] provide a way to the vision with satellite swarms and miniaturization technology. Moving one step further, we have the Starshot program by Stephen Hawking[54], a visionary project where a satellite in the form of a wafer-sized chip is shot to distant starts at ultra-high-speeds away from the Earth, using highly concentrated laser beams. Figure 2.3a shows a tiny femtosatellite called Sprite, developed by Zac Manchester, to demonstrate how hundreds of these can be deployed around the earth (or any planet) by a single 3-Unit nanosatellite called Kicksat. The concept of deployment of sprites is shown in Figure 2.3b. These sprites were supposed to be a part of the Starshot program in the future. However, the mission was a failure as the Kicksat failed to deploy sprites in space. This shows that there is a need for much advancement in miniaturization and sensor technology to make the mission successful.

Furthermore, for missions such as the Starshot program, there has to be a huge advancement in the existing satellite technology to produce tiny sensor and actuator chips that are ultra-low-power and can communicate with one another and with ground stations. Thinking big, to be small, the complete satellite should be embedded in a single pixel-shaped miniaturized chip which we call "*Space Pixels*". With a size in the range of 1 mm x 1 mm and weighing less than a gram, Space pixels can be analogous to Smart Dust[55] containing processing, sensor, actuator, and communication units onboard. Figure 2.4 shows the concept of smart dust, mainly projected to be used in terrestrial applications. We envision Space pixels to be similar to these smart dust but for space endeavours. The weight and size of Space pixels make them easy to be released in thousands in different orbits by

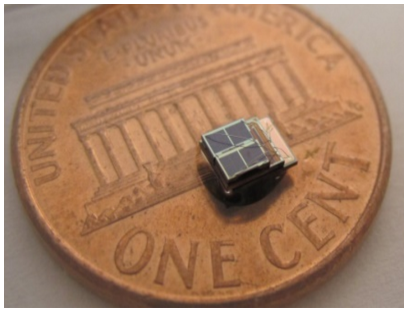

Figure 2.4: The concept of tiny smart dust, a sensor unit that is capable of processing and communication [55]

a high-altitude balloon or a small satellite. With these units, experiments such as RADAR reflectivity, atmospheric colouring, gas concentration, and meteor impacts can be done almost instantly. Not only in Earth orbits, a swarm of femtosatellites or Space Pixels can also be used in deep space explorations. They can be used for near-field atmospheric measurements in other planets and space objects such as moons, asteroids, and space stations by throwing them into orbit from landers or rover robots. In the case of remote sensing, multiple Space Pixels with micro cameras can get a bigger image in interplanetary explorations. The source of energy for these pixels can be solar or RF-based. In the case of solar, there can be a tiny solar panel embedded onboard, and in the case of RF, a large satellite or lander/orbiter on other planets can power these chips with continuous RF bursts. Space pixels are indeed an important vision for Space-IoT.

2.2.2. RADIO INTERFEROMETRY

One of the most foreseen expectations with the development of small satellite technology is taking radio astronomy into space. Though many complex radio telescopes are installed on Earth, there are many problems in listening to the RF signals from deep space: low radio frequencies are absorbed or refracted by the Ionosphere, high frequencies are absorbed by oxygen and water in the atmosphere, man-made interference on Earth, atmospheric phase fluctuations, and pointing offsets, etc. Even though space beyond the Ionosphere is suitable for radio astronomy, the technology involved in placing radio telescopes out there is different from that on the ground. Projects such as Orbiting Low Frequency Antennas for Radio Astronomy (OLFAR) aim to collect low-frequency signals (0.1 - 30 MHz) from far galaxies that can reveal information about solar, planetary bursts and the events from *Dark ages* after Big Bang, which is still unknown to us[56]. OLFAR cannot be accomplished on Earth or in Earth orbits as man-made RF interference from Earth can reach as far as the Moon. Hence, the dark side of the moon – where there is a lack of atmosphere to interfere with radio waves – would be a favourite place for radio astronomers. RF Telescopes on Earth have antennas with a diameter between 25 m - 500 m [57] and have an angular resolution of $\frac{1.22\lambda}{d}$ where λ is the wavelength of observation and d is the diameter of the antenna. Further, the lower the radio frequency larger the required antenna. The Hubble space telescope has an angular resolution of 14μdeg. Therefore, for low-frequency radio measurements in

space, a 5 km diameter antenna has to be placed in orbits that are nearly impossible with the current technologies. However, a novel approach with a swarm of small satellites in a constellation can realize the dream of radio astronomy in space.

To achieve a single, big, and virtual radio telescope in space with an angular resolution equivalent to that on Earth, an array of smaller telescopes can be used. This technique is called Radio Interferometry (RI). The design considers spatial separation between small satellites in the form of swarms carrying small telescopes, pointing at the same source of interest. The distance between two antennas is the baseline which is nothing but the diameter of the virtual giant antenna in space. Since the radio signal from a distant source arrives at the antennas at slightly different times, the cosmic address of the source can be calculated provided that the distance between small telescopes (satellites) is known. The signals from all the telescopes (at least two) are correlated to eliminate noise and obtain the signal. Though the concept of RI in space is already proposed, it is not yet demonstrated in space. RI can also help in searching for signals such as Fast Radio Bursts (FRBs) and gravitation waves from distant galaxies or *Black Holes* that span for a fraction of a second. To date, less than 100 FRBs have been discovered since their first detection in 2007[58]. Several key technologies are still to be developed for such missions using small satellite swarms with precise formation flying, and high-speed inter-satellite communication. If a stage can be set for RI in space, then a very high redundant, low complexity, highly scalable, autonomous radio astronomy can be realized.

2.2.3. SPACE ROBOTICS

Robots in space are expanding the horizons of exploration beyond the reach of human access. Though humans in space provide operational flexibility and intelligence, human space missions are long-term, expensive, and highly risky. Humans need extra care against harsh space conditions such as radiation, extreme temperatures, gravity, and pressure. While humans need consumables (oxygen, food, and water) to survive, robots can be powered by the available energy from their surroundings: light energy from the nearest star, wind, and the magnetic fields of host planets, etc. Unlike humans, they do not require to be in deep sleep during space travel, no psychological issues have to be handled and can work without taking a break. Space robots are advantageous for space exploration in many ways: they can collect fine samples in space, can work towards in-space assembly and in-space maintenance, as human assistants, mining, satellite deployments, refuelling, and orbit maintenance, constructions, repairing, re/de-orbiting, etc. Since the previous decade, robots have done a lot when it comes to space exploration. Rosetta comet lander, Pathfinder, Opportunity, and Curiosity Mars rovers have proven that robots work in space[59]. However, in some cases, a swarm of robots can perform collective space exploration with coordinated motion and pattern formation, completing the mission quickly. Future space missions involving swarm robots can perform multiple tasks simultaneously that are beyond the capabilities of a single one. Swarms provide improved performance, distribute sensing and action, and offer redundancy and fault tolerance. If one robot fails, the other robot in action can repair it autonomously.

One of the major challenges in space robotics is teleoperation where the robot is controlled by humans in space or on Earth. Communication latency is one of the major issues

that NASA is trying to handle. It takes between 5 - 15 minutes to send commands to a Mars rover and to receive telemetry back. The major delay is because of the distance from the Earth. Therefore, researchers are finding a way to make tactile teleoperation for upcoming Mars missions. The best solution for future robots in space is to make them autonomous, reliable, and self-repairable, and only receive new instructions or software upgrades from satellites if necessary. The future vision in the space industry is to send humanoid robots and advanced rovers to explore Mars, Mercury, asteroids, and Jupiter in the next ten years. Another big project from NASA is to establish a Moon base station constructed by coordinated humanoid robots [60]. The agency also plans to clean up the space junk (debris) that pose threat to ISS, other satellites, or future human flights. Recent developments at ISS include 3D printing tests, which if successful, robots not only can build small modularized satellite swarms on other planets but also repair other robots. If this technology was existing a few years back, Pathfinder and Opportunity missions to Mars would have been successful. Virtually, a robot can perform all the tasks that a human can do and much more, and also it is inexpensive and without life risks. Unlike humans, robots do not need years of training to perform tasks such as spacewalking and planetary explorations except that they should be tested rigorously before the missions. Robots, once designed, can be re-manufactured quickly and assigned on a mission immediately. They need not be brought back to Earth, unlike humans, thus making the mission twice affordable.

Space robots can come in many forms in the near future – they can be a bunch of self-deploying sensor networks such as humanoid robotics, manipulator arms, advanced rovers, plasma or rotor-based drones, crawlers, climbers, etc. Their capability will be far beyond the potential of humans: Space pixels can be mass programmed for specific tasks shot by a space robot on a distant celestial object to study weather conditions and do atmospheric measurements; humanoids can replace humans in many aspects, rovers can perform mining for samples; crawlers and climbers can perform tasks on uneven surfaces where rovers and humanoids cannot step on; drones can travel farther distances at less time performing aerial mapping and measurements; swimming robots can swim (in liquid hydrogen and other fluids on Saturn and other planets), and many more. Missions with such types of robots pose unique requirements and opportunities but also new challenges. Planet's gravity, planet-quakes, and unknown obstacles can be challenging for humanoids, unknown atmospheric perturbations can damage the drones, and unfavourable weather such as heavy winds can sweep away Space Pixels. With the rapid developments in space robotics, there is no doubt that the next interplanetary missions will first have a footprint of a humanoid on a distant planet than that of a human. Having all these said, there is a need for the development of reliable and low-latency communication to control these space robots from Earth; and the design of robot systems that are miniaturized, low-power, and easily deployable. The notion of SWANS is the first step towards realizing this.

2.3. CHALLENGES ON THE WAY TO BUILD SWANS

In the previous sections, we explained the path toward the use of SWANS in space assisting many new applications and missions. We discussed three ambitious themes, which offer new directions in the coming years. All of them invariably require building networks within space objects (e.g., satellites) to connect and coordinate multiple objects. The space-related

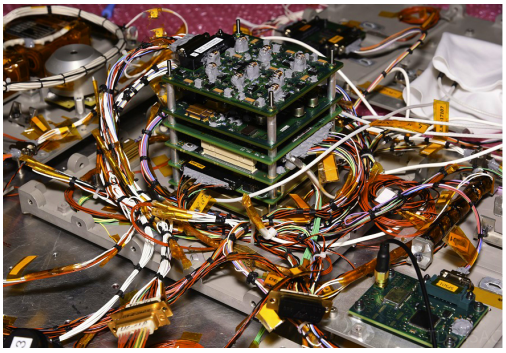

Figure 2.5: Harness in a nanosatellite of size 15 cm x 15 cm x 15 cm

scientific endeavours have umpteen possibilities and challenges. Future SWANS needs cutting-edge technology in the field of miniaturization, energy harvesting, and distributed sensor networks. We consolidate many important challenges below that are highly interesting to the sensor systems community and need to be addressed immediately to bring the vision of SWANS to reality, in turn, Space-IoT.

Miniaturization. As mentioned earlier, access to space is expensive and an enormous amount of resources (fuel, infrastructure, etc.) are required. Thus, making space objects as small as possible is a must. However, miniaturization also poses challenges – constraints on harvested energy through small solar panels, power generation, control, and regulation. Though a small amount of energy is sufficient to power up systems such as Space Pixels, we do not have any miniaturized energy harvesters to date to fit the entire power system in a tiny chip. With miniaturization, the hardware limitations such as radiation mitigation and thermal control, etc., become highly challenging.

MEMS technology for space. With the existing commercial infrastructure and MEMS technology, the development of systems such as Space Pixels is not possible because of their form factor and also the need for all the subsystems – power, processing, communication, etc., – to be embedded in a single chip.

Distributed systems. Future SWANS should have a tight coupling between the distributed sensor and actuator systems and distributed computing and communication. The idea is to build and assemble independent modules to work towards a common goal. Within a space object, such as nanosatellites, or amongst multiple such objects, many modules should be able to accomplish a huge mission by working in tandem independently but synchronously. Modules working well individually do not guarantee that the overall system is reliable, robust, and adaptive to the harsh environments in space.

Avoidance of cable harness using wireless. One of the ways to miniaturize the space object is to replace the cable harness with wireless systems. Indeed, cables account for 5-10% of the total weight in small satellites on average as shown in Figure 2.5. In bigger counterparts, this may even increase. Moreover, avoiding cables reduces the time for integration (building) of satellite time by 30%-40% while also avoiding errors and difficulties to reach every part of the space systems. It has been proved that wireless technologies such as BLE

and ZigBee work in space, yet a complete satellite has not been built using wireless communications. This is an area that needs thorough exploration. A major roadblock here is the reliability of wireless links. With wireless coming into the picture, challenging problems such as RF interference, and higher power consumption because of newly introduced wireless devices, should be addressed.

Handling a large amount of data. Any space mission these days requires high-resolution data. Data handling in large space systems involves maintenance and powering of the memory modules but the tough problem is to communicate the data back to Earth. In miniaturized space systems it is tedious to store data for a longer duration because of less space, lower power, and less protection from solar flares, etc. Until now, not much work has been done on exploring this challenge; with distributed systems and the requirement of higher resolutions, data management, and communication become an important bottleneck.

Synchronization. One of the major requirements in swarm-based radio astronomy is synchronization between individual devices in SWANS. The easiest way to achieve synchronization in space is by utilizing Global Navigation Satellite System (GNSS) signals. Using GNSS, synchronization can be achieved in nano-seconds with the COTS components. However, in non-Earth orbits such as around the Moon, GNSS is not available, thus, clock synchronization is one of the major challenges if multiple modules or objects need to work in tandem. Further, some applications such as RI require multiple telescopes (antenna arrays) to be synchronized with respect to each other with high precision - as low as 25 femtoseconds. Typical COTS crystals cannot provide such accuracy and are also affected by clock drifts unless it is atomic.

Coordination. Orbit management is a key requirement for satellite constellations in Space-IoT. Here, the spatial separation between the satellites must be maintained so that certain application requirements are continuously fulfilled, for example, to achieve global coverage of environmental phenomena on the ground. Moreover, individual small satellites in a constellation must be accurately time-synchronized for inter-satellite communication when using time-triggered communication patterns [61]. Energy constraints have an adverse influence on achieving proper coordination among small satellites as inter-satellite communications consume additional power. Alongside, orbit management takes up extra resources for computing, localization, and attitude determination and control.

Spectrum management. In applications such as RI, individual telescopes should have a minimum RF bandwidth and should be possible to tune to a broad range of frequencies. This requires the use of Software Defined Radios (SDR). It is not the scarcity of spectrum that is driving us in this direction but building an *agile* distributed system requires such flexibility. For example, one of the nano-satellites needs to take on the role of another in its group in case of failure.

Software defined systems. Making the swarms agile and programmable as well as transformable requires flexibility in designing and executing software modules. For example, RI requires constellation formation in different geometry based on the application or mission. Thus, SWANS system can be a Software Defined Satellite (SDS) system combining many innovations and notions of software-defined systems.

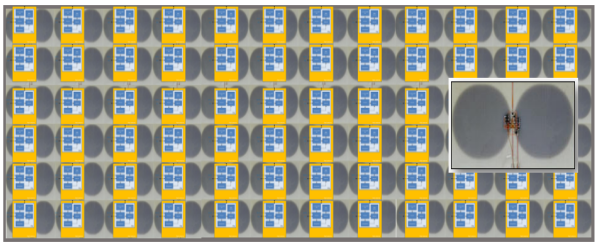

Figure 2.6: Multibeam antenna array on solar panel

Onboard control systems. The celestial objects around which the satellites are orbiting can have gravitational perturbations (gravity is not the same at all points). This makes the satellite change its orientation and altitude in orbit. Hence, SWANS need autonomous control algorithms. Especially, it is highly necessary for formation flying and high-speed inter-satellite communication systems. The embedded software needs to support such precision control algorithms.

Antenna arrays. An efficient communication requires variable antenna beams, resulting in multi-beam antenna arrays. For example, Space Pixels can also be placed on solar panels to form a multi-beam array that can be digitally controlled as shown in Fig 2.6. Controlling and operating such antenna array systems require proper coordination with different modules. For example, a space object moving at a speed of 7.8 km/s (at 500 km altitude) requires sophisticated control systems and actuators to coordinate with antenna array drivers to beam signals to the ground stations. Such issues have not been explored for pico and femtosatellites hitherto.

Machine learning to AI. In the case of robotics, developments in machine learning, distributed sensing, AI (especially for humanoids) are necessary to coordinate, repair systems, and adapt to unknown conditions on distant planets. For instance, swimming robots should be able to come out of a liquid environment when the temperature falls and when liquid starts solidifying; humanoids should be aware of the geometric ambiguities of the planet when they walk. They also need to be tactile in the case of robotic manipulators (robotic arms controlled by humans from space stations orbiting distant planets, moons, etc.).

Debris management. Space debris is a growing concern for the space community due to the increasing number of satellites and space missions, which contribute to the accumulation of debris around Earth. Space debris is not only a threat to operational satellites because of collisions but also to space stations such as International Space Station where there is human presence. Hence, satellites need to be designed keeping debris reduction in mind, avoiding collisions, and controlled reentry. While big satellites have reentry mechanisms such as a propulsion system, a similar design is challenging in small satellites such as pico and femtosatellites.

These challenges are interconnected and it is not straightforward to perform a trade-off between them, especially when so many constraints overlap. Sacrificing one requirement for the other is not an option as it may violate the concept of small satellites – miniaturized, low-power, low-cost, as defined by NASA [62].

2.4. CONCLUSIONS

The future of Space-IoT has the potential to be endless. Commercial interests show that there is a race for Space-IoT, and many companies are promising a constellation of hundreds of satellites in LEO to connect the unconnected. Space-IoT is a hot research topic in the satellite industry, and pioneering breakthroughs in technical innovations are essential to bringing Space-IoT into reality. In this chapter, we traced the new horizons for innovations in space-embedded systems in the near future. We presented our vision on many innovations that are expected in space technologies in the coming years, harnessing the developments in Space-IoT. We envisaged that wireless sensor-actuator networks will take over space systems in a big way and fulfill the insight of Space-IoT. We provided examples of innovative applications showcasing our visions for the future, which will have a significant impact on science and technology. We also listed some important challenges concerning miniaturization, resource optimization, embedded software, algorithms, wireless communications, and networking that are faced in the journey en route to realizing SWANS. Materializing SWANS is the first step towards accomplishing Space-IoT comprehensively.

In the forthcoming chapters, we present our substantial contributions, demonstrating how the challenges portrayed in Section 1.4 can be addressed in small satellites. We predominantly consider three sub-systems of a satellite communication system, positioning system, and health monitoring unit, to exemplify our contribution.

3

DEMODULATION OF BANDPASS SAMPLED NOISY FSK SIGNALS FOR SPACE-IOT

While the state-of-the-art terrestrial IoT nodes perform satisfactorily in terms of reliable communication, most of them are designed for low-power and short-range applications. One way to achieve reliable direct communication between a satellite and sensor nodes is to transmit data at high power or employ large high-gain antennas at either end. However, this would jeopardize the existing low-energy and miniaturization requirements both on IoT nodes and small satellites. Replacing large antennas with smaller ones will decrease the reception/transmission gain, resulting in a low Signal to Noise Ratio (SNR). Additionally, the RF noise level is much higher on Earth than in space, thus degrading the Carrier to Noise Ratio (CNR) and/or SNR. This can seriously affect the communication reliability in the network as signals with SNRs less than the threshold specified by the RF chip manufacturers are not decoded. Similarly, small satellites when launched in constellations come with many constraints in terms of cost, mass, and power, yet, they need to meet the demands such as high-reliability and high-speed inter-satellite & earth-satellite communications [63]. This calls for reliable wireless communication schemes from the perspective of Space-IoT.

There are many ways to ensure the successful reception of messages in satellite–sensor node communication for data transfers over hundreds of kilometres. The major ones are (i) increasing the RF transmission power on both sensor nodes and satellites. However, this is not energy-efficient, (ii) using large antennas with higher gain on satellites and the sensor nodes. This is not feasible as it opposes the goal of miniaturization, (iii) adapt/re-design low-power, long-range communication techniques, such as LoRa, to make them energy-efficient, (iv) employ existing modulation techniques, such as Amplitude Shift Keying (ASK), Frequency Shift Keying (ASK) and Phase Shift Keying (PSK), and improve them at a fundamental level to successfully decode the signals at low Signal to Noise Ratios (SNR). Thus,

there will be no need to increase the transmission power.

In this work, we choose (iv), and engage FSK as an example modulation technique for communication between a satellite and a sensor node. We present a design of an energy-efficient FSK decoder called *Teager Energy Decoder (TED)* that works even in the presence of Doppler and noise. Further, TED performs better than COTS receivers and decodes the FSK signal when the SNR is as low as 1 dB. This feature is vital for several applications in Space-IoT, where the received signal strength is low due to the need for low-power, long-distance communication.

3.1. MOTIVATION AND CONTRIBUTION

In this section, first, we motivate this work, followed by our contributions.

Motivation. Although all sub-systems of a satellite are tested thoroughly before launch, there is still a large scope for them to fail after deployment. Indeed, this work was necessitated because of a *crisis*. Two nanosatellites launched in 2017 developed stabilization and orientation issues leading to intermittent telemetry. Further, the received signals were noisy and Doppler shifted. Since the satellites were not properly stabilized, they were sending intermittent data because of the non-availability of continuous power and/or antenna orientation. The satellites were equipped with ON Semiconductor's AX5043 transmitters for transmitting signals down to the Earth with FSK as the modulation scheme. To maintain compatibility with the onboard transmitter, the same AX5043 model transceivers were used in the designated ground stations (we call sensor nodes in our context). Because of the above issues, the telemetry signals were not received by the ground station transceivers due to SNR being lower than the required threshold mentioned in the manufacturer's datasheet.

During this crisis, a few amateur radio enthusiasts around the globe were requested to help. The idea was to gather information regarding the health parameters of the satellites and command the satellite to stabilize. When some amateur radio enthusiasts could collect the received signals, they were bandpass sampled to share the information over the Internet easily. The recording rate of the signal was lowered to reduce the storage space (5 GB for 1 minute recording). If the signal is stored at a lower sampling rate, i.e., bandpass sampled, a great deal of information may not be available for Doppler correction and noise minimization while decoding. The challenge was to demodulate and decode the information from the bandpass sampled signals. As the existing FSK methods did not work effectively, we had to design a new technique to demodulate the signals.

Such low CNR/SNR scenarios can occur in Space-IoT frequently due to low-power satellite-sensor node transmissions, disorientation of antenna, and heavy RF noise in crowded areas such as cities.

Why FSK? FSK is one of the most used modulation techniques used in satellite communication. It is well known that the FSK demodulation can be performed in two ways - *coherent detection* and *non-coherent detection* [64]. Herein, our decoding algorithm employs a non-coherent demodulation technique. While coherent detection is performed at a cost, the non-coherent scheme is exempted from carrier synchronizers and phase detection circuitry. However, the non-coherent type suffers from performance degradation compared to

coherent type schemes. Further, FSK is easy to implement, and more resilient to errors and interference than Amplitude Shift Keying (ASK); it is highly tolerant to channel non-linearity and power-efficient. The demodulation can also be performed using simple hardware in a non-coherent way. While digital modulation schemes such as ASK and Phase Shift Keying (PSK) are independent of frequency shifts, FSK is potentially affected by time-varying frequency offsets. In the case of FSK-based satellite communication, the high orbital velocities (around 7.8 km/s in Low Earth Orbits) and relative motion of satellites with respect to the sensor node on earth cause significant *Doppler effect*, influencing the performance of communication systems [65]. This is one of the main motivations to consider FSK as the modulation scheme in this work, where an additional factor must be considered during decoding, i.e., Doppler shift. Additionally, a small error in FSK demodulation such as a bit reversal may lead to the rejection of an entire data packet in satellite data link protocols such as Amateur X.25 (AX.25) and High-Level Data Link Control (HDLC) [66].

A new technique: In this work, we present a new reliable, energy-efficient algorithm to decode signals resulting from direct communication between sensor nodes/gateways and satellites. We propose a scheme called Teager Energy based Decoding (**TED**) to demodulate bandpass sampled FSK signals that are influenced by Doppler shift, and low SNR. TED can decode FSK-modulated signals even when their SNR is as low as 0 dB. In our scheme, the raw signal is filtered to attenuate lower frequencies of the received FSK signal to minimize the effect of Doppler in a non-coherent way. Later, we employ the Teager Energy Operator (TEO) for demodulating the filtered FSK signals. Our proposed solution addresses all the challenges mentioned above in decoding an FSK signal. In our approach, to keep the algorithm simple, we do not compensate for the Doppler shift in the raw telemetry signal; however, we live with it while demodulating the FSK signals in real-time. Being aware of Doppler shifts in received signals in the wild is a difficult problem, which TED solves easily through signal detection. Indeed, this work is expected to help in the proliferation of Space-IoT applications, at least connecting nodes in remote/harsh environments to the IoT platforms via satellite links. In the sequel, we enlist our contributions.

Contributions. While addressing the crisis mentioned above, we built a complete receiver chain in the software and tested it.

1. We propose a novel, non-coherent approach to recover data from the bandpass sampled noisy FSK signal, influenced by Doppler shift. We detect the continuous or non-continuous FSK signal in IQ (.wav) file and then decode it.

2. We employ the Teager energy operator to suppress one of the symbol frequencies while enhancing the SNR of the other. To the best of our knowledge, we are the first to address the low SNR-based communication issues in the context of Space-IoT.

3. We have provided an end-to-end software-based receiver chain that can detect the FSK signals with low SNRs, boost the SNR of such signals, and decode them successfully.

4. The proposed TED algorithm can be applied to demodulate FSK signals, modulated at

any baud rate, from any satellite or sensor node demodulation. Hence, it can be easily employed in any "new or existing" sensor nodes, gateways, and satellites to decode the data in real-time. TED algorithm could be ported on any hardware needing only the RF front-end and a computation platform.

5. We demonstrate the performance of TED on real-world FSK-modulated signals transmitted from satellites.

Challenges. Though the challenges in the existing satellite communication technology are explored well in the literature, the concept of Space-IoT adds new demands when direct communication between low-power sensor nodes and satellites is considered. Due to the large distance separation and movement of satellites (around 7.8 km/s), several existing and new challenges need to be addressed. In Chapter 1, we listed the primary challenges related to communication in Space-IoT in brief. This section comprehensively explains the concerns in achieving communication between the terrestrial sensor nodes and the satellites:

1. Unlike techniques such as ASK and PSK, FSK is prone to *Doppler* effects resulting from the high orbiting speeds of Low Earth Orbit (LEO) satellites. The magnitude of the Doppler shift varies over time due to the orbital dynamics and the uneven curvature of Earth, thus making the demodulation of FSK signals more challenging. Even though the Doppler shift can be theoretically modelled for specific satellite communication, usually empirical data do not conform to the derived expressions due to the influence of anomalies in satellite orientation, movements, etc.

2. Bandpass signals with high baud rates are more prone to bit reversals and shifts on their way from satellite to the sensor nodes on Earth and vice versa.

3. Compensating Doppler shift during signal acquisition, before decoding FSK signals, is a well-known technique adapted in satellites and SDR-based satellite ground stations. However, Doppler correction on nanosatellites for each 'sensor node' is complicated and unscalable. Further, each sensor node on Earth should be aware of the orbit and position of the satellite at the time of communication to compensate for the Doppler shift before demodulation. Regular updating of orbital information to a low-power sensor node is arduous and may not be feasible. Thus, a Doppler-correction agnostic approach is required.

4. Miniaturized satellites generally have low gain antennas, and they transmit signals at low-power (around 1,W) [67]. Furthermore, signal degradation in the ionosphere and the channel noise lowers the SNR, thus making the decoding process tedious.

5. The transmitted signal can undergo phase changes while travelling through the ionosphere, which degrades the performance of demodulation. This may affect coherent-based FSK decoding schemes.

6. Though the antenna orientation on the satellite can be changed (unlike that of the sensor node/gateway) and be omnidirectional, it cannot be pointed to a particular sensor node on Earth when thousands of sensor nodes/gateways are distributed over

miles and communicate with the satellite at the same time. Furthermore, the polarization of the incoming signal may not be exactly matched with that of the receiving antenna. These issues significantly degrade the CNR and/or SNR, thus jeopardizing successful decoding.

7. The problem of low SNR is acute when the satellite and its antenna are tumbling, which is typical in satellites without attitude control systems.

8. The antenna on the satellite receives signals from thousands of low-power sensor nodes/gateways simultaneously. This may result in weak received signal strength. Additionally, simultaneous transmissions from the nodes may create interference at the satellite antenna, thus degrading the signal further, resulting in low CNR/SNR.

9. Particularly in this work, since non-standard amateur receivers were used, the recording rate of the signal was lower to reduce the storage space. If the signal is stored at a lower sampling rate, i.e., bandpass sampled, much information may not be available for Doppler correction and noise suppression.

3.2. THE EFFECT OF SNR AND DOPPLER IN SATELLITE COMMUNICATIONS

Before we present our system model and the proposed decoding technique, we discuss the impact of SNR and Doppler shift in satellite communication.

3.2.1. EFFECT OF SNR

We explain the influence of SNR in satellite–sensor node communication with an example. Let us consider a satellite in Low Earth Orbit (LEO) at 500 km altitude, communicating with a single sensor node on Earth. We choose Texas Instruments (TI) CC1310 transceiver on the sensor node, one of the widely used transceivers in IoT modules. We fix the communication frequency to 435 MHz, one of the Federal Communications Commission (FCC) allocated bands for satellite communications. This is also a reasonable choice of frequency considering the antenna length on the sensor node, and its low-power, long-range communication requirements. The signal from the satellite to the sensor node is FSK modulated with a frequency separation of 5 kHz. The baud rate is set to 625 bps, the lowest possible in CC1310. Assuming a Noise Figure (NF) of 0 dB and the lowest available receiver sensitivity (S) of -124 dBm for a bit error rate (BER) of 10^{-2}, we set the receiver bandwidth (RB) to 40 kHz to accommodate the Doppler shift. If the satellite is transmitting the signal (with any modulation technique such as FSK, PSK, ASK) at 1 W using 5 dBi gain antenna, which is the most common in small satellites, then the required SNR on the receiver (sensor node) just to detect the signal is given by,

$$\text{SNR(dB)} = \text{S} + 174\ \text{(dBm)} - 10\log(\text{RB}) - \text{NF}. \tag{3.1}$$

Substituting the parameters in (3.1) using CC1310's datasheet, we get SNR = 6 dB, which means, the signal power should be four times higher than the noise power for successful decoding in the best case if CC1310 is used.

To calculate the link budget, we set the gain of the antenna on the sensor node to be 2 dBi. Using Friis' equation, we get 4.7 dB link margin for the SNR of 6 dB when the satellite is straight above the sensor node, i.e., at 500 km (the elevation angle is 90°). In this case, CC1310 may decode the data successfully. However, as the distance between the satellite and sensor node increases (when the elevation angle is not 90°), the link budget decreases and becomes negative. For instance, when the elevation angle is around 45°, the link budget reduces to -0.8dB. This means that the sensor node will not be able to decode the data. In this case, even if the required SNR can be reduced to (say) 1.2 dB, then we get a link budget of 4 dB. Hence, the decoding may not be possible with the COTS transceivers such as CC1310 because of the SNR threshold. Moreover, for a fixed link budget, the CNR and/or SNR may vary significantly due to RF noise on the ground (acutely in cities), signal absorption in different atmospheric layers, and other RF interference.

3.2.2. EFFECT OF DOPPLER SHIFT

The Doppler effect is the change in the frequency of transmitted waves because of the relative speed between a satellite and a sensor node on Earth. For a satellite, the difference in frequency $\Delta f(t)$ between the observed frequency f and emitted frequency f_o is given by,

$$\Delta f(t) = f - f_0 = \frac{\overrightarrow{v_r(t)}}{c} f_0, \tag{3.2}$$

where c is the velocity of the electromagnetic wave in the medium, and $v_r(t)$ is the velocity of the satellite relative to the sensor node on Earth [68]. As the satellite sweeps in its orbit, the distance between the stationary observer on Earth and the satellite varies. This changes the viewing angle of the observer, which is called elevation. Therefore, the velocity of the satellite as observed from the sensor node location changes with the elevation angle. $v_r(t)$, also called range rate, is the first-order derivative of slant range r of the satellite that can be predicted from Two Line Elements (TLE) of the satellite [65]. TLE is a file containing the orbital information of a satellite using which its location in space at any instant can be estimated. The slant range is the line of sight distance between the satellite and a sensor node/gateway on Earth.

The slant range of a satellite at an instance t in LEO can be calculated as,

$$r(t) = \sqrt{h(t)^2 + r_e^2 - 2h(t)r_e \cos(\lambda(t) - \theta(t))}, \tag{3.3}$$

where $\lambda(t) = \arccos\left(\frac{r_e \cos\theta(t)}{h(t)}\right)$, with $h(t)$ being the altitude of the satellite that varies in case of non-circular orbits and also because of uneven curvature of Earth; r_e is the radius of Earth, and $\theta(t)$ is the elevation angle. For more details on calculating range rate, elevation, and Doppler shift for any satellite, we refer the readers to [65]. From (3.2), it is evident that the magnitude of the Doppler shift on 'M' frequencies of M-ary FSK is different. Moreover, $\Delta f(t)$ is positive if the satellite is approaching the receiver (sensor node) and is negative if it is receding.

Figure 3.1 shows the Doppler curve for a satellite in LEO, transmitting telemetry at 435.08 MHz, for a range of maximum elevation angles. When the elevation is maximum in a satellite pass, the distance between the observer and the satellite is shortest. In Figure 3.1, the

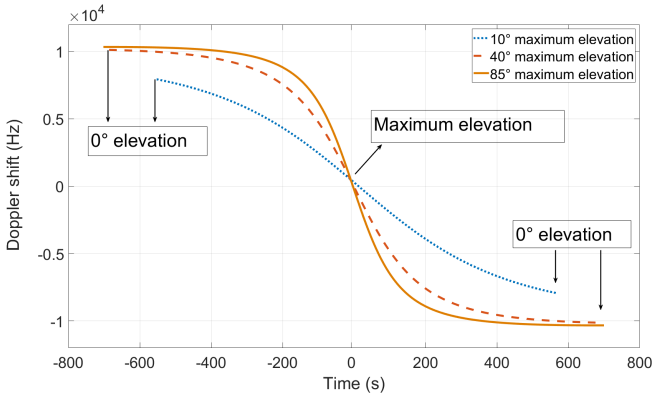

Figure 3.1: Doppler-Time curve for a different satellite-passes at a range of maximum elevation

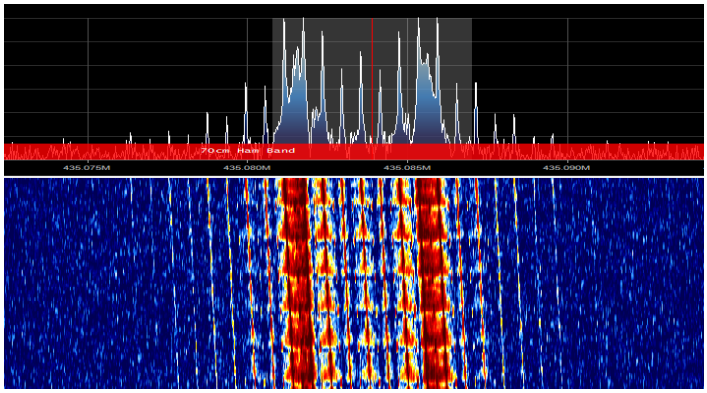

Figure 3.2: Telemetry reception using the software SDR#

zeroth second on the x-axis indicates the time at which the maximum elevation is observed – Time of Closest Approach (TCA) in different passes. We observe in the plot that the curve becomes more mirrored S-shaped when the maximum elevation is high, i.e., at 85° as shown in the figure. The magnitude of the Doppler shift varies with the elevation angle as a result of the change in the slant range. We also notice in the plots that as the satellite approaches the ground station, the Doppler frequency decreases. When the elevation angle is at maximum for a particularly visible pass (i.e., at 0 s), the satellite is at the closest approach vis-à-vis the observer, and the observed frequency represents the actual operating frequency of the satellite. As the satellite recedes, the observed frequency starts decreasing again, causing $\Delta f(t)$ to be negative. It should be noted that the observed Doppler curve for any satellite may not coincide precisely with the analytical curve due to propagation anomalies [69].

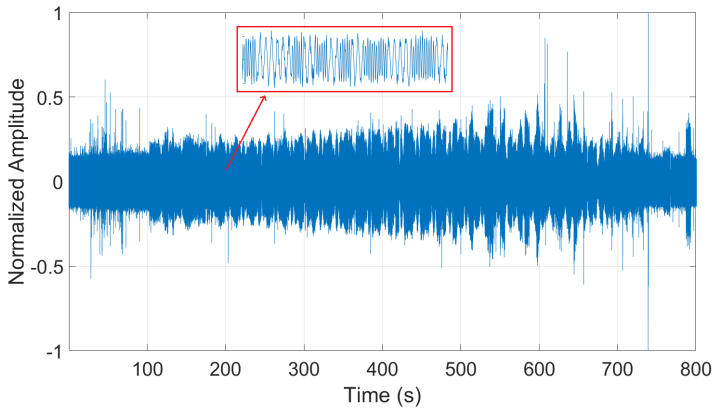

Figure 3.3: FSK coded signal from a satellite.

3.3. SYSTEM MODEL AND PROBLEM STATEMENT

In this section, we describe our system model and formulate the problem of decoding Doppler-influenced noisy FSK signals. In our work, we adopt a popular model where a binary FSK modulated signal $S(t)$ is represented as[70],

$$S(t) = \begin{cases} \sqrt{\frac{2E_b}{T_b}} cos(2\pi f_1 t + \phi_1(t)) \text{ for bit 0} \\ \sqrt{\frac{2E_b}{T_b}} cos(2\pi f_2 t + \phi_2(t)) \text{ for bit 1,} \end{cases} \tag{3.4}$$

where E_b is the energy per bit in $S(t)$, the symbol duration T_b, and f_1 and f_2 are the frequencies used to represent Space (bit 0) and Mark (bit 1) in FSK. $\phi_1(t)$ and $\phi_2(t)$ are the phase terms, which are arbitrary constants. $|f_1 - f_c| = |f_2 - f_c|$ forms the frequency deviation δf of FSK, centred at the carrier frequency f_c.

Processing high-frequency signals require high operating energy. Hence, our system model considers the signal to be bandpass sampled and down-converted to an intermediate frequency (IF) to ease the processing. This also aids the implementation of the proposed algorithm on low-power microcontrollers. However, the down-converted signal is also influenced by Doppler shift and noise (for example, from the oscillator). In our model, we neglect the phase component as we adopt a non-coherent approach for demodulation. Hence, we modify (3.4) as,

$$S(t) = \begin{cases} \sqrt{\frac{2E_b}{T_b}} cos(2\pi(f_1 t + \Delta f_1(t))) + r(t) \text{ for bit 0} \\ \sqrt{\frac{2E_b}{T_b}} cos(2\pi(f_2 t + \Delta f_2(t))) + r(t) \text{ for bit 1,} \end{cases} \tag{3.5}$$

where $\Delta f_1(t)$ and $\Delta f_2(t)$ are time-varying Doppler shifts, as represented by (3.2); $r(t)$ is a sample function of Random Process $R(t)$, which is Additive White Gaussian (AWG) with zero mean and power spectral density of $N_0/2$. To simplify the presentation, we consider the following example, using which we explain our demodulation algorithm in later sections.

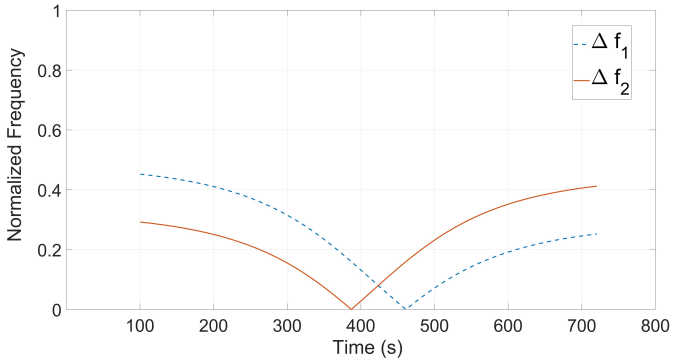

Figure 3.4: Expected Doppler shift in the telemetry signal

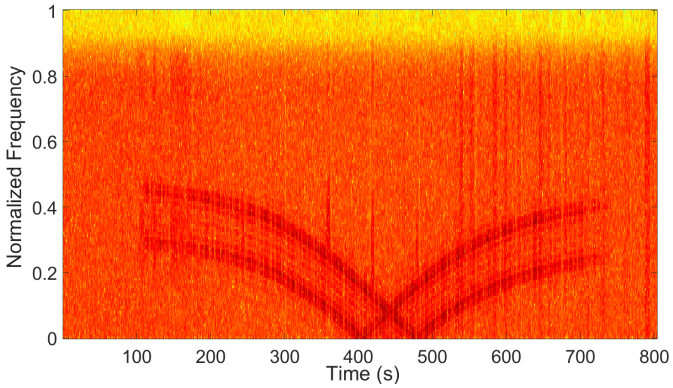

Figure 3.5: Spectrogram of the telemetry signal

Example 1. We consider a sample telemetry signal from one of our satellites, with transmission frequency $f_0 = 435.08$ MHz. The signal was recorded using a Software Defined Radio (SDR). For ease of understanding, we consider a recorded signal in the .wav file format that contains FSK signals. We chose the signal with decent SNR (>3 dB) in this example so that the FSK modulation in the signal is visible. However, in later sections, we explain how our algorithm also works with the signals when the SNR is very low. Figure 3.2 shows the online telemetry reception in SDR# software [71], indicating frequency shift when elevation was around 10°. The telemetry signal shown in Figure 3.3 was recorded with the sampling rate $f_s = 50$ kHz, and the particular pass had the maximum elevation of only 16°. The signal is FSK modulated with baseband bandwidth, $B = 1.2$ kHz, and frequency deviation, $\delta f = \pm 2$ kHz. The low-frequency component $f_1 = (435.08 - 0.002)$ MHz indicates bit 0 and high-frequency component $f_2 = (435.08 + 0.002)$ MHz indicates bit 1. The baud rate, b, of the signal is 1200. Further, we assume that there is no aliasing error.

Figure 3.4 shows the expected Doppler shift in the signal, calculated using (3.2). The spectrogram of the telemetry signal, displaying Doppler-influenced Mark and Space frequencies of FSK is shown in Figure 3.5. We assume the AWGN channel. Note that the negative frequencies are folded to the positive side in the spectrogram as the values are normalized. For a better comparison, the same has been followed in Figure 3.4. The y-axis is normalized with respect to $F_s/2 = 25$ kHz in both plots. The duration of the recording is 800 s, where 0 s and 800 s correspond to elevation $-1°$, and 455 s corresponds to TCA of 16°. We also observe in Figure 3.5 that the telemetry is not continuous but intermittent. This was due to the power fluctuations and/or frequent changes in the orientation of the satellite.

With this example, our objective is now clear – to demodulate the signal in real-time and finally get the binary data. Further, in the process, we address two supplementary objectives (i) how to make the decoding process energy efficient; and (ii) how to generalize the complete process so that it could be adopted in Space-IoT devices.

It should be noted that the negative frequencies (frequencies below center frequency) that arise due to the Doppler shift can be avoided by providing an offset to the center frequency during signal acquisition. For instance, if the center frequency is 435 MHz, and the Doppler shift range is ± 5 kHz (i.e., 434.995 kHz to 435.005 kHz), then adding an offset >- 5 kHz to the center frequency during signal acquisition sets the entire Doppler frequency to be positive. However, in our algorithm, we consider the worst-case scenario, wherein we do not provide offset to the Doppler frequency.

3.4. FSK SIGNAL DETECTION AND DECODING

In this section, we explain our novel algorithm to demodulate FSK signals that are influenced by the Doppler shift. The approach consists of two steps: *Signal detection* – to detect the FSK signal in the telemetry, and *Signal decoding* – to demodulate the FSK signal once the FSK signal is identified. We first explain the procedure for signal detection, followed by signal decoding.

3.4.1. SIGNAL DETECTION

Before we proceed with demodulation, it is important to identify the starting position of the FSK signal that corresponds to the satellite telemetry. The reasons are as follows.

1. The signal from the satellite may not be present at the beginning of the recording, like in the sample telemetry signal from Example 1;

2. The satellite communication system may be designed to send signals at specific intervals to save power (which is usually the case in small satellites);

3. The telemetry may be discontinuous due to the tumbling of satellites or other problems;

4. In our case, we had fewer samples to guess the envelope of the Doppler and also use any coherent detector.

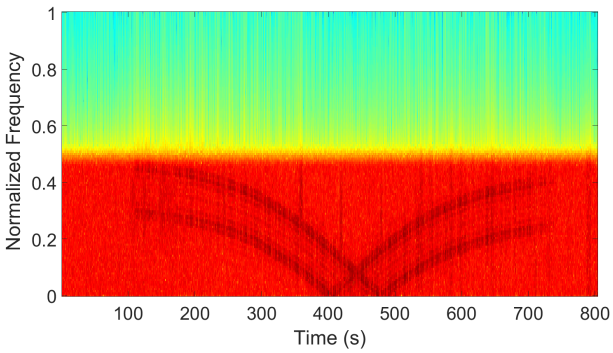

Figure 3.6: Spectrogram after the signal is processed with low pass filter

As we search for the FSK modulated signals before decoding in our scheme, the time consumed for demodulation is decreased. Especially, this is notable when the telemetry is discontinuous. Thus, the signal detection performance is improved.

The first step towards signal selection is pre-processing the raw signal to filter the noise as much as possible. This helps in minimizing decoding errors such as false detection. The next step is to identify the FSK-modulated signal in the telemetry. The final step is selecting small portions/windows of the signal for demodulation and feeding it to the signal decoding algorithm. Thus, the overall signal detection is done in three steps which we explain in detail:

A. FILTERING

The bandwidth (BW) of an FSK-modulated signal is not constant in all the telemetry signals. It varies for every pass of the satellite depending on the maximum elevation, as shown in Figure 3.1. If $(|\Delta f_1|)_{\max}$ and $(|\Delta f_2|)_{\max}$ are the expected maximum Doppler shifts for a particular maximum elevation θ_{max}, then the bandwidth of FSK modulated signal in that specific pass is given by,

$$\mathrm{BW} = 2(B+\delta f) + 2\Big(\max\big((|\Delta f_1|)_{\max}, (|\Delta f_2|)_{\max}\big)\Big). \tag{3.6}$$

Frequencies outside this bandwidth can be filtered by employing a low pass filter with cut-off frequency $BW/2$ as they do not contain FSK modulated signal. Considering the Example 1, we get, BW = 2(1200 + 2000) + 2 x 8800 = 24 kHz.

Applying a low-pass filter to the signal with cut-off frequency BW/2 = 12 kHz, we get the resultant filtered signal, whose spectrogram is shown in Figure 3.6. The order of the filter was empirically chosen as 40.

B. SIGNAL IDENTIFICATION

After filtering the raw signal, we now identify the starting location of the FSK signal. We have discussed earlier that the raw telemetry signal shows variation in amplitude (Received Signal Strength Indication) over time as the slant range changes. Hence, our approach

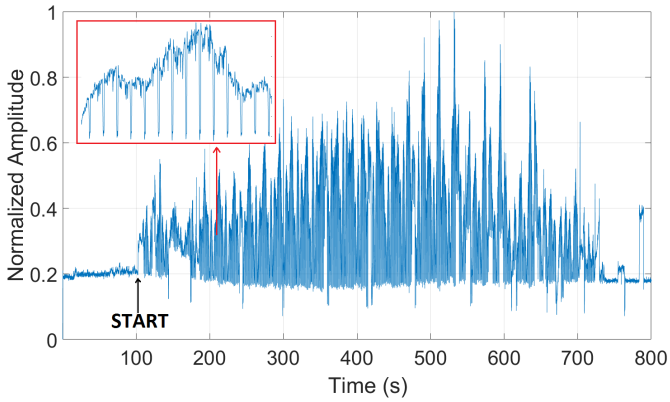

Figure 3.7: Envelope of the signal using spectrogram.

toward signal identification is modelled in three dimensions – amplitude, frequency, and time. As the first step in signal identification, we obtain the spectrogram of the signal. The spectrogram provides the energy content (amplitude) of a signal expressed as a function of frequency and time. In other words, a spectrogram is nothing but the windowed discrete-time Fast Fourier Transform (FFT) of a signal using a sliding window and represented in the form of a matrix containing complex values. The size of the spectrogram matrix depends on the selected length of FFT (L_{FFT}). The vertical axis in Figure 3.5 represents frequency, the horizontal axis denotes time, and the amplitude over time is indicated by colour scale (the darker the grayscale, the higher the amplitude).

The spectrogram of the signal results in $p \times q$ matrix where p is $L_{FFT}/2$, indicating normalized positive frequencies with respect to $F_s/2$, and q is the number of time segments in the spectrum. The $p \times q$ values are added column-wise to obtain a row-matrix having $1 \times q$ values, representing the signal's energy envelope at corresponding time segments. The presence of envelopes in the resultant signal indicates the FSK, whose rising edges can be identified. A continuous envelope represents the FSK, and discontinuity indicates the absence of the FSK signal.

We chose 256 FFT points and a non-overlapping window to obtain the spectrogram for the signal in Example 1. The values in the matrix are added column-wise to obtain a row matrix. A low-pass filter is used to smoothen the resultant signal, and the resultant waveform is shown in Figure 3.7. We chose the order of the filter to be 5 and cut-off frequency 1000 Hz, empirically. By setting a threshold of 0.25 (the noise floor is around 0.2) with respect to normalized amplitude, edge detection was performed to identify the beginning of the FSK modulated signal in the spectrogram. The corresponding timestamp in the raw telemetry signal indicates the starting of the FSK modulated signal from which a window is selected for further decoding.

C. WINDOW SELECTION

Our approach for decoding the signal does not compensate for the Doppler shift but works with the Doppler shift by minimizing its effect. To accomplish this, we adopt a matched filter-based decoding technique. If the signal's frequency is constant throughout the telemetry, then the coefficient of the matched filter can be chosen at once. However, this is not the case in satellite communication. Due to the Doppler shift, the frequency of the signal varies continuously. Hence, rather than considering the complete signal at once for decoding, we select windows/portions of FSK modulated signals one after the other, which are then fed into the decoding algorithm for further processing. We assume that the frequency of the signal is constant in these chunks.

The span of a window $\{t_i\,,\,t_j\}$ with $t_i < t_j$ depends on two factors:

1. *Bit width T_b of the signal:* The window length should be a multiple of T_b; else, the last bit with incomplete information will be neglected by the decoding algorithm.

2. *Slope of Doppler curve:* The magnitude of the Doppler shift is not constant all over the signal. As we observe in Figure 3.1, the Doppler effect is more when θ approaches θ_{max}, the maximum elevation. The matched filter will perform better if this change is as low as possible. Hence, $\{t_i\,,\,t_j\}$ for a telemetry signal is a function of the slope of the Doppler curve for a particular pass.

Using (3.2), the slope s of Doppler curve is given by

$$s_{ij} = \frac{f_0}{c}\frac{d}{dt}\left[\overrightarrow{v_r(t)}\right]_{t_i}^{t_j}, \tag{3.7}$$

which is always negative. The high magnitude of the slope indicates a higher Doppler shift. Hence,

$$\{t_i\,,\,t_j\} \propto |s_{ij}|^{-1}.$$

It should be noted that the Doppler cannot have slopes 0 and ∞, as zero slopes indicate the absence of Doppler and infinite slope indicates an abrupt change in transmission frequency when the satellite is at the same position. For the signal in Example 1, we empirically set $t_j - t_i = 1$ s when the slope is -0.017, 200 ms when the slope is -1, and 500 ms when the slope is -57. The intermittent values are approximated using interpolation. However, the relation between the slope of the Doppler curve and the window span can be generalized by fitting a curve. Hence, the window spans $\{t_i\,,\,t_j\}$ are chosen such that t_j - $t_i = kT_b$, where $k \in \{1,2,3...\}$ and it should also confine the relation with the slope.

After the first window from the raw signal is fed into the decoding algorithm, the selection of the subsequent windows depends on two cases which we explain using the Example 1. A chunk of the telemetry data is shown in Figure 3.8. Without loss of generality, let us assume that the recording starts at t_0, and the FSK modulated signal starts from t_1. At t_6, there is a break in the FSK signal and starts again at t_9. First, the starting position t_1 of the FSK signal in the telemetry is identified using the steps described in Section 3.4.1. By fixing s_t to -0.3, the windows $\{t_1\,,\,t_2\}$, $\{t_2+1\,,\,t_3\}$, ... ,$\{t_5+1\,,\,t_7\}$ are calculated using (3.7). Since the FSK signal breaks at t_6, t_8 is identified again using the steps described in Section 3.4.1.

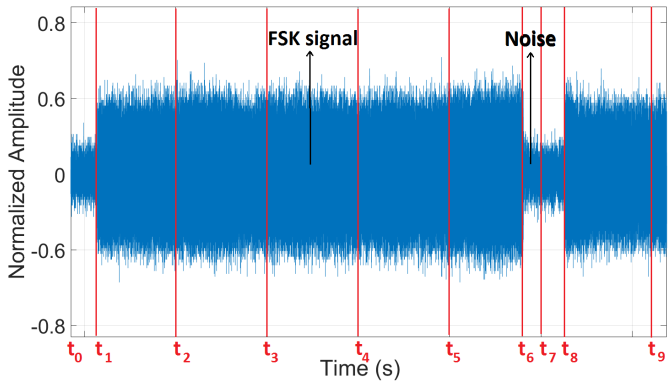

Figure 3.8: Window selection when FSK is continuous

Two cases affect the window span. They are as follows.
Case 1: If there is a continuation in FSK signal soon after t_j, then $t_j + 1$ is chosen as t_i for next window. Hence, $\{t_1\,,\, t_2\}$, $\{t_2 + 1\,,\, t_3\}$, ...,$\{t_5 + 1\,,\, t_7\}$ form the windows in this case.
Case 2: When there is a break in FSK signal, the subsequent window begins from the next starting position of the FSK signal. Therefore, $\{t_8\,,\, t_9\}$ forms the subsequent window after $\{t_5 + 1\,,\, t_7\}$ instead of starting from $t_7 + 1$ in this case.

Thus, the raw telemetry file that is low-pass filtered (as described in Section 3.4.1) is fed into a signal decoding algorithm in the form of small windows after detecting the FSK signal in it.

3.4.2. SIGNAL DECODING

We proceed to explain the decoding of the FSK modulated signal using non-coherent detection. The signal window obtained after FSK signal detection is passed through a matched filter to suppress the low-frequency component of FSK in the signal. Teager Energy Operator (TEO) [72] is operated on the resultant signal to distinguish between 0s and 1s in the signal. The overall decoding process is done in two steps, which we explain in detail below.

A. SUPPRESSION OF A FREQUENCY COMPONENT

The matched filter is a correlation-based filter where a known signal or a template is correlated with an unknown signal to detect the presence of a signal matching the template. In matched filtering, the template is a time-reversed and conjugated version of the signal that is convoluted with the same signal to suppress the unwanted part. The advantage of this type of filter is that the SNR of the signal is maximized in the presence of AWGN. Hence, using a matched filter in signal demodulation and decoding suits Space-IoT applications when SNR is low. The matched filter $h(n)$ is formulated as,

$$y(n) = \sum_{k=-\infty}^{\infty} h(n-k)x(n),$$

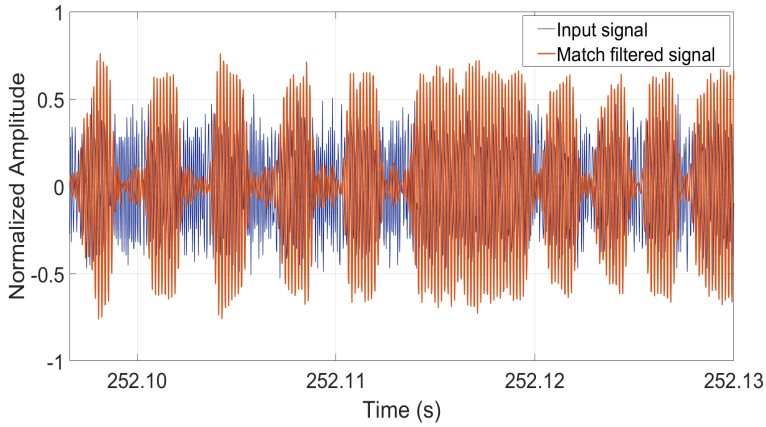

Figure 3.9: High-frequency signal suppressed as a response to matched filter

where $y(n)$ is the output signal, $x(n)$ is the input signal, and $n \in 0,1,2...$ The matched filter is best suited for demodulating noisy FSK signals as either low or high-frequency signals of the FSK can be considered as a template. Moreover, the probability of detection is high due to the increase in SNR. In an ideal case, the coefficient (template) of the matched filter remains the same throughout during convolution. However, this is not the case when the low and high frequencies of an FSK signal are influenced by the Doppler shifts. This is one of the reasons why we choose windows of the raw telemetry signal and update the filter coefficient for each chunk. Since the low-frequency component $f_1 + \Delta f_1(t)$ of FSK has more Doppler shift compared to the high-frequency component $f_2 + \Delta f_2(t)$, we try to suppress the low-frequency component using a matched filter.

As explained in Section 3.4.1, each window starts with FSK modulated signal. To search for the high-frequency component, we first take FFT of the signal over $t = \{((k-1)T_b) + 1\,,\, kT_b\}$, where $k = 0,1,2...$, and get the magnitude of the frequency. Next, we compare this magnitude between $((k-1)T_b)+1$ and kT_b until we get one greater than the other. Finally, we choose the co-efficient of matched filter to be the signal over duration $\{((k-1)T_b) + 1\,,\, \frac{(2k-1)T_b}{2}\}$, containing high-frequency component[1].

Figure 3.9 shows a portion of the FSK modulated signal where the low-frequency component is suppressed using a matched filter. It is also evident from the figure that the SNR of the matched signal is maximized. Note that if the suppression is not perceptible, the matched filter must be applied multiple times. The final step in the decoding process is to find the energy of the signal so that it can be decoded into bits by detecting zero-crossings.

It should be noted that TED executes the decoding process on the modulated signal mainly in the time domain. The most important problem for decoding FSK in the frequency domain with varying Doppler shifts is *finding the point of separation between carrier frequencies*. Most receivers achieve this by tracking the Doppler shifts. As we employ matched

[1] Choosing the span over $\{((k-1)T_b)+1\,,\, kT_b\}$ decreases the filter performance and also,$\{((k-1)T_b)+1\,,\, \frac{(2k-1)T_b}{2}\}$ is expected to be the mirror of $\{\frac{(2k-1)T_b}{2}+1\,,\, kT_b\}$.

filters in TED, the filter coefficients cannot be predefined to identify the point of separation if operated in the time domain.

B. INTERPRETING THE BITS

Since only high-frequency component of FSK is retained in the signal now, it can be treated as a single component signal. Hence, the instantaneous energy of the signal at different time intervals can be used to distinguish the signal into two levels – '1' wherever there is high-frequency component, and '0' for the rest of the signal.

Teager Energy Operator is one of the handy tools for analysing single component signals from the energy perspective. TEO for a discrete-time signal $x(n)$ is given by,

$$\psi[x(n)] = x^2(n) - x(n-1)x(n+1) \tag{3.8}$$

and in the continuous case,

$$\psi[x(t)] = \dot{x}^2(t) - x(t)\ddot{x}(t) \tag{3.9}$$

When (3.9) is applied to a continuous signal of type $x(t) = Acos(\omega t)$, the resultant signal will be of type,

$$\psi[x(t)] = A^2\omega^2 \sin^2(\omega t) + A^2\omega^2 \cos^2(\omega t) = A^2\omega^2, \tag{3.10}$$

where $\omega = 2\pi f$.

Hence, TEO is an amplitude and frequency-dependent operator because of which the amplitude of the part of the signal component suppressed by the matched filter is still reduced. This further increases the SNR of the signal. The analytical explanation of the combined effect of the matched filter and TEO in improving the SNR is as follows.

A binary FSK modulated signal $S(t)$, representing low and high-frequency components of FSK, respectively can be formulated as,

$$S(t) = \begin{cases} A_1 \cos\omega_1 t - \text{low-frequency component and} \\ A_2 \cos\omega_2 t - \text{high-frequency component,} \end{cases} \tag{3.11}$$

where A_1, A_2 are amplitudes of the signals, and $\omega_1 = 2\pi f_1$ and $\omega_2 = 2\pi f_2$. Also, $\omega_1 < \omega_2$. Let us choose the high-frequency component as a coefficient for the matched filter. Then the output of matched filtered signal $S'(t)$ contains the components,

$$S'(t) = \begin{cases} \frac{A_1}{j} \cos\omega_1 t - \text{low-frequency component and} \\ A_2 \cos\omega_2 t - \text{high-frequency component,} \end{cases} \tag{3.12}$$

where $j \in \Re$ and $j \geq 1$. Since the matched filter maximizes the SNR of the signal, the low-frequency signal of FSK along with noise is suppressed by j times using a matched filter. This is evident from Figure 3.9.

Further, when TEO is employed, the instantaneous energy of low and high-frequency components in the resultant signal becomes (using (3.10)),

$$\psi[S'(t)] = \begin{cases} \left(\frac{A_1}{j}\right)^2 \omega_1^2 - \text{low-frequency component and} \\ A_2^2\omega_2^2 \quad - \text{high-frequency component} \end{cases}$$

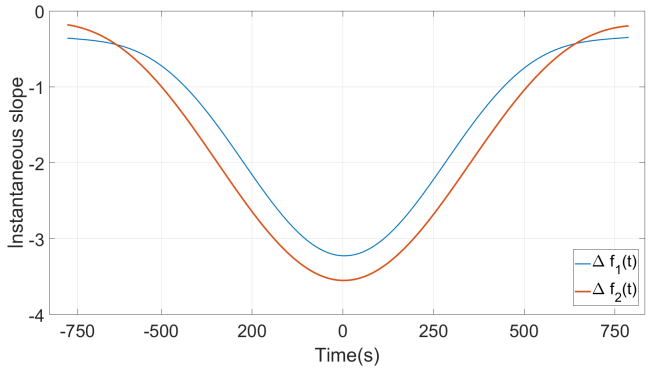

Figure 3.10: First order differential of Δf_1 and Δf_2

where the low-frequency component in the resultant signal is again suppressed by j times, and the energy (SNR) of the high-frequency signal is increased. Hence, with the combination of the matched filter and TEO, we suppress the signal's low-frequency component and noise.

Now, introducing the Doppler shift in (3.11), the FSK signal can be represented as,

$$S_D(t) = \begin{cases} A_1 \cos(\omega_1 t + 2\pi\Delta f_1(t)) - \text{low-frequency component and} \\ A_2 \cos(\omega_2 t + 2\pi\Delta f_2(t)) - \text{high-frequency component} \end{cases}$$

Applying TEO on this signal using (3.9), the resultant signal is,

$$\psi[S'_D(t)] = \begin{cases} A^2(\omega + 2\pi\Delta f_1\dot{(t)})^2 + A^2\pi\Delta f_1\ddot{(t)}\sin(2\omega t + 4\pi\Delta f_1(t)) \\ A^2(\omega + 2\pi\Delta f_2\dot{(t)})^2 + A^2\pi\Delta f_2\ddot{(t)}\sin(2\omega t + 4\pi\Delta f_2(t)). \end{cases} \tag{3.13}$$

The first-order differential of Δf_1 and Δf_2 is shown in Figure 3.10. In the plots, we observe that the high-frequency component Δf_2 has a higher slope than low-frequency component. Hence, Δf_2 tends towards zero Doppler shift faster than Δf_1. Further, from (3.13), it is evident that the output of TEO is dependent on the amplitude and frequency of the input signal. The amplitude of the low-frequency component is suppressed by the matched filter and further by TEO.

Now, applying (3.8) to the resultant signal obtained after employing the matched filter, we get an envelope of the matched filter output with retained frequency component as shown in Figure 3.11. An indication of high energy in the signal corresponds to the non-suppressed frequency component of FSK, which is $(f_2 + \Delta f_2(t))$. The zero-crossings of the envelope indicate a change in bits which can be used to represent the data in the binary form as shown in Figure 3.12. The zero-crossings occur approximately at integral multiples of T_b, and each bit must be of duration T_b. For instance, the decoded bits for the chunk of the signal shown in Figure 3.12 is "1100110011001100110011000000001001100 ...". It should be noted from (3.8) that TEO can work with just three samples at a time. Thus, our algorithm can dynamically adapt to varying noise levels and Doppler shifts effortlessly.

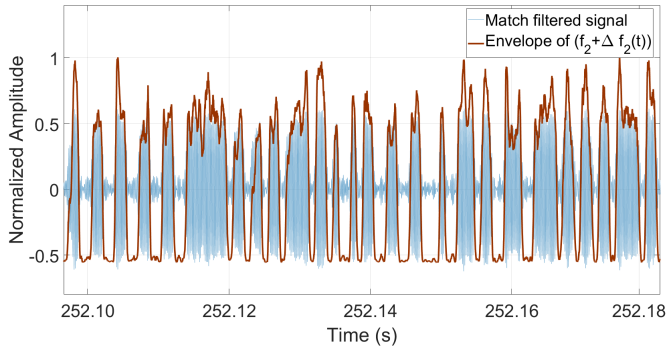

Figure 3.11: TEO employed on matched filtered signal

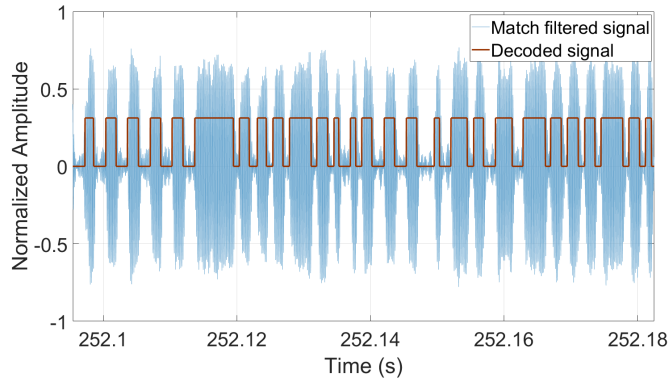

Figure 3.12: Decoded bits

We also observe in Figure 3.11 that the energy of the signal is negative when the high-frequency component of FSK is not present. Here, the negative energy corresponds to the low-frequency component. The negative energy in TEO is an awkward behaviour for an energy operator which can be best analysed at the extrema of the input signal, where the probability of such an event occurring is the highest [73]. These extrema are the high-frequency signal (whose SNR is increased by the matched filter) of FSK and noise (AWGN + low-frequency component) in the signal. We take advantage of this behaviour of TEO in our algorithm for zero-crossing detection to classify the bits.

As TED uses a matched filter and TEO, the computation complexity of TED is $\mathcal{O}(N^2)$. Additionally, TED does not require a local oscillator which is required by the current chipsets. The block representation of the procedure explained above is captured in Figure 3.13, which is referred to as Teager Energy Decoding (TED) algorithm.

3.4.3. PERFORMANCE ANALYSIS

We evaluate the performance of our algorithm using Bit Error Rate (BER). The average symbol error probability P_e for our matched filter based non-coherent, M-ary FSK modulation

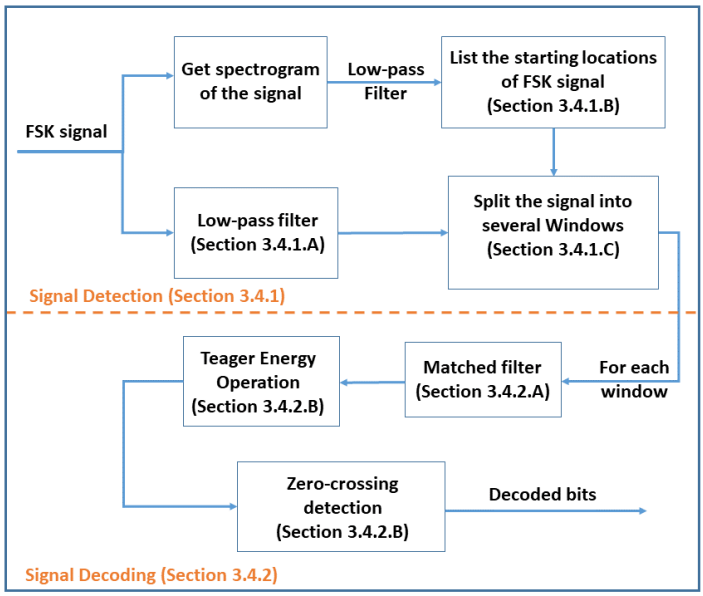

Figure 3.13: The proposed TED algorithm

is [64],

$$P_e = \sum_{i=1}^{M} \binom{M-1}{1} \frac{(-1)^{i+1}}{i+1} \exp\left[-\frac{iE_b|\cos(\mu)|\log_2 M}{N_0(i+1)}\right], \tag{3.14}$$

where $\mu = 2\pi\Delta f(t)$, $\Delta f(t)$ being time varying Doppler shift. For binary FSK, $M = 2$ and (3.14) reduces to,

$$P_e = \frac{1}{2}\exp\left(-\frac{E_b|\cos(\mu)|}{2N_0}\right) \tag{3.15}$$

For an M-ary FSK, the bit error probability P_b is given by,

$$P_b = \frac{M}{2M-2} P_e$$

Substituting $M = 2$, we get $P_b = P_e$ i.e., symbol error probability equal to bit error probability for binary FSK. Figure 3.14 shows the BER for TED algorithm for different values of E_b/No and Doppler shifts Δf. We observe in the plots that the BER changes as the Doppler shift changes. For a small increase in Doppler shift, for example, $\Delta f = 0, 1000$ and 3000, the BER is not affected much. However, a further increase in the Doppler shift affects the BER significantly.

3.5. EVALUATION

In this section, we present the results of the performance evaluation of TED. The experiments were done using multiple telemetry signals from two distressed satellites. We also

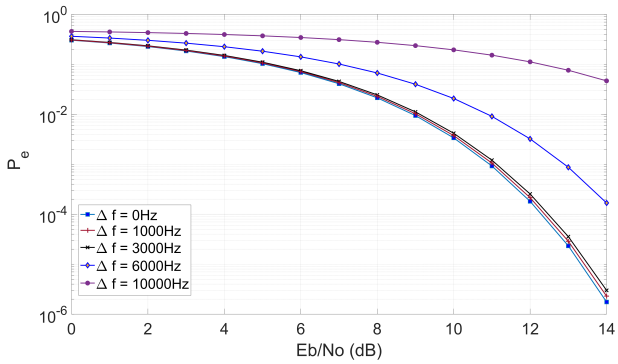

Figure 3.14: Bit Error Rate vs E_b/N_0 for different Δf

compare TED's performance with that of CC1310 and AX5043 transceivers. We choose these COTS transceivers because of their popularity, and usage in satellite communication systems and wireless sensor nodes. Here, we consider only one-way communication – i.e., from satellite to the sensor node, as the same can be implied the other way around. In all our experiments, we do not adopt any error correction techniques as we want to evaluate the performance of TED in the worst-case scenarios.

3.5.1. EVALUATION SETUP

We consider the telemetry signals from two satellites, orbiting in LEO at 505 km and 511 km altitude, respectively. Both the satellites were transmitting signals in amateur frequencies – 435.080 MHz and 437.095 MHz, respectively, at 1 W transmission power. The communication modulation scheme used was binary FSK, with a frequency deviation of $\delta f = \pm 2$ kHz. The baud rate was 1.2k. Both satellites used AX5043 transceivers onboard. The telemetry was sent continuously down to Earth with each data packet containing 930 bytes. Note that the system evaluation in uplink or downlink is equivalent in our case as Doppler and SNR problems can exist on both sides. Moreover, in the downlink, we can perform the evaluation thoroughly due to the extensive setup.

To extensively evaluate our algorithm, we developed a custom board mimicking sensor nodes, housing two COTS RF transceivers – CC1310 and AX5043. The developed board is shown in Figure 3.15 (antennas not shown). The decoding of data for the aforementioned FSK parameters is performed by both the transceiver chips by tweaking the example source codes provided by the manufacturers. In addition, the board was also equipped with NXP's LPC1768 ARM Cortex-M3 microcontroller to configure and control the transceivers.

We also use "HackRF One SDR" to receive raw bandpass sampled IF signal in MATLAB. Then we employ the TED algorithm to decode the data. The incoming RF signals on the SDR were recorded at 50 kHz. The main receiver antenna, having 2 dBi gain, is connected to both SDR and the sensor node board using a splitter. The overall experimental setup is shown in Figure 3.15.

To get the best performance from CC1310 and AX5043, transceivers, the Doppler compensation was done using NXP's LPC1768 ARM Cortex-M3 microcontroller on the sensor

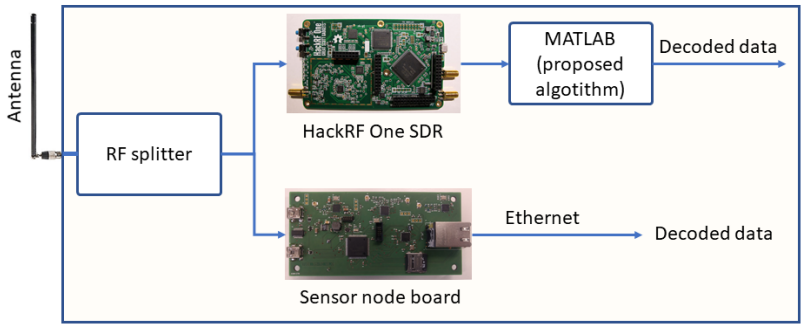

Figure 3.15: Experimental setup

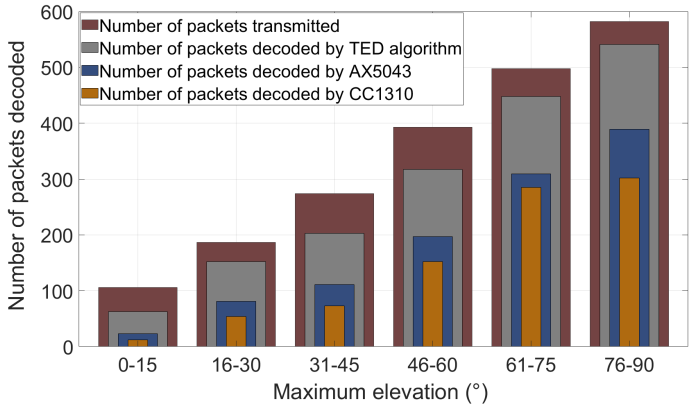

Figure 3.16: Number of packets decoded in different cases

board. This was achieved by tuning the transceivers' centre frequency using the satellites' TLE information provided by the space organizations. If this was not done, then the receiving bandwidth of both the transceivers had to be increased (up to 50 kHz), while the centre frequency was shifting because of the Doppler effect. However, Doppler compensation was not done in the case of SDR as the TED algorithm performs well even in the presence of Doppler.

The telemetry was decoded online simultaneously on MATLAB (using our algorithm) and on the board (emulating sensor node) using both the COTS transceivers. The obtained results in all three cases (SDR, CC1310, AX5043) were compared. The number of data packets decoded by the TED algorithm and sensor node for different elevations of the satellite passes is shown in Figure 3.16. For comparison, we consider the number of packets decoded successfully without bit error, averaged over a range of maximum elevation in every satellite pass. The data plotted in the figure was obtained from averaging over 50 telemetry signals containing more than 2000 data packets in total.

We observe from the results that the TED algorithm outsmarted the COTS transceivers in decoding for all the satellite passes. From the recorded data, we later observed that the SNR of the received signals varied approximately between -2 dB and 10 dB. Whenever the SNR was above the required threshold for CC1310 and AX5043, they decoded the signals successfully. However, the TED algorithm performed well even when the SNR was as low as 1 dB. As observed, the performance of AX5043 was better than CC1310. The reason was that the transmitter used on the satellite was also AX5043, thus providing the matching settings with the ground station receiver.

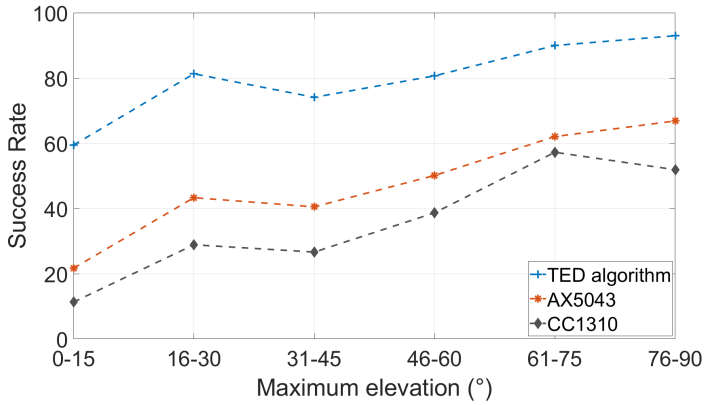

Figure 3.17: Success rates of decoding in different cases

To quantify the performance, we define **Success Rate** – the ratio of the total number of packets decoded without bit error and the total number of packets present in the telemetry. The Success Rate in all the cases – TED algorithm, CC1310, and AX5043 for different satellite passes are shown in Figure 3.17. It is evident from the figure that the TED algorithm had the Success Rate of 92.96% for maximum elevation in the range 76°-90°. While AX5043 capped at 66.8% for maximum elevation range 76°-90°, CC1310 had the maximum Success Rate of 57.23% for 61°-75° elevations.

To evaluate the complexity of TED and the feasibility of executing it on a low-power microcontroller, we ported TED onto Texas Instrument's Cortex M4 based MSP432 development board. The microcontroller operating frequency was set to 16 MHz, and the bandpass sampled raw telemetry signals from SDR were transferred to MSP432 over RS-232 using MATLAB. We observed a similar performance by TED on the microcontroller to that in MATLAB. This proves that TED can be employed on low-power embedded devices such as MSP432 for real-time decoding of signals. These results prove that our FSK demodulation solution substitute commercially available hardware receivers when system energy consumption and communication reliability are of concern.

3.5.2. COMPARISON WITH OTHER SDR BASED SOLUTIONS

Apart from the COTS transceivers, we also evaluate the performance of the TED algorithm with other SDR based open-source FSK demodulation techniques. We choose "demod" utility from cubehub[74] in combination with "multimon-ng" to decode Doppler compensated FSK signal [74]. We modified the utility to support our FSK parameters since it supports demodulation for only signals with the 9600 baud and 48000 sampling rate. Further, it does not take care of the Doppler shifts. Hence, we use one of the famous satellite Doppler compensation tools called "gpredict" to remove the frequency offsets before feeding the signal to demod utility. The implementation of the system is done using GNU Radio, and the block diagram of modules used is shown in Figure 3.18. For more details on the implementation of these utilities, we point the readers to [74] and [75]. The telemetry signal from

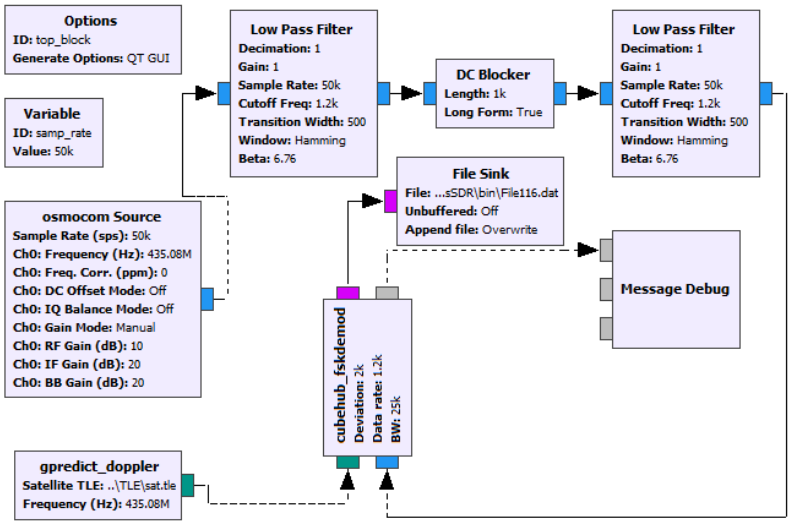

Figure 3.18: FSK demodulation using GNU radio

the SDR is passed through our proposed algorithm and the GNU Radio setup. The demodulation outcomes for different satellite passes with different bit errors in every data packet are shown in Figure 3.19. Different telemetry signals with varying SNR containing 2048 data packets in total are considered for the experiment. The figure shows that the TED algorithm demonstrated the Success Rate of around 85% against 54% of the GNU Radio setup when no bit error is allowed in the decoded packets. However, the Success Rates of both setups increased as the bit error count in a packet increased. For a maximum bit error count of 20 in 930 B packet, TED algorithm decoded 1910 packets, and the GNU radio setup decoded 1467 packets.

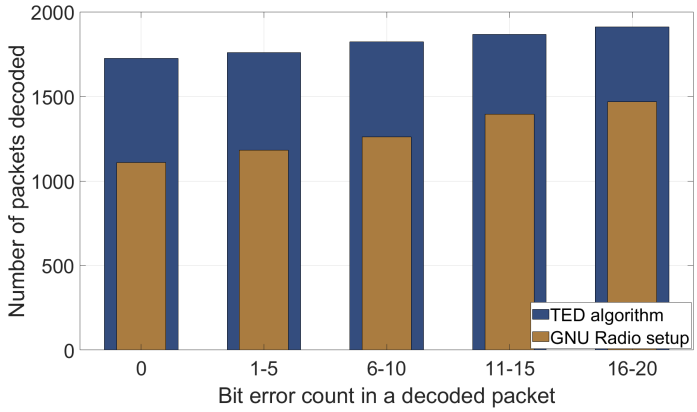

Figure 3.19: Number of packets decoded with bit errors

3.5.3. COMPARISON OF TED WITH A CONVENTIONAL DEMODULATION TECHNIQUE

We compared the performance of TED with a conventional FSK demodulation technique. We simulated binary FSK signals in MATLAB with the carrier frequency 435 MHz and frequency deviation of 8 kHz. The data rate was set to 1.2 kbps, and 1200 subsequent bits formed a packet. These FSK signals were passed through a channel with additive white Gaussian noise having varying SNRs between 0 dB and 6 dB. For every SNR consideration, we generated 100 FSK signals to find statistically stable values. Further, the Doppler shift was introduced to these noisy FSK signals to simulate the real-time scenario. These FSK signals were sampled at 50 kHz, and they were demodulated using TED and non-coherent envelope detection using a trapezoidal numeric integration method; we call it *CONV* method. Figure 3.20 shows the number of packets that were not successfully decoded (even a single bit error leads to the rejection of the packet) by both TED and CONV methods for FSK signals with different SNRs, and Doppler shifts of 1 kHz, 6 kHz, and 11 kHz. The results obtained in each case are averages taken over 100 trials. We observe in the plots that CONV algorithm failed to decode all the signals with SNR<5 dB. TED outperformed CONV by decoding the signals with SNR as low as 0 dB. Further decrease in SNR led to an increase in bit errors in both cases. The primary reason for the bit errors in the case of the TED was the noisy coefficients of the matched filter, as they were the chosen templates for decoding the entire packet.

3.5.4. ANALYSIS OF SIGNALS WITH LOW SNR

It is also important to assess TED against COTS receivers for signals with low SNRs. We consider two sets of several raw telemetry signals from satellites, one with SNR>6 dB and the other with <6 dB (the reason for 6 dB limit being provided in Section 3.2). Figure 3.21 and Figure 3.22 show chunks of two such signals as samples. In the case of signals with SNR>6 dB, CC1310, AX5043, GNU Radio setup, and TED algorithm decoded most of the packets successfully. In other cases, only TED decoded the packets. It is evident from

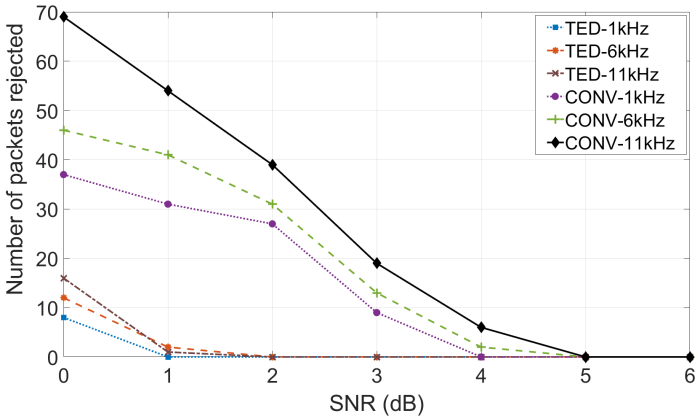

Figure 3.20: Number of packets that are rejected for signals with different SNRs

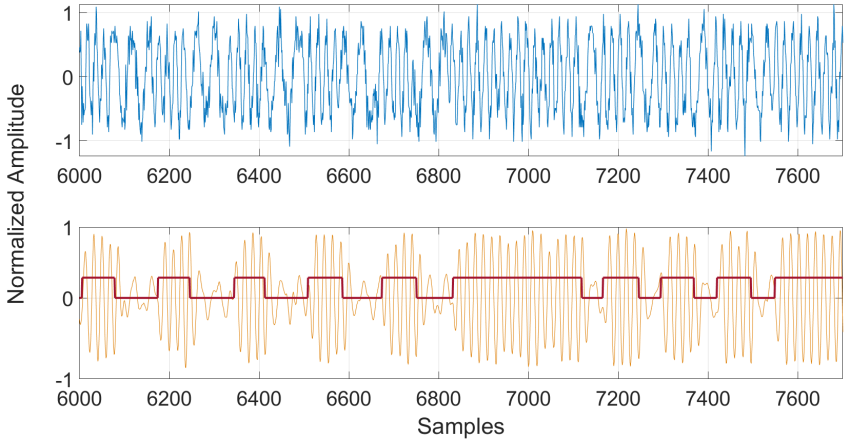

Figure 3.21: Signal with SNR>6 dB

both the figures that the combination of matched filter and TEO aids in suppressing the noise and identifying the signal. In Figure 3.22, we notice that TED introduced an extra bit around sample 4700 (as indicated in the figure). Such bit errors were removed by comparing their bit width with the expected bit width T_b of the signal. As we noticed, the performance of TED drops when SNR falls below 1 dB or when Doppler-shift is abrupt within the time ((number of samples-per-bit)/(sampling rate)). It is around 800µs in our case. Further, higher Δf_1 implies higher $f_1 + \Delta f_1$ leading to the decreased performance of the matched filter.

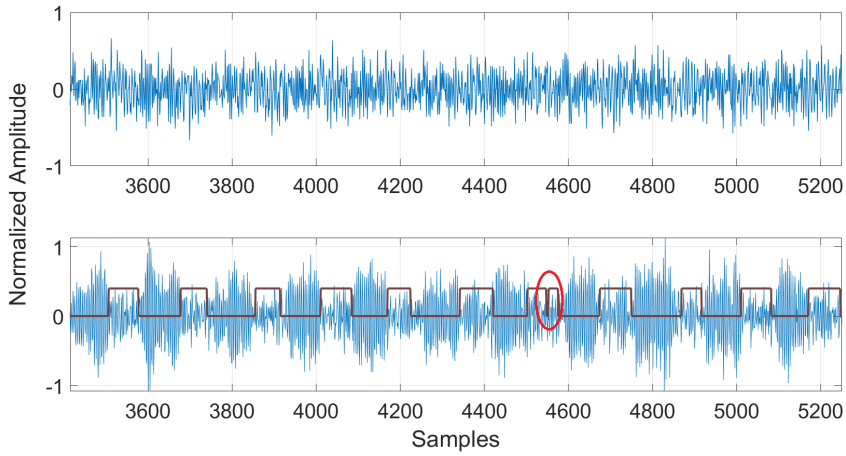

Figure 3.22: Signal with SNR<6 dB

3.6. RELATED WORK

We find ample works related to FSK based satellite communication in the literature. However, only a few works can be related to the context of Space-IoT due to the low-power, long-range requirements. Wannsarnmaytha, *et al.* [76], proposed a novel FSK demodulation method using Short-Term DFT (ST-DFT) analysis for LEO satellite communication systems. Using ST-DFT, the algorithm looks for instantaneous energy spectral peaks in the time-frequency plane of the signal to identify mark and space bits. This algorithm may not be efficient when the SNR is low, for example, 1 dB. A hardware-based reconfigurable nanosatellite communication system using FPGA and SDR for FSK demodulation was proposed by Nivin, *et al.* [77]. They implemented a Cross-Differentiate Multiplier type of demodulator on FPGA for FSK decoding online FSK data. Gomadam, *et al.* [78], presented an FSK modulation and partial coherent detection scheme for time-varying channels. They considered a simple analytical model of the Doppler effect for compensation. An investigation on the effects of Doppler dispersion in matched filters that use frequency translation for Doppler compensation has been provided by Remley [79]. A matched filter detector using frequency translation for Doppler compensation was implemented and analyzed statistically. A matched filter-based technique was proposed in [80] to detect complicated signals subjected to a wide range of possible Doppler shifts using conjugate functions or Hilbert Transforms. A 100 tap bandpass delay line was used in conjunction with a resistor weighting matrix to synthesize signals and filter their characteristics.

An open source software “demod” makes use of open source libraries such as “modified multimon-ng”, “doppler” and “gpredict” to decode FSK signals that can tackle Doppler problem [74, 75]. This is one of the best available solutions that can be integrated with SDRs and decode the signal online or offline. However, the software is restricted to FSK signals with a baud rate of 9600 and sampling rate of 22.05 kHz or 48 kHz. Guimaraes, *et al.* [64], explored the practical aspects of FSK modulation with non-coherent matched filter detection.

The performance of a non-coherent correlator receiver and a non- coherent matched filter receiver simulated from a realistic implementation-oriented model was studied. They also discussed that the matched filter receiver could achieve superior performance by adopting the realistic model. However, the performance of their proposed system in the presence of the Doppler effect is not discussed. To the best of our knowledge, this work is the closest to ours found in the literature, however not in the context of Space-IoT. Unlike the existing work in the literature, our work provides an end-to-end FSK demodulation technique in the context of Space-IoT where the SNR of received signals can be as low as 1 dB (TED decoded 90 % of the packets when SNR is around 1 dB as shown in Figure 3.20) for successful decoding. Additionally, the existing work entails Doppler compensation of telemetry signals before decoding them, while TED performs even in the presence of Doppler shift. With Space-IoT as the primordial outlook, it is necessary to tackle the challenges of long-range, low-power communication between sensor nodes and satellites, as mentioned earlier. In this work, we have addressed one such challenge in decoding the low SNR signals between satellite – sensor node communication in the presence of Doppler shift.

3.7. CONCLUSION

With the proliferation of IoT applications, we envisage that satellite-based IoT application is the next frontier to support remote, harsh, and rural areas. In Space-IoT, the terrestrial sensor nodes are expected to communicate directly. Additionally, the miniaturization of satellites may end up with designing small antennas. With a smaller antenna, communication with lower frequencies is at stake because of low SNRs. Higher frequencies are power-hungry while energy is scarce with small harvesters. Thus, there is a need for low-power, long-range communication techniques for Space-IoT.

In this work, we presented a non-coherent FSK demodulation technique for bandpass sampled telemetry signals from nanosatellites. The proposed scheme can decode the signals with low SNRs, hence, providing an extended range. A matched filter based non-coherent detection approach is used to suppress one of the frequency components of FSK. We applied the *Teager Energy Operator* to decode the signal. The algorithm was evaluated for its performance by comparing it with a commercially available telemetry decoder. We showed that the results from the TED algorithm are significantly close to the proprietary decoder, and in low SNR cases, it even performs better. As demonstrated earlier, TED has a success rate of 92.96% compared to the nearest hardware solution that provides 66.8% decoding. Thus, we envisage that the TED algorithm can be a substitute for proven hardware in nanosatellites. Additionally, there is no requirement for TLE since TED is immune to the Doppler shift. This would bring the cost of deployment significantly down. This technique can be used not only for satellite–sensor node communication but also in inter-satellite networks and terrestrial IoT alone.

We summarize the findings of this work as follows. ① Satellite–sensor node communication is affected by Doppler shift heavily. Thus, either Doppler compensation is necessary to decode the signals, or a Doppler-correction agnostic approach is required. ② Techniques such as matched filters can be employed to suppress the noise and unwanted frequency component in the FSK signal, even in the presence of a Doppler shift. It also improves the SNR of the signal. ③ TEO is an amplitude and frequency-dependent operator, and it can be

used to quell the noise further, thus improving the SNR. ④ Space-IoT calls for low-power, long-range, and energy-efficient communication technologies while SNR of the signals can even go below 0 dB. This is one of the reasons why LoRa is widely adopted in terrestrial IoT devices. With TED, we demonstrated that even with conventional techniques such as FSK, decoding signals with very low SNRs is possible.

Future work. This work demonstrated how an existing modulation technique could be adapted for Space-IoT by addressing the issues at rudimentary levels. The future work includes enhancing the performance of the algorithm through error correcting codes and extending it for demodulation of M-ary FSK modulated signals. Moreover, TED can be made further energy efficient by implementing it on an RF SoC, and a fair comparison can be made with the existing FSK-based RF SoCs. Additionally, the algorithm needs to be improved to facilitate decoding the signals with SNR < 0 dBm if attainable. This will extend the communication range without any trade-off with the transmission power. Similar solutions can also be explored on other modulation techniques such as ASK, PSK, and LoRa as they are widely adopted in terrestrial IoT networks. While this work gives an insight into the effect of Doppler shift on sensor node – satellite communication, care should be taken while employing other modulation techniques. Several new challenges may arise. For instance, LoRa, which already consumes a high bandwidth (minimum 125 kHz) for communication, is forced to increase the receiver bandwidth further due to the Doppler shift. This may also lead to spectrum licensing issues when thousands of satellites need to communicate with billions of IoT nodes on Earth. Further, new revolutionary networking and communication standards in the context of Space-IoT must be evolved as discussed.

In this chapter, we have demonstrated an approach to improve the energy efficiency and decoding performance of the communication subsystem of a satellite. In the next chapter, we target another critical subsystem of the satellite - the Attitude Determination and Control System (ADCS), and portray how we make it energy-efficient. While ADCS comprises several sensors and actuators, such as magnetorquers, Satellite Positioning System (SPS), inertial motion units, star trackers, reaction wheels, and sun sensors, we choose the SPS unit as it is a widely adopted localization approach in small satellites.

4

HUMMINGBIRD: AN ENERGY-EFFICIENT GPS RECEIVER FOR SMALL SATELLITES

Location information is an essential aspect of many terrestrial and space applications. Global Positioning System (GPS) is a widely accepted technique for satellites to identify their locations in Low Earth Orbits (LEO) and Medium Earth Orbits (MEO). Positioning helps in various satellite applications such as surveillance, mapping, and estimating sea levels and areas of forest and lakes. Advanced applications such as high-resolution imagery, radio interferometry, finding the ice levels on glaciers, and movement of pollutants also need exact positioning. For instance, Planet Labs' constellation of 88 satellites can provide up to 3 m multispectral imaging resolution [81]. For such use cases, high position accuracy (sub-meter) is critical. Additionally, a satellite also needs to know its position for its orbit correction and navigation.

While big satellites typically do not have any constraints on energy consumption for GPS subsystems, this is not the case in miniaturized satellites. Most of the small satellites such as CubeSats and picosatellites are severely power-constrained because of their restricted solar panel size. The GPS receivers are seen as one of the subsystems constantly consuming a significant portion of energy, even up to 20% of the power budget in CubeSats [30, 31]. Even though there are many GPS receivers commercially available, most of them are optimized for terrestrial applications. They may not be energy-efficient to employ on small satellites or would not even be functional for space applications. Hence, with the rise in demand for small satellites over the past decade, the need for low-cost, low-energy spaceborne GPS receivers is also increasing.

Duty-cycling. One of the most common energy conservation techniques proposed for spaceborne GPS receivers is duty-cycling [82]. Here, the receiver is turned ON until a position fix is acquired, and then it is turned OFF for a specified duration to save energy. This

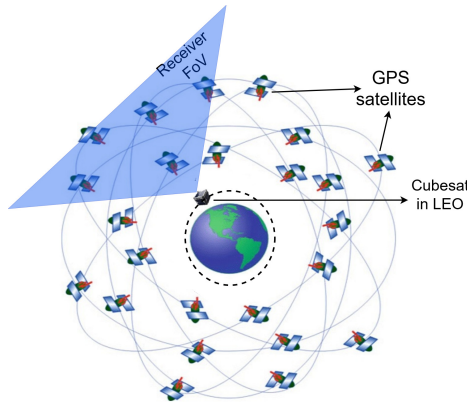

Figure 4.1: A scenario, demonstrating the visibility of GPS satellites for a GPS receiver antenna mounted on a CubeSat in LEO

technique is efficient only when the Time To First Fix (TTFF) of the receiver is relatively short. TTFF is the time taken by the receiver to get locked to at least four GPS satellites, acquire signals and navigation data, and obtain the position fix. On account of duty-cycling, if the receiver takes more time to get a position fix (or TTFF) every time it is turned ON, then there may not be any significant minimization in energy consumption. However, attaining a short TTFF in spaceborne receivers can be challenging, unlike in terrestrial systems where cell tower data can be used to achieve a faster fix [83, 84]. During TTFF, most of the energy is consumed for searching the GPS satellites and acquiring the signals [85]. Unless the local time and information about the GPS constellation are known a priori, the receiver has to search for the visible GPS satellites to get the first fix.

Doppler shift. Majority of the acquisition time is spent on searching for a GPS satellite's Psuedo Random Number (PRN) code in the presence of Doppler shift, and on the time to read the navigation data [85]. The Doppler shifts in GPS signals are due to the high orbital velocities of the GPS satellites (around 3.9 km/s) and GPS receivers (around 7.8 km/s at 500 km altitude) mounted on satellites. While generic GPS receivers are designed to consider the Doppler shift of around ±10 kHz on Earth, the receiver on a satellite in LEO can experience Doppler shifts up to ±80 kHz. This impacts the TTFF significantly as the receiver has to blindly search for the visible GPS satellites that are within the Field of View (FoV) of the receiver (Figure 4.1). Additionally, when there is no prior information on the GPS constellation and time, the acquisition search takes place for all the GPS satellites in the entire Doppler range during correlation, even if the satellite is not visible at that moment. Therefore, the TTFF for a receiver in space can go as high as 25 minutes, and in such cases, duty-cycling may not be beneficial [86].

The problem. Once the receiver locks to a GPS satellite, the almanac (coarse information on the position of GPS satellites at a given time) and ephemeris (precise location of the GPS satellites) can be downloaded, which takes 12.5 minutes and 30 s, respectively. Most small satellites may not be equipped with attitude control systems, which are commonly present in big satellites, leading to tumbling (spinning) on all three axes, including the GPS

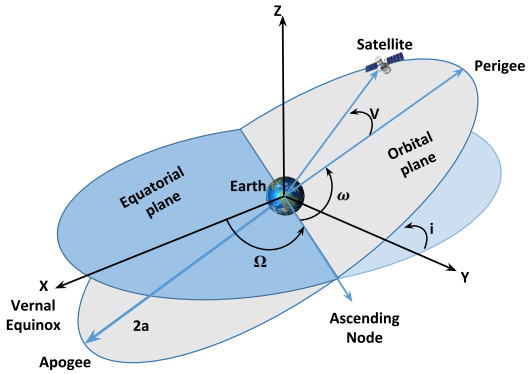

Figure 4.2: Satellite orbital dynamics

receiver and antenna. While it is beneficial to keep the energy consumption low in satellites with or without attitude control, it is essential to search the GPS satellites as quickly as possible and download the ephemeris and almanac when the receiver antenna is disoriented (rotating). This is a kind of a challenging *catch-22* situation, wherein the approximate GPS location and time are required by the receiver to get a faster fix but cannot be obtained without having a position fix. Furthermore, energy-saving must not be at the cost of position accuracy. Missions involving payloads such as cameras may need high position accuracy.

Our solution. Due to the high orbital velocities, a duty-cycled GPS receiver usually has to lock on to a new set of GPS satellites each time it wakes up. Thus, TTFF is one of the major factors that affect the performance of spaceborne GPS receivers in terms of energy consumption. Hence, we mainly focus on a specific problem - reducing TTFF to minimize energy consumption. In this work, we present an algorithm to minimize the energy consumption of the GPS receiver by exploiting the orbital information included at launch time. To demonstrate this, we also focus on designing and developing a low-power GPS receiver (employing an off-the-shelf GPS chip) for satellite applications. We design a space-qualified, low-power GPS receiver subsystem, called μGPS , that is energy-efficient[1]. While TTFF is a major factor that affects the energy consumption of duty-cycled spaceborne receivers, we mainly concentrate on significantly improving the TTFF by proposing an energy-efficient algorithm – Fast Fix and Forward/Propagate (F^3). The algorithm minimizes the time and energy to get the first fix. We reduce the TTFF significantly by readily estimating the visible satellites and the Doppler frequencies for the respective GPS satellites, thereby reducing the frequency search space for PRN codes.

Specifically, our contributions are as follows:

1. We design a low-power miniaturized GPS receiver subsystem called μGPS for space applications and present the in-orbit results.

[1]Analogy of the hummingbird is used in the title to highlight that our solution is *small*, *fast* and *energy-efficient* as the bird

2. We present a complete solution to minimize the energy of spaceborne GPS receivers considerably.

3. We use a COTS GPS chip (where raw GPS data output is available) to keep the design low-cost rather than designing a proprietary GPS module. Thus, our solution could be used in almost all situations.

4. With in-orbit data from a launched nanosatellite with our μGPS , we demonstrate that our proposed algorithm, F^3, performs well even when the satellite is tumbling, and the GPS antenna is disoriented.

5. The TTFF with μGPS and F^3 is only a few seconds more than the time required to download the ephemeris from one GPS satellite, hence it is extremely fast.

4.1. FUNDAMENTALS OF SATELLITE ORBITAL DYNAMICS AND GPS

Before we present our energy minimization technique and algorithm to reduce TTFF, we briefly explain the satellite orbital dynamics and the fundamentals of GPS for civilian use.

4.1.1. SATELLITE ORBITAL DYNAMICS

Most of the satellites in Low Earth Orbits (LEO) form an elliptical orbit with Earth as one of the focal points. The geometry of such an elliptical orbit is shown in Figure 4.2. The entire satellite orbit and the position of a satellite in space at any time can be determined using the six *Keplerian orbital parameters*:

1. *Semi-major axis (a)* of the elliptical orbit.

2. *Eccentricity (e)* of the ellipse.

3. *Inclination (i)* is the angle between the orbital and equatorial planes;

4. *Argument of perigee (ω)* is the angle between the perigee and ascending node vectors.

5. *Right ascension of ascending node (Ω)* is the angle between the vernal equinox and the ascending node vectors. This angle is thus measured along the equatorial plane.

6. *Mean anomaly (v)* is the angle between the perigee and the satellite's current position vectors.

More details on the relation between these elements can be found in [87]. North American Aerospace Defense Command (NORAD) provides the complete orbital element information and the Keplerian elements as Two-line Element (TLE) that is unique to a satellite. Using TLE, anyone can track the satellite, and the TLE is available for public use. NORAD updates it once a day or two. The position is estimated using TLE and is accurate to 2 km and the position data becomes stale over a few days [86].

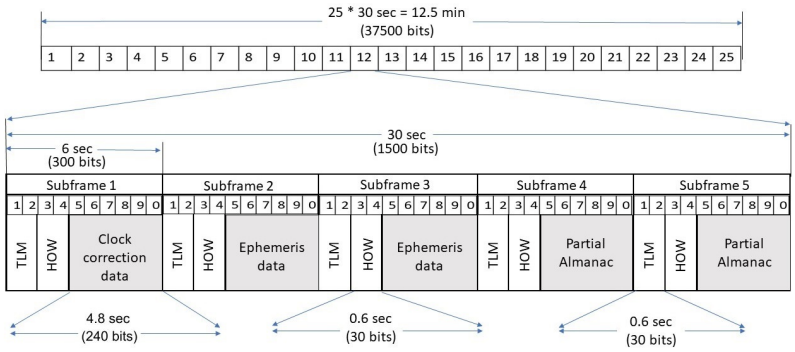

Figure 4.3: Data frame format of signal from a GPS satellite

4

4.1.2. FUNDAMENTALS OF THE GPS

The GPS constellation consists of 31 active satellites transmitting navigation messages on the same carrier frequency. The satellites are orbiting at an altitude of 20200 km above the Earth. The orbit geometry is such that at least four satellites are visible at any location on the Earth all the time. All the satellites transmit GPS data in the same frequency band using Code Division Multiple Access (CDMA). Each satellite has a unique PRN code which is used to identify the satellites. The navigation message (actual data) is transmitted at 50 bps. GPS uses three frequency bands for transmitting navigation data – L1, L2, and L5. The codes used for the L1 band (1.575 GHz) Coarse Acquisition (C/A - for civilian use) are 1023 bits long and are transmitted every 1 ms. As shown in Figure 4.3, a single navigation message frame consists of five sub-frames, transmitted every 30 s. Each sub-frame is transmitted every 6 s. All the sub-frames consist of the information of the time at which the next sub-frame will be transmitted along with the clock corrections. Subframes 2 and 3 together constitute the *ephemeris*[2] information, which is a set of time-varying parameters that are used to calculate the position and velocity of the corresponding GPS satellite. Subframes 4 and 5 contain a partial almanac, which has coarse information about the state and position of all the GPS satellites. The receiver has to wait for one subframe (6 s), one navigation frame (30 s), and 25 navigation frames (12.5 minutes) to download the GPS time, ephemeris, and almanac, respectively. While the almanac is valid for around two months after which the accuracy of the data becomes poor, the ephemeris is valid for around 4 hours only.

There are three major steps performed to get a position fix:

1. **Acquisition:** First, the receiver has to search for the signals from the visible GPS satellites. Even though all the GPS satellites transmit at the same frequency, there may be a Doppler shift, and the receiver has to lock onto the satellite's frequency. This search is done by correlating the received signal with the pre-saved PRN codes of GPS satellites. If the received signal matches the PRN code of a satellite, then the receiver is said to be locked onto that satellite. To get a 3-dimensional (3D) fix, the receiver must get locked onto at least four GPS satellites.

[2] An ephemeris gives the trajectory of space objects *i.e.*, the position (and possibly velocity) over time.

2. **Decoding:** Once the receiver locks to a GPS satellite, it decodes the received signal to get the information on GPS time, ephemeris, clock bias, etc.

3. **Positioning:** With the help of the decoded data, the 3D position of the receiver is estimated using trilateration.

A scenario demonstrating the visibility of GPS satellites for a GPS receiver antenna mounted on a CubeSat in LEO is shown in Figure 4.1. The time taken by the receiver to startup, acquire satellite signals, receive navigation data, and calculate its current position for the first time after the receiver is turned ON is called *Time To First Fix* (TTFF). Typically, the TTFF is classified into three different start types based on the data already stored in the GPS receiver.

Cold start. Typically, a cold start is performed whenever the receiver has been powered down for more than two weeks. The receiver does not know its last position or time during cold start, and it has no valid ephemeris or almanac data. A typical cold start will take at least 12.5 minutes – without considering any software optimization – when the almanac stored in the memory is not valid. Even when there is a valid almanac, the receiver can take more than 5 minutes to get a position fix, which is typical [88].

Warm start. In this case, a valid almanac is present in the receiver's memory, and the current position is within 300 km from the last active position. However, ephemeris is not present in its memory. A typical warm start takes between 35 s to 4 minutes.

Hot start. A receiver starts up in this mode when warm start conditions are met, and a fix had been established within the last two hours. The receiver has valid ephemeris data for at least five satellites.

The ephemeris data contains precise corrections to the almanac data and is required for accurate positioning. It is continuously updated, and thus, the ephemeris data within a deactivated GPS receiver will become stale after ~4 hours. We point the readers to [89, 90] for more information on the GPS theory. With this foundation, we now motivate this work, and also we try to list the problems in detail in the sequel.

4.2. CHALLENGES AND WORKAROUND

As discussed earlier, performing localization in small satellites is a challenge because of many constraints. This section summarizes the challenges encountered in designing a low-power GPS receiver for space applications and the possible solutions.

4.2.1. CHALLENGES

Using GPS is the easiest method for satellites in LEO orbit to keep track of their positions. Given that the satellites are being miniaturized, their power budgets are also being reduced correspondingly. While CubeSats can dissipate as low as 1 W, femtosatellites have an even lower power budget of approximately 200 mW [26]. If 140 mW is the average power spent on the GPS receiver in these small satellites, there is hardly any power left for the other subsystems to operate (more so in pico and femtosatellites). Furthermore, the current state-of-the-art receivers may not work when a satellite is tumbling at high rates (~30°/s). As GPS is one of the most power-consuming subsystems in small satellites, it is highly desirable to reduce its energy consumption.

As explained earlier, duty-cycling the GPS receiver operation is a standard method to reduce energy consumption. Generally, due to the high orbital velocity of the satellites, the GPS receivers need to find a new fix each time they wake up. This technique is power-hungry and inadequate if the TTFF is high. This work, therefore, focuses on developing a low-power GPS subsystem and an algorithm that significantly reduces energy consumption without sacrificing position accuracy.

Several non-trivial challenges exist that need to be addressed in order to realize μGPS and the F^3 algorithm. Further, nanosatellite applications make it much harder. We list them briefly here.

- **Visibility of GPS Satellites.** On terrestrial GPS receivers, there is a possibility that the same GPS satellites may be visible even after 4 hours. Therefore, even if the receiver is duty-cycled multiple times, it can get a faster fix. However, satellites in LEO revolve around the Earth in just 90 minutes (at approx. 500 km altitude). Hence, the visibility of GPS satellites changes rapidly, while the receiver needs to update itself for new acquisitions more frequently. This would not be an issue when the receiver is continuously ON as it can get locked to more than four (six to ten usually) GPS satellites as a backup in case it loses track. However, it is tricky in the case of duty-cycling to conserve energy. The receiver, when turned ON each time, will be far away from the previous position and has no idea of which satellites it should search, thus resulting in longer TTFF.

- **High Doppler shift.** A satellite in LEO travels at a velocity of up to 7.8 km/s at approx. 500 km orbit. The GPS satellites themselves travel at 3.8 km/s. Due to the high relative velocity between them, the Doppler search range can be as high as ±80 kHz compared to that on Earth (±10 kHz). Alongside this, the rate of change of the Doppler offset is also significant. This increases the receiver frequency search range during initial signal acquisition, and re-acquisition in case the GPS satellite is lost after locking. This implies an increase in the TTFF significantly, and it can be as high as 25 minutes [86]. Hence, reducing TTFF is a challenging task for spaceborne GPS receivers.

- **Higher performance at low-power.** The acquisition and decoding of the navigation message must be performed as quickly as possible. A slight delay of 10 ms in the algorithm points the satellite 78 m away when the speed is 7.8 km/s. Hence, the receiver should contain high-performance hardware while it has to be low-power. In other words, there is a need for a low-complexity algorithm.

- **Attitude control**: When the satellite attitude is uncontrollable, which is usually the case in small low-power satellites, the receiver antenna orientation with respect to the GPS constellation may be unfavourable when the satellite is tumbling (spinning). This leads to a loss of GPS signal, resulting in the search for GPS satellites multiple times. In some cases, the receiver may not get the complete almanac, ephemeris, and clock corrections from any of the GPS satellites due to antenna disorientation. This leads to no fix and also drains the battery on account of signal acquisition.

4.2.2. A POSSIBLE WORKAROUND

All the above challenges can be addressed with workarounds. However, they require some compromise through the use of additional devices or losing space. We list them below.

1. Multiple receiver antennas can be mounted all around the satellite so that the signals from all the visible GPS satellites can be acquired and locked continuously even if the satellite is tumbling. However, this comes at the cost of sacrificing the mounting space for solar cells as the small satellites are covered by body-mounted solar cells to harvest maximum energy.

2. As an alternative to Assisted GPS (A-GPS), the GPS almanac and ephemeris data can be uploaded to the receiver from multiple ground stations on Earth to improve TTFF. However, this requires additional ground stations and is not cost-effective.

3. Updated TLE can be uploaded to the satellite from the ground stations continuously to propagate the orbit position when the receiver is OFF. But, again, this requires multiple ground stations.

4. In terrestrial GPS receivers, there are algorithms to get a faster fix (~2 s TTFF) if the position of the receiver does not change more than 300 km [91]. Such techniques can be applied on spaceborne receivers but require duty-cycling at a higher rate (in LEO, a receiver has to be duty-cycled once every 20 s approximately). This is not energy-efficient.

In this research, we try to address all the aforementioned challenges. We present an algorithm that does not need any additional requirements, such as multiple antennas or ground stations. Further, the duty-cycling period is selected optimally to minimize energy consumption while designing a spaceborne GPS receiver. To demonstrate these, we design and deploy a space-qualified GPS receiver on a nanosatellite. To the best of our knowledge, we are the first to provide such a complete solution and test it in stringent conditions by launching our module in LEO.

4.3. DESIGN OF μGPS RECEIVER

Unlike GPS receivers for terrestrial use, the μGPS on a satellite has to sustain the harsh environmental specifications of space – extreme temperatures, vibration during launch, vacuum, and radiation. All the components used should be reliable as there is no chance of repair after launch. Furthermore, the software must also be of high reliability, albeit the mission fails. Considering these requirements, we set the following design goals.

G1 The dimension should be as small as possible; however, it must withstand vibrations and be robust. Based on the structural requirements and the mounting, our μGPS receiver has the dimension 40 mm × 30 mm × 2 mm. The available power budget is 150 mW, and the mass budget is 50 g. It should be noted that the power budget provided here is similar to/lower than the generic commercial miniaturized GNSS receivers for small satellite applications [92–94]. Typically, the power budget for a CubeSat is around 1 W, and the GPS subsystem consumes 10% to 20% of the total available power [26, 95, 96].

G2 An in-orbit accuracy of 30 m (with a minimum of 99.7 percentile) for the position and velocity of 30cm/s (99.7 percentile) is sought.

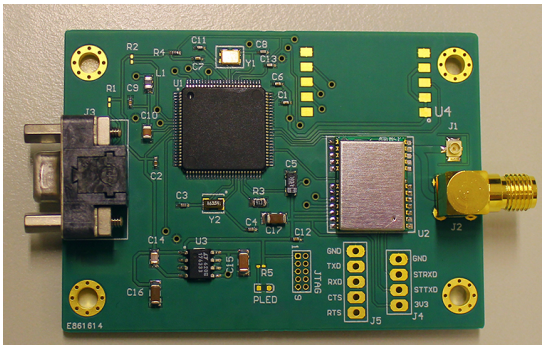

Figure 4.4: μGPS Receiver

G3 The navigation solutions must be sent to the On-Board Computer (OBC) at 1 Hz in a custom format.
G4 The GPS should provide clock synchronization to the satellite's main OBC like any commercial receiver using Pulse Per Second (PPS) output.

The μGPS, that we developed is shown in Figure 4.4. The receiver weighs 20 g. The maximum power consumption of the receiver is 145 mW, which is within the limit imposed by the structures team (**G1**)[3]. The receiver houses a *customized* low-power GPS chip with frontend - Venus series from Skytraq, supporting GPS L1 frequency (1.54 GHz). It provides the navigation solution in NMEA format [97] as a standard, like any other commercial consumer and space-grade GPS receivers. The chip also provides raw GPS data such as ephemeris, GPS time, pseudo-range, clock corrections, and other required data to estimate the position. The On-Board Computer (OBC) has no computational power to parse these data and execute the algorithm. Hence, the receiver also includes a low-power ARM microcontroller, MSP432 on which the navigation solution is computed, and to power duty-cycle the GPS front-end. Before the launch, the GPS chip was subjected to emulation by sophisticated equipment that completely mimics the dynamics of space and GPS satellites. The observed accuracy by the chip was 10 m (at 99 percentile) for the position and 10cm/s (at 99 percentile) velocity, catering to **G2**. The reasons for selecting the aforementioned GPS chip are its low-power operation, accuracy, and most importantly, the availability of raw data. The microcontroller sends the navigation solution to the OBC at 1 Hz (**G3**). It should be noted that we used high-reliability COTS components in the design and qualified them for space in LEO. However, for the orbits above LEO, we suggest using the space-grade counterparts of the COTS components due to extreme temperature changes and high radiations.

Since the OBC clock drifted 2 s per day, an important requirement for the μGPS was to provide real-time clock synchronization to the OBC periodically. The receiver sends the Pulse Per Second (PPS) signal on one of its output pins to the OBC. PPS is the pulse given out every second after it obtains the position fix. Since the time synchronization has to be in microsecond accuracy, the delay in communication between the OBC and the receiver is also included in the algorithm. The GPS receiver also corrects its clock periodically, meeting

[3]The μGPS can be miniaturized further. As we see in Figure 4.4, there is empty space

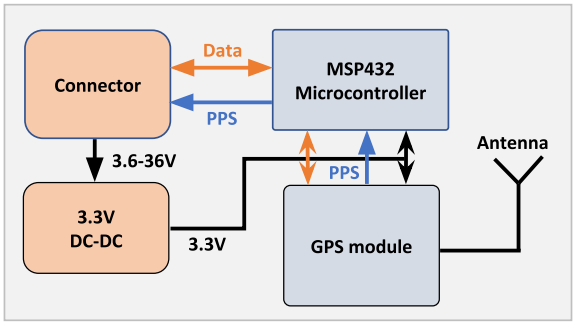

Figure 4.5: Electrical block diagram of the GPS receiver

the goal **G4**. The receiver supports both SMA-based active and passive GPS antenna, and we chose Tallysman 2410W because of its robustness to sustain in the harsh space environment.

The overall component cost of the receiver was ~$200 (commercial GPS subsystems for small satellites cost around $3000-$4000). The receiver has passed all the environmental tests such as reliability, thermal, vacuum, vibration, and radiation, adhering to space systems requirements. We execute our proposed algorithm Fast Fix and Forward (F^3) on the microcontroller to reduce energy consumption.

4.4. DESIGN OF THE F^3 ALGORITHM

The basic idea behind the Fast Fix and Forward (F^3) algorithm is to duty-cycle the GPS chip to minimize energy consumption while having improved TTFF. The basic idea is as follows. First, the TTFF is reduced. Later, the receiver is duty-cycled at specific intervals. When the GPS chip is OFF, the state vectors (position and velocity) are propagated using the TLE of the satellite. Since continuous TLE propagation is prone to deviations, we correct the error by getting the true position from the GPS intermittently. Then, the TLE is updated/corrected for bias for further propagation. The functional diagram of our algorithm is shown in Figure 4.6, and the methodology is implemented in five main steps explicated below.

4.4.1. REDUCING THE TIME TO FIRST FIX (TTFF)

GPS signal acquisition is a search process. This process requires replication of both the code and the carrier of the GPS satellites to acquire the signal. Hence, the process is two dimensional – the range dimension, associated with the replica code, and the Doppler dimension, associated with the replica carrier. To perform the search, the receivers utilize the tracking loops such as Phase Locked Loop (PLL) and Delay Locked Loop (DLL). When the code phase and the Doppler frequencies of signals are unknown, the corresponding search space is large. Thus, the expected search time increases, and it can take up to 25 minutes because

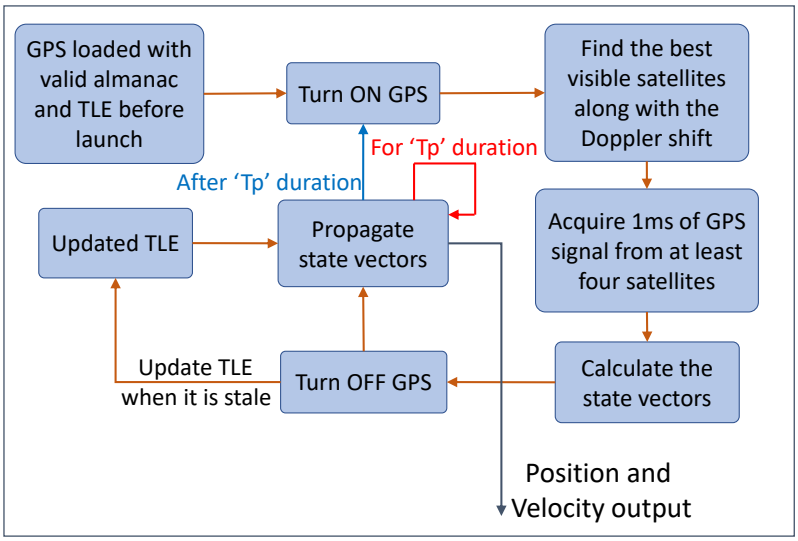

Figure 4.6: Functional block diagram of the F^3 algorithm

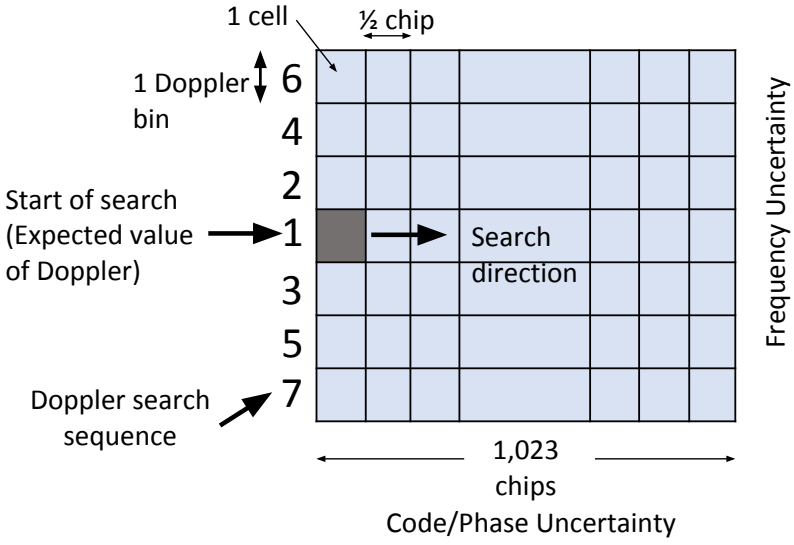

Figure 4.7: C/A code search pattern

of the high Doppler shift range of received signals in satellite orbits, as mentioned earlier. Therefore, we try to reduce the search time.

The initial C/A code search usually involves replicating all 1023 C/A code phase (1 ms signal = 1023 chips) states in the range dimension. The code phase is typically searched in increments of 0.5 chips. Each code phase search increment is a code bin. Each Doppler bin is rough $2/(3T)$ Hz, where T is the search dwell time (the longer the dwell time, the smaller the Doppler bin). The combination of one code bin and one Doppler bin is a cell. In a typical receiver, the default bandwidth of the search bin is set at 250 Hz [84]. Figure 4.7 shows the two-dimensional C/A code search pattern. Each bin also needs to search for a correct PRN code phase. This search period is called the dwell time. Predicting the Doppler shifts (using estimates of the receiver and GPS satellites' position and velocity) reduces this dwell time. This is possible only when the approximate receiver position is known, or the prior position is within 300 km [91]. There are many methods proposed to reduce the search space in frequency axes but the process is always two dimensional [89, 90]. In our proposed method, we reduce the search space to one dimension.

Our approach: During the launch, the receiver is loaded with the parent satellite's TLE, the almanac of GPS constellation, and the ejection time of the satellite[4]. The receiver uses this information when it is turned ON for the first time. Note that the almanac does not cause any storage overhead as all the GPS chips reserve onboard storage space for the almanac. However, the TLE file comprises 138 characters (138 bytes), which can be easily accommodated in the microcontroller. On the first cold start of the GPS receiver, it estimates its position in the orbit using the loaded TLE as the approximate launch time is known. Using the almanac, the best visible GPS satellites at that position are calculated, and their Doppler frequencies are estimated. Now, the two-dimensional search space converges to one dimension i.e., single-row search space, as the Doppler frequency is known. Hence the complexity of the TTFF algorithm reduces to $\mathcal{O}(N)$ from $\mathcal{O}(MN)$, where M is the number of Doppler bins and N is the number of chips. However, the reduction in code/phase uncertainty is not possible unless accurate ephemeris is known. Now, it is necessary to show that the estimated Doppler frequency is within 250 Hz due to the Doppler bin size, and the search stays within a single bin for different code phases.

Error bounds. Even though the tracking frequency is identified now, there is a possibility that the almanac and TLE used for calculation may not be accurate. It has been shown that the TLE provided by NORAD is accurate to a few meters and deviates as high as ±2 km on continuous propagation for days [86]. The almanac will remain valid for around two months and accurate enough to get ±3 km accuracy on the day of the launch of the receiver [98]. Hence, the estimated position has a combined maximum error of 10 km. However, the maximum error from the almanac can go up to 50 km if it is two months old [98].

The estimated satellite ejection time and the actual time is assumed to be accurate to ±5 s, else the satellite orbit will change. Therefore, the receiver's estimated position may have deviated by 78 km in ±5 s with the assumption that the velocity of the receiver is 7.8 km/s. Hence, the maximum possible error in estimated position = *Error from TLE* + *Error from almanac* + *Error from ejection time* = 4 + 6 + 78 = 88 km. For ease of calculations, we round this on the higher side to 100 km.

[4] Ejection time of a satellite is known prior to the launch to place the satellite in the defined orbit.

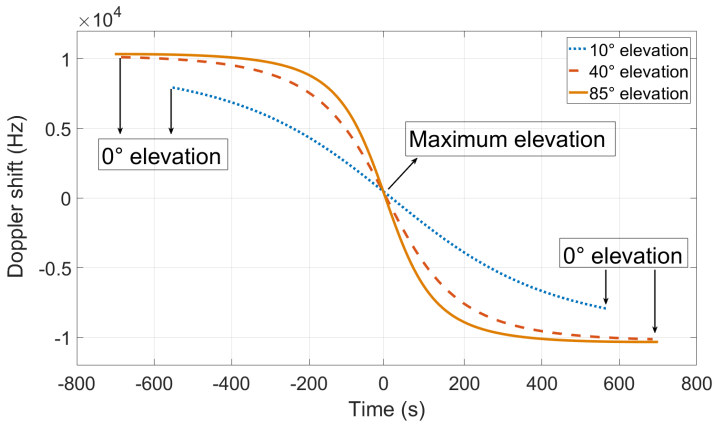

Figure 4.8: Doppler shift observed for different elevation between the observer and a satellite at 500 km

The Doppler frequency f observed by the receiver is given by,

$$f = \left(1 + \frac{\Delta V Cos\theta}{c}\right) f_o, \tag{4.1}$$

where ΔV is the relative velocity between the receiver and the GPS satellite, θ is the angle between them along the velocity vector, c is the velocity of light, and f_o is the transmitted signal frequency. For GPS L1, $f_o = 1.575$ GHz.

Figure 4.8 shows the Doppler frequency observed for different elevation (angles) between the observer and a satellite at 500 km, travelling at 7.8 km/s. We observe from the plot that the Doppler frequency is zero when the elevation is maximum, i.e., 90°. The same also holds when we substitute $\theta = 90$ in Eq. (4.1). Additionally, when the elevation approaches its maximum, the slope of the curve also reaches its extreme. This indicates that the rate of Doppler shift is more around the maximum elevation, so the estimated Doppler frequency using error-prone TLE and almanac. Let us consider the scenario where a GPS satellite is visible to the receiver as depicted in Figure 4.9. Let the relative velocity ΔV, be $|(3.8 + 7.8)|$ km/s, which is the maximum possible. The receiver is at the vertex of the cone, and the GPS satellite is anywhere on the circumference of the plane surface, let us say Position A. The rate of Doppler shift is maximum when the GPS satellite moves along the diameter of the circle, crossing the maximum elevation point, and then touching the circumference of the circle at, say, Position B. As per our consideration, the maximum possible error in the estimated position of the GPS satellite is 100 km. Hence, the radius of the circle is 50 km. Considering the LEO orbit that extends up to 2000 km above the earth, the altitude of the cone is the difference between the altitude of the GPS satellite and the altitude of the receiver in LEO, which is, 18,200 (20,200 - 2000). Note that, as the distance between the GPS satellite and the receiver decreases, the Doppler rate increases. Hence, we consider the farthest possible LEO orbit. Now, we have the angle between the slant range and the altitude vector, $\phi = 0.158°$.

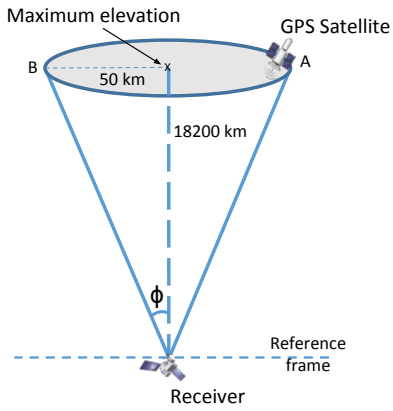

Figure 4.9: A scenario where estimation of a GPS satellite's position is off by the maximum possible error distance.

The maximum error in the Doppler frequency= ± (Doppler shift at Position A - Doppler shift at maximum elevation point).

Substituting $\Delta V = 11.6\,\text{km/s}$, $\theta = 90 - \phi = 89.842$, $c = 3\text{x}10^8\,\text{m/s}$ and $f_o = 1.575\,\text{GHz}$ in Eq. (4.1), we get the maximum Doppler Shift of approximately ±170 Hz, which is less than ±250 Hz – the frequency search bin size of the receiver. Therefore, with the maximum position error of 100 km in estimating the position of a GPS satellite, it is possible to reduce the satellite search space to one dimension, thus improving the TTFF. Since modern receiver chips contain multiple channels, the search can be done in parallel to speed up and identify multiple satellites as fast as possible. At the end of the search, at least four GPS satellites must be locked to get the position fix.

4.4.2. TIME SYNCHRONIZATION

At this stage, it should be noted that the receiver clock is not synchronized to that of the GPS satellites even though a minimum of four satellites are found. Therefore, it is necessary to download at least one navigation frame from these satellites, including ephemeris and GPS time. This takes around 30 s as explained in Section 4.1.2, after which the GPS receiver is synchronized with the GPS time. In the case of tumbling satellites, the GPS signals are intermittent; thus it may take a longer duration. It should be noted that the GPS time can be downloaded in just 6 s if the tumbling speed (degrees/second) is $\frac{1}{6}^{\text{th}}$ of the Antenna FoV and is oriented perpendicular to the direction of the incoming signal. In literature, we find methods to estimate the position just by using the Doppler measurements but they are not worthy for satellite applications because of the long TTFF issues [91]. However, with our improved TTFF methodology, the same algorithms can be used for tumbling satellites when there is no possibility of downloading ephemeris. We do not explain this in detail as it is out of the scope of this work but we show the results in 4.5. Because of the quick lock to the GPS satellites, coarse estimation of the position is possible even when they are tumbling at high speeds or on satellites where the power is too low to turn ON the receiver for 30 s.

4.4.3. DUTY-CYCLING THE RECEIVER

Once we have the ephemeris downloaded and the receiver clock is synchronized, the position of the receiver and measurement error are calculated using classic algorithms such as the least square error method or Kalman filter. Indeed, the position accuracy can be improved with a custom designed state estimation algorithm but this is out of the scope of this work as we mainly concentrate on minimizing the energy consumption without jeopardizing the position accuracy much. Further, $F^3$is independent of the estimation/tracking algorithm employed. For more details on the position estimation algorithms, we point the interested readers to [89, 90]. As mentioned earlier, we duty-cycle the receiver to conserve energy. The receiver is ON for a short duration just to synchronize the GPS time and correct the receiver's clock offsets. When the GPS front-end is OFF, the microcontroller on the receiver propagates the previous position using TLE. Let us formulate our energy minimization problem as follows.

Our main objective is to minimize the consumed energy $E_c = n(T_{ON}\text{x}P_G + P_M(T_{ON} + T_{OFF}))$ where T_{ON} is the total time for which both GPS chip and microcontroller are ON. T_{OFF} is the time during which only the microcontroller is ON, n is the number of times the GPS chip is duty-cycled, P_G and P_M are the power consumption of the GPS chip and the microcontroller, respectively. However, the duty-cycling period depends on the following three conditions.

1. *Available energy.* The receiver cannot consume more energy than the available energy, E_A, at any moment.

2. *Propagation time.* The receiver cannot propagate the TLE for more than T_P s – starting from the time at which the GPS chip is turned OFF – to stay within the error limits of propagation and to maintain navigation accuracy. Hence, the GPS chip has to be turned ON after every T_P s for error correction. Through T_P, we consider the GPS accuracy error in our optimization problem.

3. *Navigating duration.*: The GPS chip has to be ON for at least T_{ON} duration so that the position fix can be obtained.

If T_{TTFF} is the time taken by the receiver for the first fix, T_{nav} is the time taken to compute navigation solutions; our energy minimization problem can be formulated as a Linear Programming model as given below,

$$\textbf{Minimize } E_c = n(T_{ON}\text{x}P_G + P_M(T_{ON} + T_{OFF})) \textbf{ s.t.}$$

$$E_c \leq E_A \tag{4.2}$$

$$T_{OFF} \leq T_P \tag{4.3}$$

$$T_{ON} = T_{TTFF} + T_{nav} \tag{4.4}$$

$$\text{and } T_{OFF} \geq 0; T_{TTFF}, T_{nav}, E_c, n, P_G, P_M > 0. \tag{4.5}$$

Since we have already optimized T_{ON} with our proposed algorithm, it is clear from the above equations that, to minimize E_c, n should be minimized as the rest of the parameters are constant for a particular receiver. However, it is also true that E_c has a trade-off

with T_P. If the state vectors can be propagated using TLE for a longer duration (higher T_P) while maintaining the accuracy within the threshold (as per the requirement), then T_{OFF} increases. Thus, n can be reduced, and the chip can be turned OFF for a longer duration in a considered period. During the duty-cycling, when the GPS chip is OFF, the power reduces to ~6 mW, wherein only the microcontroller is active.

4.4.4. UPDATING TLE AND ALMANAC

The TLE and almanac go stale over days, leading to increased errors in position measurements when used for propagation. Since GPS gives the true position (depending on the accuracy of the navigation algorithm), we use the position provided by the GPS receiver to update the TLE and GPS almanac.

The solution provided by the GPS navigation algorithm will be in Earth Centered Earth Fix frame (ECEF) and the TLE is the True Equator Mean Equinox (TEME) frame that is the subset of Earth Centred Intertial (ECI) frame [89, 90]. ECI coordinate frames have their origins at the centre of mass of Earth and are called inertial, in contrast to the ECEF frames, which rotate in inertial space in order to remain fixed with respect to Earth's surface. The relation between the ECEF and ECI frame can be given using the rotation matrix as,

$$P_{ECEF} = \begin{bmatrix} cos(\omega_g) & sin(\omega_g) & 0 \\ -sin(\omega_g) & cos(\omega_g) & 0 \\ 0 & 0 & 1 \end{bmatrix} P_{ECI}, \tag{4.6}$$

where ω_g is the rate of Earth's rotation.

We use NORAD SGP4 function to update the TLE from the estimated position and velocity. SGP4 is a well-known and widely used technique in the Aerospace industry to estimate the position of the satellite at any given instant [87, 99]. However, we do not restrict ourselves to using only the SGP4 since there are numerous methods to update TLE. Moreover, the TLE propagation accuracy affects the duty-cycling period as explained in section 4.4.3. The elements of TLE and almanac are in the format,

$$y_i = f_i(a, e, i, \Omega, \omega, \nu, B^*) \qquad i \in \{1, ..., 7\}, \tag{4.7}$$

where y_i is the i^{th} state estimate, B^* is the ballistic coefficient used in the SGP4 propagator, and the rest are the orbital elements as explained in [99].

Once we have the position in ECI format, the TLE and partial almanac (update details only for the satellites whose ephemeris have been downloaded) are updated using the relations between the estimated state vectors and orbital elements as described in [89, 90].

4.4.5. PROPAGATION USING TLE

When the GPS chip is off, the microcontroller propagates the state vector using TLE. We use NORAD SGP4 orbit propagator to estimate the next position depending on the prior position. This is the inverse operation of the calculations performed in 4.4.4. Usage of stale TLE leads to erroneous propagation compromising the position accuracy. Since we update the TLE periodically, as mentioned earlier, the error in propagation is corrected.

4.5. EVALUATION

We evaluated the performance of our GPS receiver and the proposed technique by means of long duration simulation and real-time tests in the LEO orbit. The evaluation setup for both cases is as follows.

4.5.1. EVALUATION SETUP

A. SIMULATION

We used Spirent GSS6700 simulator (Spirent is one of the top companies that offers GNSS simulators with satellite orbit simulation) to test the performance of our GPS receiver. The simulator is capable of providing a coherent simulated signal from the GPS satellite constellation. It especially considers the LEO scenario by adjusting the Doppler frequencies and satellite visibilities for the set receiver orbit. It also incorporates atmospheric effects and errors in the simulated signal so that the receiver will experience the same effect as that in orbit. The simulator provides RF output over an antenna. In this simulation process, even though the receiver is stationary, it experienced a high relative Doppler shift and high velocity as if it is in orbit. The maximum Doppler shift considered in simulation is ±80 kHz, as explained in Section 4.2.1 and Section 4.4.1.

For simulation, the receiver orbit was considered to be 520 km, the same as that of the nanosatellite. Mbed LPC1768 microcontroller was used as OBC of the nanosatellite to record data and clock synchronization from the GPS receiver and validate the results. The TLE[5] of the receiver orbit and the latest GPS almanac was given as input to the simulator and also stored on the receiver microcontroller. The simulator was also updated with the latest Ionospheric error models.

B. IN-ORBIT EVALUATION

The receiver was fixed on the nanosatellite and was launched at an altitude of 520 km. The receiver was attached to one of the side panels inside the satellite, as shown in Figure 4.10. The antenna was placed in such a way that it points to deep space. The antenna placement is shown in Figure 4.11. The data from the receiver was recorded by the OBC and sent to the ground station whenever there was visibility.

For both simulation and in-orbit evaluation, we set the following values to the parameters described in Section 4.4.3, unless mentioned otherwise.

We set T_{ON} = 33 s as the complete TTFF and navigation algorithm execution including TLE, almanac update was performed within 32.8 s. The continuous power of 150 mW was available from the nanosatellite. The TLE propagation error was within the threshold of 30 m position and 0.3 m/s velocity at 3σ level as per the requirement when $T_P \leq 300$ minutes. Note that, as T_P increases, T_{OFF} increases, thus maximizing the energy savings.

4.5.2. SIMULATION AND IN-ORBIT RESULTS

With our experiments, we present the impact of the proposed algorithm on various factors as follows.

[5]This was provided by the space organization responsible for the nanosatellite

Figure 4.10: Placement of the μGPS receiver in the nanosatellite

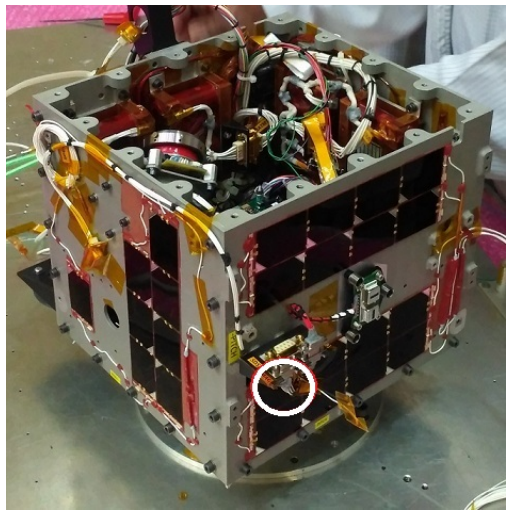

Figure 4.11: Antenna placement on the nanosatellite

A. ENERGY CONSUMPTION

To evaluate the energy savings of the receiver 'in-orbit', we consider three scenarios.

Scenario A (SA): The receiver is continuously ON. Here, there is no requirement for the propagation of orbit since a continuous GPS fix is available. Our algorithm is not executed in this case.

Scenario B (SB): The receiver is duty-cycled once in 50 minutes (to get an accuracy of 10 m) and our TTFF algorithm is not used. During duty-cycling, when the GPS chip is OFF, the microcontroller is continuously ON, propagating the state vectors.

Scenario C (SC): The receiver is duty-cycled once in 50 minutes but with improved TTFF (using our algorithm).

The performance of one of the best available commercial spaceborne GPS chips from Skytraq, the state-of-the-art methodology, and our F^3 algorithm are evaluated in the above

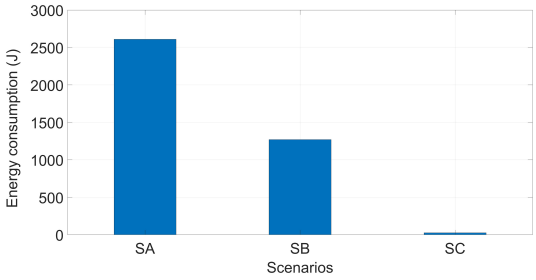

Figure 4.12: Energy consumption on different scenarios

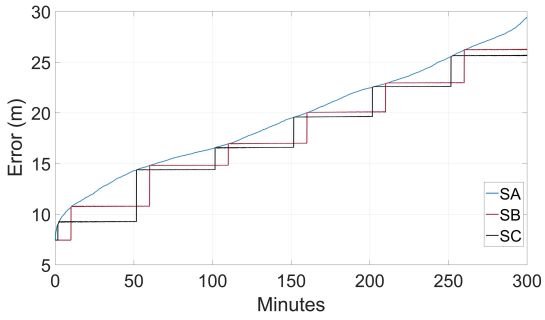

Figure 4.13: Accuracy of the solution

three scenarios, respectively.

The energy consumption of the receiver in the above three scenarios for 5 hours is shown in Figure 4.12. The total power consumption of the receiver was ~145 mW, wherein the microcontroller consumed ~6 mW and the GPS chip consumed ~139 mW power. It is evident from the plots that our F^3 algorithm saves energy significantly. In SA, the receiver is continuously ON, consuming maximum energy. In SB, even though the GPS chip was duty-cycled, it was a cold start for it every time it is turned ON. The TTFF went up to 20 minutes. In SC, the maximum TTFF was 33 s, thus saving 96.16% compared to that in SA, and 92.7% to that of SB.

B. ACCURACY

Figure 4.13 shows the accuracy of the navigation solution in the aforementioned scenarios, tested in orbit. Since velocity is the function of position, we show the error only in the Z direction (along with altitude) as it was the maximum in all the cases. In SA, the error is within 10 m (99%) always. However, in SB and SC, the state vectors are propagated after the GPS chip is turned OFF, resulting in the propagation of position error. It should be noted that, in SB, the receiver continues to propagate for a few minutes even after the GPS chip is ON, as the fix has not happened yet. We observe from the plots that TLE propagation also propagates the error from the GPS solution. In the first three months after launch, we observed that the propagation error was within 10 m (99%) when the GPS was duty-cycled

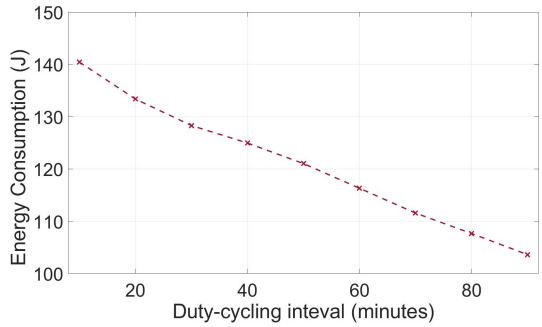

Figure 4.14: Impact of duty-cycling interval on energy consumption

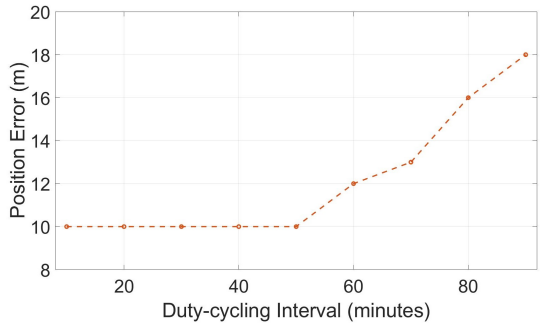

Figure 4.15: Impact of duty-cycling interval on position error

once every 50 minutes.

C. DUTY-CYCLING

We evaluate the impact of duty-cycling time on energy consumption using a simulator. The receiver was turned on at different intervals from 10 s to 90 minutes for 300 minutes. The results are shown in Figure 4.14. We observe from the plots that as the GPS chip is turned ON less and less, the energy consumption decreases almost linearly. When it is duty-cycled every 90 minutes[6], the energy consumption was at the minimum.

Since the position accuracy is dependent on the TLE propagation duration T_p, the duty-cycling duration also impacts the accuracy. The position error for different turn-ON intervals of the receiver is shown in Figure 4.15. We observe in the figure that the error is within 10 m for turn-ON intervals until 50 minutes. Further increase in the interval leads to more error because of incremental error from TLE propagation. Hence, even though the energy consumption decreases with the increase in duty-cycling interval, it comes at the cost of sacrificing the position accuracy.

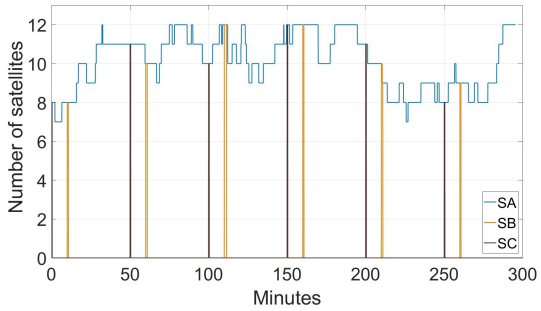

Figure 4.16: Visibility of GPS satellites

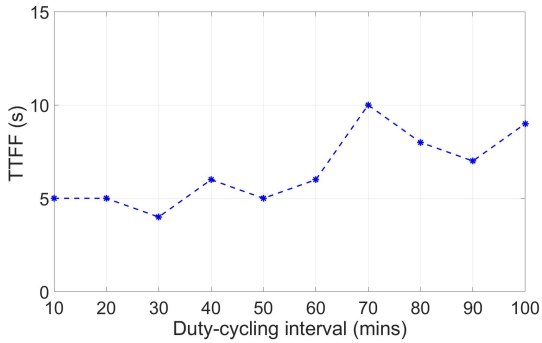

Figure 4.17: TTFF at different duty-cycling intervals

D. SATELLITE VISIBILITY

We also evaluate our F^3 algorithm for visibility of GPS satellites using a simulator to assess the performance of the TTFF. Figure 4.16 shows the results in all scenarios. In SA, more than four GPS satellites are visible always as there is a continuous fix. In SB, the TTFF was around 10 minutes. Even though the number of satellites visible was more than four during the acquisition phase, there was no fix. We do not know the exact reason as the solution is being calculated by the commercial chip and the algorithm is unknown. In SC, the receiver gets fixed to the visible satellites at a faster rate due to improved TTFF.

E. TTFF VS DUTY-CYCLING

To evaluate the trade-off between TTFF and the duty-cycling interval, the receiver was duty-cycled at different intervals between 10 and 100 minutes in orbit. The TTFFs averaged over 10 trials are shown in Figure 4.17, and the CDF of TTFF obtained for all the duty-cycling intervals is shown in Figure 4.18. As we observe in Figure 4.17, the average TTFF for any of the duty-cycling intervals is between 4 s to 10 s. However, irrespective of the duty-cycle period, the maximum TTFF observed during the evaluation was 33 s. This is because the ephemeris downloaded from all the GPS satellites is valid for four hours. If the receiver is

[6] GPS receiver turned on every 90 minutes and once fix is done, it is turned OFF.

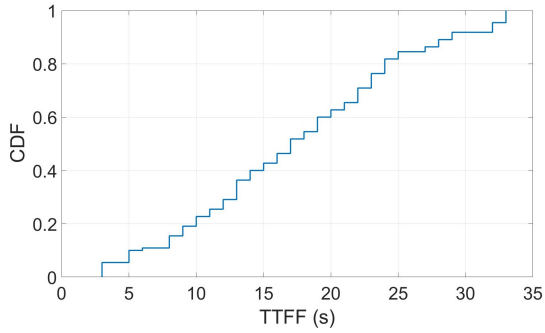

Figure 4.18: CDF of TTFF for different duty-cycling intervals

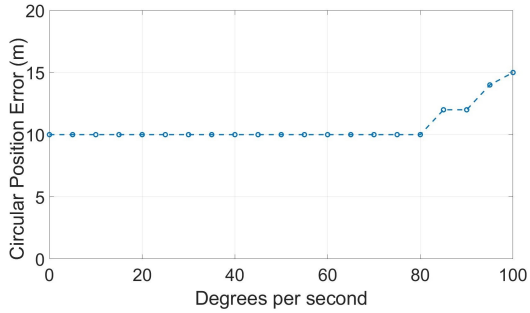

Figure 4.19: Circular position error at different tumbling rates

duty-cycled within four hours, it does not have to download ephemeris again (which takes 30 s to complete the task). However, the receiver may need to download information related to GPS time and clock drifts that can take a few seconds depending on the sub-frame being sent from respective GPS satellites. As seen in Figure 4.18, the maximum TTFF was 33 s (cold start), and the minimum (hot/warm start) was 3 s. This latency is acceptable for any of the satellite missions (so the mission of the nanosatellite) when the receiver has to download the ephemeris directly from the GPS satellites. As per the CDF plot, 60 % of the time, the TTFF was within 20 s. Therefore, the TTFF does not solely depend on the duty-cycling interval but also on the validity of the ephemeral data.

4.5.3. TUMBLING

The receiver antenna was mounted on the satellite body during the simulation and rotated to emulate the tumbling scenario. F^3 was implemented on the receiver to get a faster fix. We measured Circular position error (difference in position as estimated by the receiver and the true position provided by the simulator) and the TTFF at different tumbling rates. The results were shown in Figure 4.19 and Figure 4.20 respectively.

Observing Figure 4.19, when the rate was less than 80°/s, the receiver was able to download the ephemeris in 33 s and get the position accuracy of 10 m. The accuracy obtained

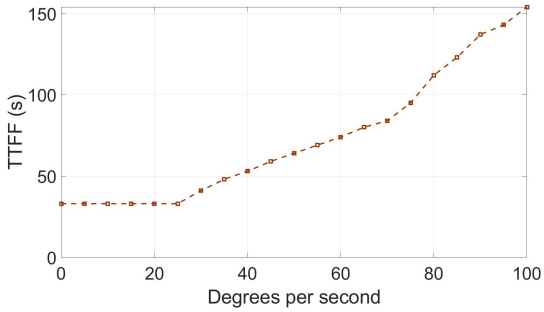

Figure 4.20: TTFF at different tumbling rates

Table 4.1: Comparison between the performance of different state-of-the-art GPS receivers

	Chen et al.	Aalto	Aurora	CAN-X2	μGPS
Power	0.143 W	0.16 W	1.1 W	1.6 W	0.145 W
Position Accuracy	12 m	100 m	30 m	20 m	10 m (99%)
Energy savings	22.7%	–	–	–	96.16%

was 15 m when the rotation rate was around 100°/s. This is considerable against the case where no fix is obtained without F^3 algorithm when the satellite was tumbling at the rate of 10°/s and higher. As the tumbling rate increases after a certain extent (80°/s in our case), there will be carrier phase error introduced in the received signal. Hence, position error increases.

The TTFF during different tumbling rates is shown in Figure 4.20. Until 25°/s, the TTFF was 33 s as the receiver could get locked to the visible satellites quickly. Beyond this rate, the receiver loses track of the visible satellites or receives only a partial signal (as explained before, 6 s is required to receive one subframe from a GPS satellite) because of tumbling. Hence, the receiver spends more time in acquisition mode to get locked to the visible/possible GPS satellites.

4.5.4. COMPARISON

We compare the performance of different state-of-the-art GPS receivers. Chen et al. [31], Aalto [96], Aurora [95], CAN-X2 [88] and μGPS are spaceborne receivers that are considered for comparison. The results are depicted in Table 4.1. It is clear from the table that μGPS , when employed with F^3algorithm, saves considerable energy, providing a decent position accuracy. Most of these state-of-the-art works do not report their acquisition and tracking algorithms. While Chen et al. use a rudimentary least square method to estimate the position, in μGPS , we use an adaptive Kalman filter to estimate the position and velocity [90].

4.6. RELATED WORK

We list some of the relevant and important works – not necessarily spaceborne – related to energy minimization and improving TTFF for GPS receivers.

For terrestrial applications. Patil et al. proposed two methods to reduce the TTFF for smartphones by avoiding the download of the ephemeris data, thus reducing the energy consumption of the receiver [100]. The first method bypasses the need for downloading the ephemeris and the second method enhances the rate at which ephemeris is downloaded using Assisted GPS (A-GPS). An energy-efficient GPS acquisition technique with sparse-GPS is proposed by Misra et al. [30]. They present a new computing framework for GPS acquisition via sparse approximation. They show that the energy consumption can be reduced 5-10 times more than a stand-alone GPS, with a median positioning accuracy of 40 m. Liu et al. designed a cloud-offloaded GPS (CO-GPS) solution that allows a sensing device such as a mobile phone to duty-cycle its GPS receiver and log just a few milliseconds of raw GPS signal for post-processing. The position information is extracted later on a back-end server [101]. A novel multi-step algorithm for low-energy positioning using GPS is proposed by Orn et al. [91]. With a prototype receiver, they demonstrate that the position can be computed using only two milliseconds of GPS raw data. The system includes a GPS receiver that collects the raw GPS data and a server that utilizes Doppler navigation and coarse time navigation to estimate the positions.

Recently, Chen et al. established an energy model for a standard GPS receiver architecture to analyze the impact of key software parameters on the GPS energy consumption [31]. Their findings show that energy consumption increases as more GPS satellites are tracked. Their approach is to track only a subset of the visible satellites that are just enough to produce equally accurate positions. They also present a method called *SatProbe* allowing low energy and fast indoor/outdoor detection based on raw GPS processing [102]. Bissing et al. proposed a new method to shorten the TTFF by exploiting the shape of the likelihood function in the collective detection of satellites, thus minimizing the energy in constrained situations like continuous position tracking on small wearable devices.

These works either require a centralized server or assisted GPS (internet/cell tower) to speed up the TTFF. This is not practical in the case of space applications.

For space applications. Leung et al. implemented a signal acquisition-aiding concept based on an analytical orbit model, which regularly calculates the approximate position and velocity of the receiver [86]. They use the data from the satellite orbit model to improve TTFF when there is a temporary loss in the fix. Power saving in small satellite GPS receivers by duty-cycling the receiver is investigated by Hartmann [103]. The author also attempts to combine orbital propagation with duty-cycling. Anghileri et al. presented a concept aiming at improving the TTFF performance of navigation receivers by defining a set of clock and ephemeris data (CED) with reduced size [85]. These newly defined message types could be added to the transmission schemes of today's and future GNSS satellites to reduce the TTFF. There are other state-of-the-art receivers that have been tested successfully in the orbit but they are not energy-efficient to suit small satellite requirements even if they employ duty-cycling [88, 95, 96]. In these works, duty-cycling is performed in a traditional way by turning ON the receiver whenever the position error exceeds a fixed threshold. However, they do not

concentrate on the TTFF, thereby spending energy by retaining the receiver ON until a fix is obtained. With such methods, duty-cycling may not be even beneficial to reduce energy consumption when the TTFF is longer. On the contrary, our algorithm improves the TTFF as well as duty-cycles the receiver, thus achieving energy minimization.

Filling the gap. In most of the aforementioned methods, even though a small portion of the received GPS signals is used for estimating the position, the post-processing is done outside of the receiver. Moreover, all the state-of-the-art techniques are analogous to A-GPS, where the ephemeris, almanac, clock corrections, and other navigation parameters are acquired through a secondary channel (e.g., GPRS). However, in the case of a spaceborne GPS receiver, these details are completely unknown unless they are uploaded from ground stations frequently. Though propagating TLE to estimate the position is a known technique, it requires updating the new TLE to the satellite from the ground station more often (e.g., once a day), and the satellite may not be equipped with telecommanding capabilities in some cases. Hence, none of the above work can be directly used for a low-power receiver in space. Further, the existing energy-saving techniques such as duty-cycling for spaceborne GPS receivers may not be beneficial if TTFF is huge. To this end, we propose an energy-efficient algorithm to reduce the TTFF significantly so that the duty-cycling technique is highly efficient. To evaluate our algorithm, we design a low-cost, low-power GPS receiver for spaceborne applications.

There are plenty of works on GPS algorithms in the context of TTFF, energy savings, accuracy, etc., for terrestrial applications. However, most of the solutions require Assisted GPS (AGPS) that relies on an Internet connection. Hence, they cannot be adapted for space applications. In the existing spaceborne GPS receivers: (i) none of those provides TTFF of 33 s, which we have achieved, especially when the satellite is tumbling and duty-cycled; (ii) there is no facility to execute our algorithms on the receiver; (iii) most of them are not low-cost; and (iv) in terms of algorithm, the state-of-the-art include duty-cycling the receiver. When the receiver is OFF, TLE is used to estimate the position and velocity based on the previous measurement. However, when the receiver is turned ON again, it enters acquisition mode and takes time, thus more energy is spent to get TTFF. Our algorithm gets the TTFF at the earliest, thereby saving energy.

4.7. CONCLUSION

The Global Positioning System is a widely adopted localization technique. With the increasing demand for small satellites, the need for a low-power GPS for satellites is also increasing. To enable many state-of-the-art applications, the exact position of the satellites is necessary. However, building low-power GPS receivers that operate in low earth orbit poses significant challenges. This is mainly due to the high orbiting speed (~7.8 km/s) of small satellites. While duty-cycling the receiver is a possible solution, the high relative Doppler shift between the GPS satellites and the small satellite contributes to the increase in the Time To First Fix (TTFF), thus increasing energy consumption. Further, if the GPS receiver is tumbling along with the small satellite on which it is mounted, longer TTFF may lead to no GPS fix due to disorientation of the receiver antenna.

In this work, we presented the overall design of a low-power, low-cost GPS receiver for spaceborne applications. We provided the nuances of GPS technology and its applicability in space, covering the constraints and requirements. Specifically, we showed how TTFF can significantly contribute to the energy consumption of the GPS receivers and in turn, the small satellite on which it is mounted. We explained the orbit dynamics that increase the TTFF. Since there is inflated energy consumption during TTFF, we proposed an energy-efficient algorithm called F^3 that decreases the TTFF despite higher relative Doppler shift in low earth orbits. Further, F^3 reduces the complexity of the traditional GPS navigation algorithm to be used in other scenarios. We tested our GPS receiver in in-orbit experiments by mounting it on a nanosatellite that was launched recently. We have evaluated the performance of F^3 and observed that the maximum TTFF was 33 s. We showed that up to 96.16% of energy savings can be achieved when compared to the state-of-the-art receivers.

Future work. The future work includes extending the F^3 algorithm for multi-GNSS constellations such as GLONASS and GALILEO. As a result, the receiver does not need to wait for the entire ephemeris to be downloaded from a single constellation. The navigation data received from at least four satellites of different constellations can be used to arrive at the first fix. Hence, the TTFF can be further improved, much better than 33 s.

Up till now, we have seen how energy minimization can be accomplished in the communication and ADCS units of a satellite. In the next chapter, we present a new isolated health monitoring system for small satellites. This proposed system is not only energy-efficient but also measures the different health parameters of a satellite reliably.

5

AN ISOLATED HEALTH MONITORING SYSTEM FOR SMALL SATELLITES

As discussed in Chapter 1, the rate of launching satellites is growing significantly, mainly due to the recent innovations in space systems. Alongside successful launch missions, the failure rate of satellites has also surged significantly. According to NASA, a whopping 35.2% of the small satellites launched between the years 2000 and 2016 have failed completely [32] (see Figure 5.1). Of these failures, the causes of breakdown are unknown for 16% of the satellites despite planned redundant systems. Further, the failure rate had increased to 43% between the years 2009 and 2016 according to the statistics by NASA, which is presented in Figure 5.1. Studies also show that ≈41% of the satellites failed within one year after launch [104]. If the reasons for failures can be determined for a satellite, then the satellite may be revived to some extent by sending appropriate commands from the ground station. Further, such failures can then be avoided in future satellites.

To accomplish global coverage, Space-IoT relies on a constellation of hundreds of satellites. If a few satellites stop working, then there will be an impact on the coverage. Critical applications, such as tracking, cannot endure such coverage risks. Having a backup satellite in orbit is an alternative but there will be a limit to their numbers. Hence, a failed/failing satellite should be revived whenever possible.

How can a failed satellite be revived? In most cases, if the source of failure can be identified, the satellite may be saved by telecommand from the ground station. For instance, one of the basic subsystems used in satellites is a star tracker that helps to determine the satellite's attitude precisely from the visible star positions. A star tracker helps payloads such as a high-definition camera that require precise pointing. Suppose it is possible to identify that the star tracker is not functional and consumes a lot of power, attempting to drain the battery, then the satellite can be revived by turning it off and relying on a gyroscope and magnetometer for attitude determination at the cost of measurement accuracy. Naturally, most satellites have multiple health monitoring self-help capabilities and regularly transmit

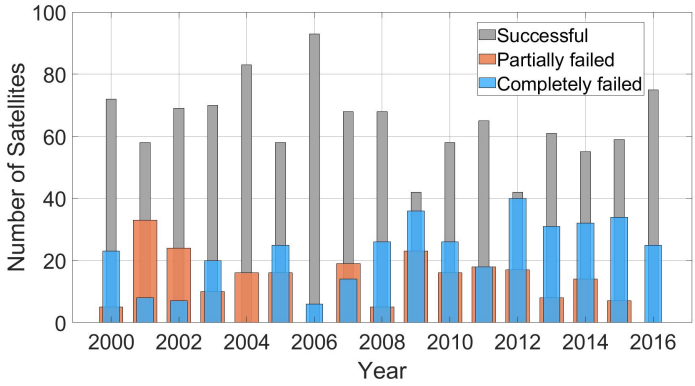

Figure 5.1: Number of small satellites launched and the failure rate since 2000 (NASA statistics).

housekeeping data, such as primary satellite bus voltage, current, and status of different subsystems, to a ground station over its communication channel. Hence, any indication of a subsystem's failure can be traced. Most of these solutions are based on software and hardware diagnostics incorporated within different subsystems of a satellite. However, if the critical subsystems such as the power and communication unit fail to operate, then the reason for failure can only be guessed at the best.

Typically, health monitoring systems in existing satellites are tightly coupled in terms of hardware and software. Any fault in the subsystem can affect its onboard health monitoring modules as they are electrically connected. Thus, in this chapter, we propose a simple, self-powered, independent, and miniaturized module called Chirper that can provide a secondary channel for the health monitoring system for satellites. The name, Chirper, symbolizes the sound a bird makes when it wants to communicate. Chirper is electrically isolated from the satellite subsystems. It can monitor the satellite health parameters at regular intervals and then transmit them to the ground station independently. Based on this health data, efforts to save the satellite can be taken.

How can Chirper help in saving a satellite? A satellite can have both hardware and software-based onboard fault detection system, and they can report the source of failure to the ground stations via the onboard communication channel [105–107]. However, if the primary power system or the communication channel is faulty, then there is no means to identify the cause of the failure or to revive the satellite. According to the literature, 45% of the failures in satellites is caused by a fault in electronics. While 32% of these electronic faults are due to the failure in the Attitude Determination and Control System (ADCS)[1], 27% is from the power system, 12% from the communication system, and 29% due to undetermined reasons [32, 104]. Some failures can also be due to the domino effect, i.e., the failure of one subsystem leads to the failure of interdependent subsystems in the satellite. For instance,

[1] ADCS comprises of sensors such as an Inertial Motion Unit (IMU), star tracker, GPS module, magnetorquers, and reaction wheels

there may be unexpected tumbling due to a failure in the attitude control subsystem. Due to this, the power system can get affected as the solar panels are not pointed towards the sun continuously. For more details on the satellites that failed due to different reasons and the causes of different failures, we point the readers to [32, 104]. Chirper can monitor the source of major faults in a satellite that can arise due to unexpected voltage/current consumption levels, unforeseen tumbling, and thermal issues.

The Chirper is equipped with multiple isolated voltages and current measurement probes. These probes can measure both voltage and current consumption on different satellite subsystems in real-time and transmit the information to the ground station directly with its onboard communication module. Further, Chirper also embeds a low-power 9 Degrees of Freedom (DoF) Inertial Motion Unit (IMU) to measure other critical statuses of the satellite, such as tumbling (spinning) rate and attitude of the satellite (see Figure 5.2). The thermistors placed at different locations of a satellite connected to the Chirper using wires measure the temperature in those locations, thus modelling the thermal information.

The health parameters are transmitted at regular intervals to the ground stations over a low-power, long-range onboard communication system. If any of the subsystems under observation behave abnormally leading to power setbacks or communication blackouts, the information received from Chirper at the ground stations can aid the satellite manufacturer to take further steps to save the satellite. Even if there is faint telemetry from the satellite that is not being detected by the ground stations, the Chirper on the satellite can detect those signals or even decode them if the transmission frequency of the satellite is within the Chirper's supported frequency range. Further, Chirper is independent in its operation and electrically isolated from the satellite (parent). Hence, any damage in the subsystems of the satellite will not harm the Chirper, and the failure can be diagnosed without it being a part of the satellite. The complete isolation also ensures the safe and independent operation of the Chirper, providing redundancy in health monitoring.

Since Chirper is designed only to detect faults and monitor the satellite, it cannot fix the problem on the satellite on its own. However, the data received from it can aid in reviving failed satellites. Additionally, the received information has substantial weight in portraying the lessons learned to avoid such problems in the future. Most of the big satellites have bus monitoring systems and redundancy as a part of the Reliability Availability Maintainability, and Safety (RAMS) system. However, they are not completely independent and electrically isolated/contactless. To the best of our knowledge, we are the first to design such an independent, completely isolated hardware-based satellite health monitoring system for small satellites with the features mentioned above. In addition, the functionality can be expanded by allowing a Chirper to communicate with its parent satellite (say, via a wireless link) so that the emergency telecommand could be done via the Chirper too.

In this chapter, we present the design and working of the Chirper and provide insights into the common failures of the satellites and in-depth evaluation.

Motivation. The work presented here was necessitated because of the failures of two nanosatellites as mentioned in Section 3.1. In one of the satellites, the reason for failure was identified as follows.

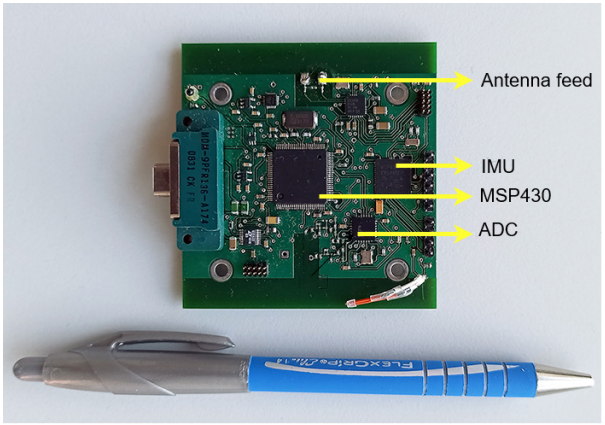

Figure 5.2: Chirper, a simple, self-powered, independent, and miniaturized satellite health monitoring system.

The satellite had a high-definition infrared camera as the primary payload, and its main mission was to capture photos of Earth at night (the anti-sun-lit side of the Earth). The satellite worked only for a few hours after the launch, and there were intermittent signals from the satellite for a few days. The satellite was even not responding to the telecommand signals, such as reboot and power-saving mode, sent blindly[2] from ground stations around the globe. The cause of the failure could not be determined. Twenty days later, there was a transmission from the satellite. From the telemetry received, it was identified that the heater system got damaged, and it was consuming all the available power from the battery as it malfunctioned around four hours after the launch. The primary bus voltage had dropped from 48 V to 8 V. Due to this, the battery drained intermittently, and the discharge cycle count crossed the allowed threshold, spoiling the battery. With the heater system and battery completely dead, the satellite is functional only when there is sunlight as the solar panel is intact but the primary mission was declared a failure, leading to a loss of $20 M. The heater system was optional, and even without it, the satellite would have been functional. Suppose there was a system that was independent of the electric power from the satellite that could send the status of the heater to the ground stations, the optional heater system could have been turned off immediately by sending commands to save the satellite and its battery. Apart from this nanosatellite, many other expensive satellites, such as Boeing's Intelsat 29e [108] costing anywhere between $400 and $450 M, failed in 2019 due to unknown reasons.

Contributions. The contributions of this chapter are as follows:

(**1**) We present a novel design of a miniaturized, low-cost, hardware-based isolated health monitoring system for satellites. To the best of our knowledge, we are the first to design such a solution.

[2] Blind commands are the configuration commands sent to the satellite even though, there is no telemetry from the satellite and its status is unknown.

(**2**) We implemented Chirper in a small form factor (5 cm x 4 cm, 32 g) by employing simple sensing and processing units using high-reliability space-qualified components. The design is open-source making it highly beneficial to the entire space community.

(**3**) We propose a novel methodology and a model to measure the low DC voltage based on capacitance technology that does not need any electrical contact for measurement. We are the first to provide such an isolated voltage measurement solution, and this technique can be used not only in the space domain but also in terrestrial applications.

(**4**) The proposed Chirper design is retrospective. It is flexible to be mounted anywhere - inside or on the body of a satellite - almost of any size. No customization or additional testing is required on the satellite.

(**5**) We conducted extensive measurements of Chirper through simulation (for isolated DC voltage measurement) and real-world testing by mounting it on an actual satellite. Further, by launching it on a high altitude balloon[3], we showed that the Chirper is functional even when it is tumbling (when the harvested power is intermittent).

5.1. REQUIREMENTS FOR THE CHIRPER DESIGN

Before proceeding with the design of Chirper, it is crucial to know the cause of critical breakdowns in a majority of the satellites. With this knowledge, Chirper can be equipped with specific components and features to detect these failures. These requirements were elicited from the known cases of satellite failures since 2000 [32, 104].

5.1.1. MAJOR CAUSES OF FAILURES IN SATELLITES

We categorize the prominent causes of failure in satellites as follows.

Mechanical or thermal failures. Structural failure in a satellite is mainly caused by collision with space debris. Mechanical failures are caused by unexpected faults in thermal mechanics (extreme heat or cold damaging the electronics), and external forces such as solar flares. Thermal control is one of the crucial subsystems of satellite development. The outer-body temperature of a satellite can go as high as 123° C and as low as -170° C depending on its orbit. It is important to maintain the temperature of electronics inside the satellite within their operating range [104, 109]; failing to do so can damage the electronics system severely, leading to the loss of the mission. Out of the satellite failures between 1980 and 2005, 32% were caused by mechanical or thermal failures [104].

Electronics. A survey from S. Tafazoli shows that almost 45% of mission failures are caused by a fault in electronics [104]. There are many reasons for electronic failure:
(1) If the active thermal control systems such as heaters fail to maintain the required temperature range inside the satellite, the electronic components can stop working. Especially, the battery is the most sensitive component in a satellite as they have a smaller operating range (0 - 60° C typically).

[3]The Chirper was stipulated to be launched in mid-2020 but it was put off due to the COVID-19 situation.

(a) Deployable type where the solar panels are deployed after launch

(b) Body mounted type where the solar cells are mounted on the satellite body

Figure 5.3: Solar panel configurations

(2) With the advent of Space Internet of Things[63] and satellite constellations, there is an enhanced interest in small satellites that are developed using COTS components as they speed up the manufacturing lead time, reduce cost, and increase productivity [9, 63, 109, 110]. However, most of the COTS components used in small satellites may not be tested for sufficiently long duration in the harsh space environment. COTS electronics in space have a higher chance of failure and swift performance degradation than space-grade components. Unlike COTS, space-grade electronics are radiation-hardened and support a higher operating temperature range, typically -55° C to 125°C. It is a fact that most of the small satellites do not use radiation-hardened electronic components, and the failure of such satellites is not a rare occurrence. Alongside, such components may not work in prolonged exposure to the vacuum in space. Hence, the subsystem built using COTS components should be monitored for its failure continuously.
(3) Radiations caused by cosmic rays, the intense magnetic field of Earth, and solar flares can cause, (a) Single Event Upsets (SEU): the change of state in electronics caused by a single ionizing particle such as ions, electrons, photons striking a sensitive node in an electronic device; and (b) Single Event Latchups (SEL): a type of short circuit that can occur in an integrated circuit in non-space-grade electronics components, leading to temporary or permanent damage to the subsystems. In the case of SEL, there may be power shorts wherein high current flows through electronic components, pulling the nominal voltage down. One of the solutions to fix the SEL is to perform a complete hardware restart of the subsystem as early as possible after the latchup. While SEL is resolved automatically in some satellites, this is still a manual process (by telecommand) involved for main subsystems such as OBC and power in the satellites with traditional designs. Prolonged SELs may permanently damage the system because of the high current. Chirper can monitor the SEL by monitoring the power consumption of subsystems and inform the ground stations for further actions.

Unexpected tumbling. When a satellite is ejected from the deployer, it starts tumbling (spinning) randomly. The tumbling rate and orientation depend on the force and course at which the deployer ejects the satellite. Depending on the type of solar panel, communication antenna configuration, and payload requirement, it may be necessary to stabilize the

tumbling in three axes as quickly as possible. Especially in the case of deployable solar configuration as shown in Figure 5.3a, it is essential to point the solar panels towards the sun by de-tumbling the satellite as quickly as possible to charge the batteries. If not, the batteries may be undercharged due to the intermittent sunlight. In the case of body-mounted solar configuration, the solar cells are mounted on the surface of the satellite as shown in Figure 5.3b. Though there may not be any problem with power in this case, a frequent break in the communication can be expected due to the rotating antenna [111]. The stabilization of the satellite is carried out by the ADCS in the satellites that can frequently fail [32, 104], leading to intermittent or no communication, or exhausting battery charge/discharge cycles. There are also several instances where Inertial Motion Sensors (IMUs) fail to sense the exact tumbling rate in three axes, leading to mission failure [104, 112, 113]. However, Chirper can independently estimate the tumbling rate of the satellite using its onboard IMU.

Software. Software failures are caused mainly by undetected software bugs, or the scenario that caused the bug was not reproducible on the ground during the trial. Additionally, blind and erroneous telecommands sent to the satellite can also introduce software bugs. However, we do not elaborate on the software bugs as it is out of the context of this work.

Miscellaneous failures. Apart from the aforementioned failures, the source of other not-so-frequent failures is next to impossible to pinpoint. It is also not possible to retrieve telemetry to investigate the reasons for a breakdown if there is a critical failure in the power or communication subsystem. As per a survey from NASA, the reason for failures are unknown for 16% of the total satellites failed between 2000 and 2016 [32].

5.1.2. DESIGN REQUIREMENTS

From the analysis of the major causes of failures in satellites, we list the following functional and non-functional requirements for the health monitoring system.

R.1: The utmost requirement is that the system must be electrically isolated from the satellite. This is to ensure that any malfunction (such as an electrical short) in the Chirper should not damage the other functional parts of the satellite and vice-versa. This scenario is analogous to Heisenberg's uncertainty principle, which says, "At worst, a sort of Heisenberg Uncertainty Principle occurs, where the attempts to characterize the behaviour of the system has distorted that behaviour to the point where the information obtained may be useless" [114].

R.2: it should be possible to monitor the supply voltage and the current consumption of the subsystems and payloads in an electrically isolated way.

R.3: the system should have its own power system to avoid leeching on the satellite's power system.

R.4: the system should have its own communication channel so that the status of the satellite can be known even if the satellite's communication module is faulty.

R.5: the system should determine the attitude of the satellite as well as the tumbling rate.

R.6: it should measure temperature at different locations of the satellite to validate the satellite's thermal system.

R.7: the system must facilitate flexible installation on different classes of satellites, without requiring any customization on the satellite. This will reduce configuration and management efforts for end-users.

Chirper meets all the above design requirements and monitors the critical faults in the satellites as specified by NASA and others in the literature [32, 104, 115].

A satellite in Low Earth Orbits (LEO) - ≈ 600 km altitude - has a revisit time of around 1.2 hours, i.e., a satellite is visible to the same ground station for communication again after one hour and twenty minutes. If there is any malfunction within this revisit time, the fault can be noticed only when the satellite is in contact with the designated ground station. Additionally, the satellite visibility duration (0 to 15 minutes for LEO satellites) may not be sufficient to decide and act on recovering the satellite by telecommand. Therefore, the Chirper communicates with ground stations in UHF amateur band, specifically between 435 MHz and 438 MHz (it can be tuned anywhere between 150 MHz and 960 MHz though), as fixed by the manufacturer. In this frequency range, the data from the Chirper can be received by amateur radio enthusiasts worldwide and sent to the manufacturer so that they can be ready with a decision to revive the satellite on its immediate next visibility.

It should be noted that a satellite may be equipped with a redundant module for each subsystem, which is usual in space-grade satellites, however, there are many instances where both the systems failed [104, 108, 116, 117]. Further, the health monitoring mechanism is generally integrated in OBC in the satellites, and they are software-based. Therefore, it is beneficial to incorporate a miniaturized isolated module such as Chirper to monitor the health of a satellite.

5.1.3. CHALLENGES IN DESIGNING THE CHIRPER

There are many challenges in designing a space-qualified Chirper. In this section, we list the major design challenges that need to be addressed.

Electric isolation. The Chirper must be electrically isolated from the satellite. In any case, a faulty Chirper (if it fails) should not damage a functional satellite. Achieving this is challenging when the isolated low DC voltage (0 to 48 V) measurement at high resolutions (e.g., in steps of 1V) is considered. There is hardly any work in the literature that performs isolated voltage measurements for low DC voltages.

Miniaturization. The system should be miniaturized and flexible to mount so that it can be integrated easily into a satellite. The mass should also be minimized to avoid unnecessary launch costs. Miniaturizing a space-grade module is challenging as most of the radiation-hardened components are bigger than their COTS counterparts. Miniaturization also constrains the size of the energy harvester, i.e., solar cells.

Communication. Because of miniaturization, the communication module should employ a miniaturized antenna while there should be reliable communication between the satel-

lite and the ground station. While the communication range should be as far as 2000 km for LEO satellites, the RF transmission power is also limited by the availability of energy from the tiny solar cells.

Power storage. While there may be power available when the solar cells point towards the sun, there won't be any power generation for Chirper when the satellite is on the anti-sunlit side of the earth (eclipse period). Sufficient power required to operate the Chirper should be stored when harvesting that can be utilized during the eclipse period. The space-grade batteries are huge (around 50 mm in length, and 10 mm in diameter), and high-capacity electrolytic supercapacitors are not suggested for space environments. Moreover, batteries also require stringent operating temperature conditions[4], –10° C to 50° C, which enforces special thermal insulation. Additionally, the satellite may not be equipped with attitude control systems, and the solar cells should generate sufficient energy even when the satellite is tumbling.

Reliability. The Chirper must be highly reliable in terms of operation. The electronic components chosen must work in a harsh space environment continuously. While space-grade components are bulky, very expensive, and are not conducive to low-power operations, there are limited non-space-grade integrated circuits that suit all the requirements of the Chirper.

Data processing. The Chirper should be equipped with its own low-power processing unit that can reliably process all the required health parameters and transmit them to the ground stations.

5.2. CHIRPER DESIGN

A faulty Chirper (if it fails) should not damage the functional satellite for which, even the voltage and current measurements of different subsystems must be isolated. Achieving this is challenging when it especially comes to isolated low DC voltage (0 to 48 V) measurements at high resolutions (e.g., in steps of 1V). There is hardly any work in the literature that performs an isolated voltage measurement for low DC voltages. Additional challenges include low-power long-range communication, power storage (while bulk batteries cannot be used), and reliability. Taking into account the requirements listed in Section 5.1.2, we propose a novel design of Chirper while addressing the challenges listed in Section 5.1.3.

The Chirper hardware comprises high-reliability space-qualified components. These components are generally manufactured and tested for avionics, military, and space applications. They are robust to harsh environments such as extreme temperature, vibration, and vacuum-like space-grade components. While they can tolerate radiation in LEO, they support the temperature range (-55 °C to 125 °C) as that of space-grade materials. They are also better than general COTS components (including industrial and automotive grade) in terms of reliability and failure rates.

When it comes to geosynchronous orbits with an altitude as high as 36000 km from the

[4]Temperature inside satellite can vary between -10° C and 80°C

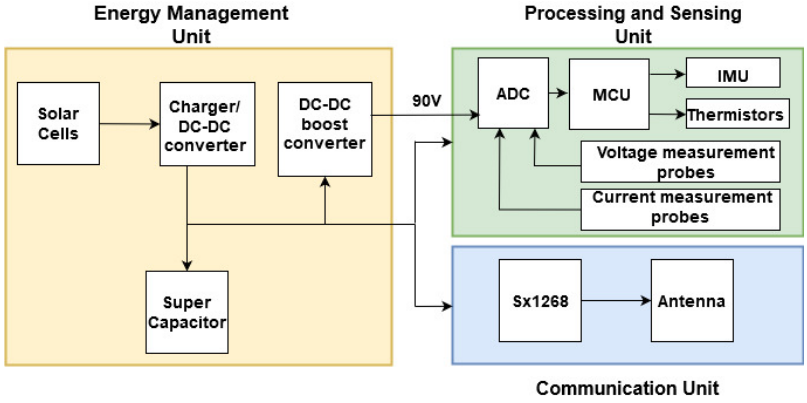

Figure 5.4: The block diagram of the Chirper showing three main units – energy management, processing, and communication unit

5

Earth, the radiation and temperature are extreme, and even these highly reliable components may fail. Hence, these components must be replaced with their space-grade counterparts for Chirper in geosynchronous orbits. However, designing a space-grade Chirper is out of the context of this work but the functional design and proposed algorithms are still the same.

5.2.1. ELECTRONICS

The block diagram of the Chirper is shown in Figure 5.4. The design consists of three main units: (i) Energy harvesting and power management; (ii) data processing and sensor unit, and (iii) communication unit. These units are explained in detail in the sequel.

A. ENERGY HARVESTING AND POWER MANAGEMENT

The Chirper is powered by space-grade solar cells – CTJ30 from CESI, each with a dimension 2 cm × 2 cm that delivers a maximum of 2.4 V, 70 mA. This specific cell is chosen because of its high efficiency of 28.5 % for such a tiny size. Alternatively, any other space-grade solar cell/cells can be used but it may impact the amount of harvested energy. Though Chirper is functional with just one solar cell, we recommend having at least one solar cell on each side of the satellite so that continuous energy will be available irrespective of the attitude of the satellite. The solar cells power the entire electronics through a solar charger IC ADP5090 from Analog Devices that can simultaneously charge a supercapacitor and deliver 3.3 V to the rest of the system. As soon as the satellite is deployed and the Chirper's solar cells are radiated, the supercapacitor starts charging, and the entire electronics is powered up. The supercapacitor acts as an energy bank when the sunlight is not incident on the solar cell. It was quite a challenge to find a tiny supercapacitor, that sustains in a vacuum and works in space. We chose Murata's DMT334R2S474M3DTA0 470 mF supercapacitor having the dimensions 2.1 cm × 1.4 cm × 3.5 mm because of its wide temperature range and robustness. Chirper is flexible to be mounted anywhere inside or outside a satellite; however, at least one solar cell mounted on the surface of the satellite is connected through the wires to the

Chirper.

There is flexibility to place the Chirper anywhere inside or outside a satellite. The only restriction is for the solar cells, whose mounting location needs to be carefully chosen to get good exposure to the sun. Further, if the Chirper is placed outside the satellite, then it has to be covered with Multi-Layer Insulation (MLI) sheet to avoid exposure to extreme temperatures.

B. SENSING AND DATA PROCESSING

A low-power space-qualified microcontroller MSP430FR5969-EP from Texas Instruments is used as the data processing unit. It operates at 16 MHz frequency. It supports up to 16 ADC channels to which the thermistors and isolated voltage and current measurement sensors or a combination of them can be connected. The principle and implementation of isolated voltage and current measurement units are explained in Section 5.3 in detail. Further, one I2C and SPI channel from the microcontroller is facilitated over the Micro DB-9 connector to connect any external sensors if required by the satellite manufacturer. A low-power onboard miniaturized IMU ICM-20948 from InvenSense equipped with a 3-axis accelerometer, 3-axis gyroscope, and 3-axis magnetometer is used to estimate the body tumbling rate and attitude of the Chirper, and in turn, the host satellite.

C. COMMUNICATION

There are many design choices for the communication unit to transmit the signals. Techniques such as Frequency Modulation, Phase Modulation, and Amplitude Modulation call for high RF transmission power (as high as 1 W) to cover the LEO altitude of 2000 km. As the harvested power is limited, we choose LoRa as the modulation technique to transmit the telemetry. Moreover, when the satellite is tumbling, if the Chirper's antenna is disoriented along with that of the satellite, then the telemetry received may contain a low Signal to Noise Ratio (SNR). It is very crucial in such situations to decode the signals successfully. LoRa supports SNR as low as -20 dBm. This leaves us to choose Semtech's SX1268 chip as it has proven flight heritage. SX1268 supports RF frequencies between 410 MHz and 810 MHz to be tuned for transmission/reception and the maximum transmission power of 22 dBm. We tune it to the UHF amateur frequency (anywhere between 435 MHz, and 438 MHz as fixed by the International Telecommunication Union (ITU) for a satellite). In this frequency range, the data from the Chirper can be received by amateur radio enthusiasts[5] all over the world; they send the collected information to the manufacturer/owner so that they can take necessary action. We chose amateur frequencies for two reasons: (a) When a satellite breaks down, it may not be in the visibility of the designated ground station. Thus, a network consisting of such radio enthusiasts around the globe will be handy when emergency telecommand is needed; and (b) Multiple signal receptions by the enthusiasts in the neighbourhood can help in providing data integrity (and redundancy) during the intermittent and/or broken signal reception.

SX1268 supports both Frequency Shift Keying (FSK) and LoRa modulation schemes. FSK can also be employed on Chirper, provided that the receiver antenna on the ground station must have a very high gain to meet the link budget calculations. The selection of LoRa

[5] Radio amateurs are enthusiastic about space technology and they track satellites continuously.

or FSK is left to the satellite manufacturer. For LoRa, we choose the spreading factor SF7 at 125 kHz bandwidth over SF12 to reduce the airtime. However, SF12 achieves a longer communication range and better sensitivity compared to that SF7 at the cost of bandwidth and airtime. The maximum payload size is limited to 222 bytes because of the chosen SF factor. However, there is no limitation for FSK.

Note that Chirper telemetry and the main satellite communication can co-exist and operate simultaneously provided that both the units are not employing the same modulation technique, and are on the same frequency band. If multiple satellites with Chirper mounted on them are in the field of view of a ground station, the chances of RF interferences are extremely low as the frequencies are allocated by ITU depending on the satellite orbit to avoid RF interference as much as possible.

A fixed UHF dipole antenna of gain 0 dBi is used in Chirper for transmitting telemetry and also to monitor the status of the host satellite's communication system. This is an easy way to find out whether the communication subsystem is working, and at what power. It should be noted that an RF limiter is placed between the receiving path of SX1268 and the antenna to avoid saturation or damage to the chip because of RF coupling from the host satellite's high-power RF transmission. An optional U.FL connector is also provided in the Chirper to connect an external antenna if the Chirper is placed inside the satellite. The external antenna must be omnidirectional so that the ground station can receive the signals even when the satellite is tumbling. The overall power consumption of the Chirper is around 250 mW when transmitting at 22 dBm, and at most 125 mJ of energy is required to sense, process, and transmit once with LoRa (at 22 dBm) at SF7.

While we present the Chirper design and communication details for satellites in LEO, Chirper can also be mounted on satellites in Medium Earth Orbits (MEO) and higher. In this case, all the components used must be of space-grade counterparts due to extreme temperature changes and radiations. Additionally, the ground station must have a very high gain antenna to receive the signals from Chirper even if the telemetry is on LoRa.

5.2.2. SOLAR CELL CONFIGURATIONS AND ENERGY HARVESTING

The Chirper is powered by six individual solar cells that are connected in parallel to each other. The solar cells must be chosen optimally for the given real estate. As the cells are typically small, the energy harvested from them is limited. Despite this, the Chirper needs to operate in all instances, including the case when the solar cells are intermittently pointed towards the sun during tumbling. Therefore, it is necessary to analyse the harvested energy from all the solar cells in sun-pointing conditions and optimize it for reliable measurement and data transmission. At the same time, sufficient energy should also be stored in the supercapacitor so that the Chirper can operate even during the eclipse (when the satellite is on the anti-sun side of the earth).

While the satellite orbit and the tumbling rate (from onboard IMU) are known, it is possible to predict the attitude of the satellite with respect to the sun to estimate the amount of energy that can be harvested at any time. However, this requires additional sensors on board, such as a sun sensor, to determine the sun angle. Further, Chirper needs to ensure continuous and accurate timekeeping without any clock drifts along with the Sun-Earth visibility model stored onboard. Any reboot cycle on the Chirper disturbs this timekeeping.

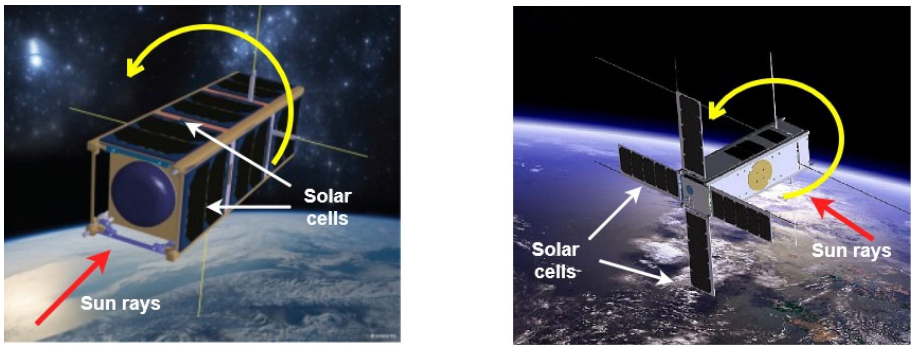

(a) Solar cells are mounted on five sides of the satellite. Only the side without solar cell is facing towards the sun

(b) Deployable solar cells on a tumbling satellite. The yellow arrow shows the tumbling direction

Figure 5.5: Solar cells configuration - body mounted type and deployable type

With a solar power model, we first explain why six solar cells are necessary, even though the Chirper can be operated with one cell.

Why six solar cells? Though the Chirper can be powered using a single solar cell, we choose to mount at least one cell on each side (considering a more common cuboid satellite) of the satellite for energy harvesting. We explain the need for six solar cells by providing example configurations with five and two cells. Let us consider a scenario in which the solar cells are mounted on five sides of a cuboid satellite. Assuming that the satellite is not tumbling, there may be a case where the side without a solar cell is pointing towards the sun continuously, as depicted in Figure 5.5a. Even if the satellite is tumbling in the direction indicated by the yellow arrow in Figure 5.5a, the sun rays are not incident on any of the five solar cells. In such cases, no energy is harvested, and the Chirper is switched off until the sun rays are incident again. This gets worse as the solar cell count decreases. Let us consider another scenario in which the solar cells are deployable, as shown in Figure 5.5b. The tumbling direction (marked by the yellow arrow) and the incidence of the sun rays are shown in the figure. Even in this case, the solar cells are not illuminated irrespective of whether the satellite is functional or not. Hence, if all the sides are mounted with at least one cell on each side, Chirper will always be powered. Thus a minimum of six solar cells are required to ensure the reliability of operation. However, the number of solar cells to be used is left to the satellite manufacturer.

Now, we proceed to provide a model for the amount of energy generated by the solar cell configuration at any time, irrespective of whether the satellite is tumbling or not.

A. ENERGY HARVESTING

In this section, we provide a theoretical basis for estimating the total harvested power by six solar cells at any time. It is easy to estimate the total harvested power when the solar panel is at a constant incident angle with respect to the sun. However, it is not easy to find the total power when the satellite is tumbling. We thus provide an analytical study to find the average minimum harvested power independent of the tumbling rate and/or orientation

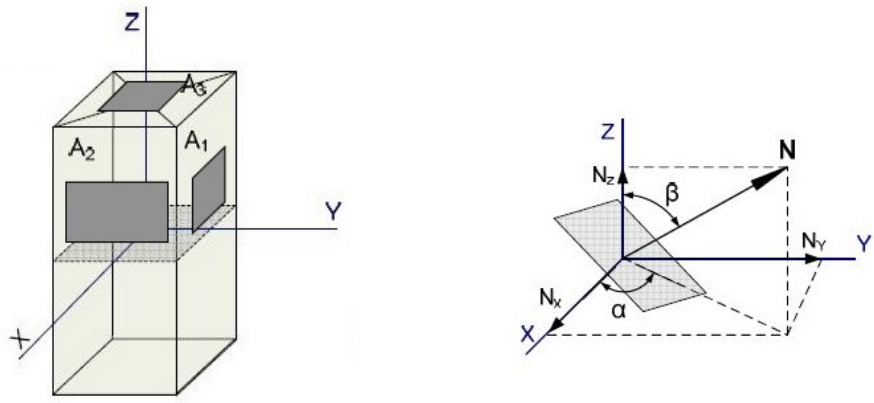

(a) Three solar cells mounted on three sides of a satellite (b) The geometry of the solar cell when incident to the sunlight

Figure 5.6: Placement of solar cells on a satellite and geometry of sunlight incidence

of the satellite. This is an important result that helps in designing the electronics on the Chirper.

For a cuboid satellite tumbling in any direction, at most three sides are pointing toward the sun. Let us consider three solar cells having equal area, each mounted on three sides of a tumbling satellite, as shown in Figure 5.6a. Let N be the normalized vector to each solar cell that is parallel to the sun's incident rays as shown in Figure 5.6b. If N_x, N_y, and N_z are the three imaginary vectors along x, y, and z axes, then the amount of power generated for any cell at any time depends on the angles α and β, and the horizontal and vertical inclination of the cell with respect to the vector N. According to Lambert's Cosine law, the radiant intensity or luminous intensity observed from an ideal diffusely reflecting surface or ideal diffuse radiator is directly proportional to the cosine of the angle between the direction of the incident light and the normal to the surface [118]. Hence, the average power 'P' generated by a solar cell can be given as,

$$P = P_k A \eta, \tag{5.1}$$

where P_k is the solar constant and equals 1367 W/m^2, A is the area of the cell that is incident to the sun rays, and η is the efficiency of the solar cell.

The total projected area, A_t, of all the cells combined in the direction of the sun for 90°rotation is [118],

$$A_t = \int_0^{\pi/2} \int_0^{\pi/2} (A\sin\beta\cos\alpha + A\sin\beta\sin\alpha + A\cos\beta) d\beta d\alpha. \tag{5.2}$$

$$\implies A_t = A\left(2 + \frac{\pi}{2}\right) \tag{5.3}$$

Note that the negative values of angles are discarded as the cell is illuminated for angles between 0 and $\frac{\pi}{2}$. Considering three solar cells, the average area A_{avg} of the cell on each

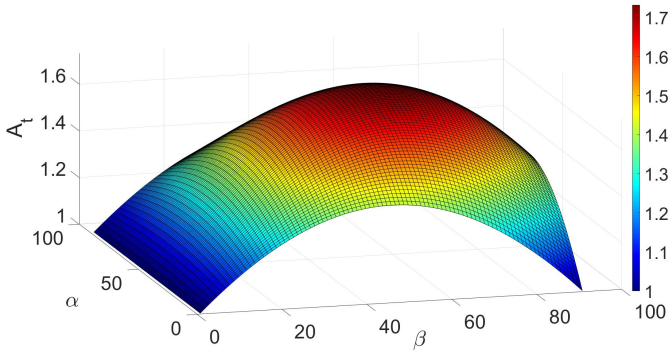

Figure 5.7: The total area of the three solar cells in parallel is a cosine function of the angle between the incident sun rays and the surface of the solar cell

side that is incident to the sun during tumbling is,

$$\frac{1}{A_{avg}} = \frac{1}{A_t}.\int_0^{\pi/2}\int_0^{\pi/2} \mathrm{d}\beta\,\mathrm{d}\alpha \implies A_{avg} = \frac{A_t}{\pi^2/4} \tag{5.4}$$

For all values of α and β in steps of 1° between 0 and $\pi/2$, the values of A_t are shown in Figure 5.7. From (5.2), we observe that the minimum and maximum values for A_t are 1 and 1.732, respectively.

Substituting (5.1) and (5.3) in (5.4), we get the average power P_{avg} generated during tumbling as,

$$P_{avg} = 1367 \text{ x } A\Big(\frac{8+2\pi}{\pi^2}\Big)\eta. \tag{5.5}$$

For the six-cell solar configuration, we considered CTJ30 solar cells from CESI. The area of each cell is 0.0004 m^2, and η = 28.5%. Substituting these in (5.5), there will be a minimum power of 155 mW harvested at any time irrespective of whether the satellite is tumbling or not.

B. CHOOSING THE DUTY CYCLE

With the available harvesting power of 155 mW, we need to choose an optimal duty-cycle period for operating the Chirper, thus minimizing energy consumption. The maximum eclipse duration for a LEO satellite is around 35 minutes [119] in its complete orbit of 2 hours (around 500 km altitude). During this period, i.e., the satellite is on the anti-sun side of the earth, and there is no energy harvesting. Hence, we need to ensure that the energy stored in the capacitor during the sunlit duration of 1 hour 25 minutes (=5100 s) lasts for at least 35 minutes of the operation of Chirper.

When the Chirper is turned ON, it collects the health parameters of the satellite, processes them, and then transmits them over LoRa communication unit. We call this an active period. The transmission duration (airtime) of LoRa depends on the spreading factor chosen and the transmission bandwidth. The spreading factor has to be wisely chosen as it impacts the link budget, in turn, the transmission distance. We choose SF7, 125 kHz

bandwidth, and the maximum available transmission power of 22 dBm (contributing to the worst-case power consumption). The airtime for transmission of 222 bytes in SF7 is around 370 ms, which results in the total time required for the Chirper to sense, process, and transmit is around 500 ms. Hence, the energy consumption for one transmission (250 mW × 500 ms) is 125 mJ. For FSK, it is lower due to shorter airtime ≈250 ms to transmit at 9.6 k baud rate. Hence, we consider the worst case of 125 mJ per active period. When the Chirper is not active, the microcontroller is in sleep mode, and the rest of the electronics are turned OFF to consume only 1 mW power.

If $P_A = 250$ mW is the active mode power and $P_S = 1$ mW is the sleep mode power of the Chirper, the duty-cycle can be represented as $t_{\text{ON}} + t_{\text{OFF}}$ which is nothing but the total orbital period, i.e., 2 hours. t_{ON} is the duration equivalent to TN_t, where T is the duration of transmission and N_t is the number of transmissions in one orbit. t_{OFF} is the duration when the Chirper is in sleep mode. Now, let us calculate the number of active periods, i.e., the regular intervals at which there will be a transmission. We start by budgeting the energy harvested and the energy spent in one orbit. We know that energy harvested during the sunlit period, $E^{(t)}$,

$$E^{(t)} \geq E^s + E^e, \tag{5.6}$$

where E^s is the energy spent during the sunlit period and E^e is the energy spent during an eclipse. Further, we know that energy harvested during the sunlit period is 155 mW x 5100s = 790.5 J. Now,

$$\begin{aligned} E^s &= P_A * t_{\text{ON}} + P_S * t_{\text{OFF}}, \\ &= 0.125N_t + 5.1 - 0.0005N_t \text{ Joules} \end{aligned} \tag{5.7}$$

Similarly,

$$\begin{aligned} E^e &= P_A * t_{\text{ON}} + P_S * t_{\text{OFF}}, \\ &= 0.125N_t + 2.1 - 0.0005N_t \text{ Joules.} \end{aligned} \tag{5.8}$$

Substituting (5.7) and (5.8) in (5.6), we get $N_t \leq 3156$. This means that there can be a maximum of 3156 transmissions in a single two-hour orbit period, i.e., once in every 3 s before the harvested energy is completely exhausted.

However, this can be increased to 30 s as the nominal visibility period[6] of a satellite in LEO varies between 30 s to 15 minutes [111]. Hence, the Chirper can transmit at least once in 30 s to ensure that the ground station receives a packet in all the visible passes.

C. CAPACITANCE OF THE SUPERCAPACITOR

When the satellite is in an eclipse, the supercapacitor is the only energy source. The capacitance of the supercapacitor that stores the harvested energy depends on the eclipse duration, the duty cycle period, and the energy consumption of the Chirper. Since we set the duty cycle period to be 30 s, we obtain the total energy required for the Chirper to be

[6]The visibility period is the duration for which the satellite is visible at a particular ground station. This period depends on the geographical location of the ground station, the orbit of the satellite, and the maximum angle at which the satellite is visible in that particular satellite pass.

functional during an eclipse is 10.82 J with $N_t = 70$ (70 transmissions in 35 minutes). The capacitor's maximum charge voltage is 4.2 V. Hence, the capacitance required is 1.22 F. We choose Murata's three DMT334R2S474M3DTA0 470 mF capacitors in parallel, summing up to the total capacitance of 1.41 F. These capacitors are charged completely when the satellite is on the sunlit side.

5.3. ISOLATED DC VOLTAGE AND CURRENT MEASUREMENT

In this section, we explain the design and working principle of the proposed isolated DC voltage and current measurement techniques. Before we proceed with our solution, we present the design choices available to measure DC voltage without any electrical contacts.

5.3.1. DESIGN CHOICES FOR LOW DC VOLTAGE MEASUREMENT

There are a limited number of options available for isolated DC voltage measurement.

1. Isolated DC-DC converters: The easiest way to measure DC voltage with isolation is by using DC-DC converters that offer isolation. The isolation is based on transformers or LED - photodiodes (optocoupler based). This system is not only bulky but also requires one part of the system to be electrically connected to the parent satellite. Any electrical short in the system can shut down the entire satellite.

2. Surface potential measurement: Surface potential sensors such as the EFS series from TDK measure DC voltage on the surface of a conductor [120]. These sensors provide complete isolation as they can be placed up to 10 cm away from the conductor, and mainly, there is no electrical contact required. However, these sensors are expensive and intended for detecting DC voltages over large ranges (0 to 1000 V). Generally, they provide a measurement resolution of 10 V which is not sufficient to measure the DC bus voltage (0-48 V) of a satellite. At least a resolution of 1 V is necessary as the bus voltage varies between 44 V to 48 V during nominal operation.

3. Capacitance on the cable insulation: There are a few works in the literature where coupling capacitance formed between the conducting wire and its insulation is measured to estimate the voltage. However, this technique is widely used for AC voltage measurements or to detect only the presence of high DC voltage.

None of these existing techniques can be used in our application as they do not provide complete isolation, or the resolution required by the Chirper. The unavailability of an isolated DC voltage measurement technique that suits the requirements of the Chirper motivated us to develop a new capacitance-based isolated DC voltage measurement technique.

5.3.2. DC VOLTAGE MEASUREMENT

The proposed technique to measure DC voltage on the main power bus of the satellite and other subsystems is based on the capacitance theory. A simple capacitor is created using two aluminium plates X and Y, and a dielectric material is sandwiched between them as

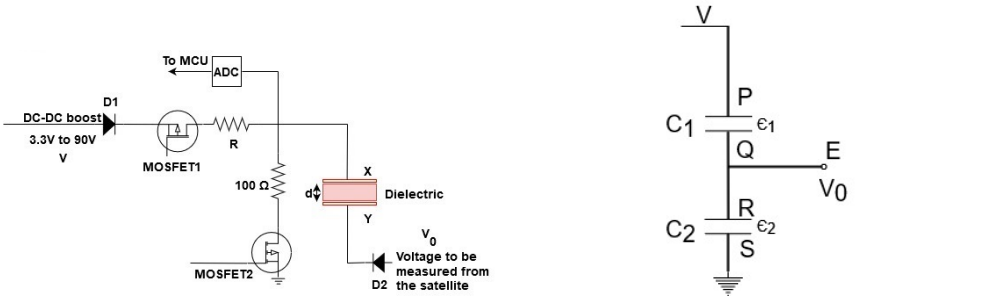

(a) Circuit diagram of the proposed low DC voltage measurement technique

(b) Working principle of the proposed voltage measurement model

Figure 5.8: Circuit schematics of the proposed Isolated DC voltage measurement technique

shown in Figure 5.8a. Plate X is connected to a DC power supply on the Chirper. Plate Y of the capacitor is connected to the voltage line to be measured on the satellite. The charging or discharging time of the capacitor depends on the voltage on plate Y, which can be measured by the microcontroller on the Chirper.

Working principle: To explain the working principle of the measurement technique, let us consider two capacitors C1 and C2, with dielectric 'ϵ_1' and 'ϵ_2' respectively, in series as shown in Figure 5.8b. A potential of 'V' is applied between the terminals P and S. The charge stored on each capacitor is equal to capacitance × voltage across its parallel plates. Let terminal 'E' be a tap from the junction point of two capacitors. If a potential 'V_0', such that $V_0 < V$, is applied on terminal 'E', then the charge stored across C1 and C2 varies proportionally to V_0. If V_0 is the voltage under measurement, it can be calculated by measuring the charge across C1 during its charge and discharge cycles. To ensure isolation, we modify this circuit as shown in Figure 5.8a, where the dielectric medium of C2 is replaced by vacuum, and plates Q and R are merged to form plate Y. Plate X is connected to a DC power supply V through a resistor 'R'. The charging/discharging of the capacitor is controlled by the microcontroller using two MOSFETS as shown in the figure. Both the Chirper and the host satellite will share a common ground.[7] A non-conductive dielectric medium is sandwiched between the plates X and Y. Since there is no electrical contact between them, the Chirper and the voltage line to be measured are isolated. As a safety feature, two diodes D1 and D2 make sure that there will not be any reverse current flow to the Chirper as well as the satellite voltage line. The capacitance 'C' of the capacitor is given by,

$$C = \frac{A\epsilon_0\epsilon_r}{d}, \tag{5.9}$$

where A is the area of plates X and Y, ϵ_0 is the absolute permittivity, a constant, and ϵ_r is the relative permittivity of the dielectric used, and d is the distance between the plates.

[7] all the subsystems of the satellite are connected to the electrical ground and the satellite structure to avoid the static charge that can arise due to charged plasma and cosmic rays in space

The area of the plates must be as small as possible for miniaturizing the system. However, this leads to a low capacitance, leading to less charging and discharging time that may be in the order of nanoseconds. Such a low-resolution time measurement is not possible with a 16 MHz MSP430 microcontroller. Hence, the charging/discharging time must be set to an extent that it can be measured by the microcontroller. Additionally, to avoid noise and offsets in the measurement, the capacitance between the plates should be much larger than the stray capacitance of the PCB traces and cables used for voltage measurement. Decreasing the distance between the plates to increase the capacitance can be an option, however, this is not suggestible as more gap between the plates ensures good isolation. From (5.9), the only way to increase the capacitance is by choosing a material with a high dielectric constant. Additionally, the charging time can be controlled by the resistor 'R'.

For a fixed capacitance 'C', the electric charge 'Q' stored in the dielectric is proportional to the voltage difference between plate X and Y. That is, $C = \frac{Q}{V-V_0}$, where V is the charging voltage applied on plate X and V_0 is the voltage on plate Y that needs to be measured. It should be noted that the charging voltage must be greater than V_0. Hence, if the maximum voltage that needs to be measured is 48 V, then $V > 48$ V. As the Chirper operates at 3.3V, a step-up converter should be used to boost the 3.3V input above V_0. We use LT3482 from Analog Devices to boost the input voltage of 3.3 V to 90 V, its maximum capability. The instantaneous voltage 'V_C' across the capacitor at time 't' is given by,

$$V_C = V\left(1 - e^{\frac{-t}{RC}}\right). \tag{5.10}$$

Initially, let us assume a case where plate Y is at the zero potential ($V_0 = 0$), and the capacitor is completely discharged. Let t_0 be the time taken to charge the capacitor to V volts (it is 90 V in our case) from zero. This is always a constant. In another case, when $V_0 > 0$, plate Y is initially at a potential of V_0. As soon as MOSFET 'M1' is switched ON and 'M2' is switched OFF, the capacitor starts charging towards V from V_0. Let the time taken to charge the capacitor from V_0 to V be t_v. The difference between the time 't_0' taken to charge the capacitor from 0 to V, and the time 't_v' taken to charge the capacitor from V_0 to V (where $0 < V_0 < V$) is equal to the time taken to charge the capacitor from 0 to V_0, i.e, $t_0 - t_v$. Hence, from (5.10),

$$V_0 = V\left(1 - e^{\frac{-(t_v - t_0)}{RC}}\right). \tag{5.11}$$

t_v is measured from the time when 'M1' is turned ON until the capacitor is fully charged. The voltage level on plate X is measured by the microcontroller using a high voltage analogue comparator as shown in Figure 5.8a. When M1 is turned ON, and M2 is OFF, one plate of the capacitor is at V_0, and another at V. Hence, the capacitor tends to charge from V_0 to V. It should be noted that both M1 and M2 are turned OFF when the voltage on plate X is being measured. Once t_v is measured, the capacitor is discharged by turning 'M2' ON and 'M1' OFF. We perform this cycle every 1 ms, and measure the capacitor voltage using ADC. Note that the capacitor is charged to V at $t = \infty$ according to (5.9). Hence, we consider the full charge condition to appear at 99.3% of V, which requires five times the time constant.

The nominal area of each capacitor plate is chosen to be around 1 cm^2 at a distance of 0.5 mm with a thin conjugated polymer as a dielectric medium having $\epsilon_r = 800$. This results in the capacitance of C = 1.42 nF between A and B. We choose R = 20$M\Omega$ to set a charging

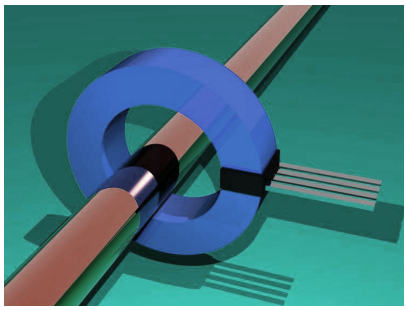

Figure 5.9: Isolated DC current measurement

time of 142 ms that can be easily measured by the 16 MHz microcontroller. However, we do not impose any restrictions on the value of the charging resistor, the size of the plate, the distance between the plates, and the dielectric property of the material. The goal is to have proper isolation while the capacitor is miniaturized.

5.3.3. DC CURRENT MEASUREMENT

The isolated DC measurement is straightforward. We adapt the existing non-intrusive method of estimating the current flow in the current-carrying wire. According to Ampere's law, the magnetic field generated around the wire is proportional to the current flowing through it. In other words, $B = \frac{\mu_0 \mu_r I}{2\pi r}$, where B is the magnetic flux density, μ_0 is the free space permeability, a constant, μ_r is the material permeability which is nearly unity for air, I is the current flowing through the wire, and r is the distance between the sensor and the wire. We use a TLE4997E2 hall effect sensor placed in the air gap of a flux concentrator as shown in Figure 5.9. The hall effect sensor provides a voltage output proportional to the magnetic flux around it. Thus, this method provides complete galvanic isolation.

5.4. EVALUATION

We evaluated the performance of Chirper in the following scenarios to establish its functioning.

(i) The proposed DC voltage measurement technique was validated with simulation and real-time voltage measurements.

(ii) The entire Chirper was mounted on a test system, and tests were conducted along with the Chirper in a space laboratory.

(iii) The Chirper was mounted on a helium balloon to emulate the distance, test the line of sight communication, and mimic the tumbling scenarios. In all these cases, we conduct different tests on the Chirper. In this section, we first provide the simulation results of the dc voltage measurement tests followed by tests on the satellite and balloon launch tests.

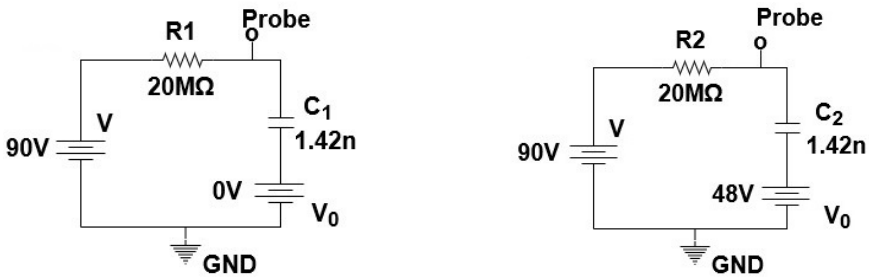

(a) $V_0 = 0$ (b) $V_0 = 48\,V$

Figure 5.10: Equivalent circuit of our proposed DC voltage measurement method

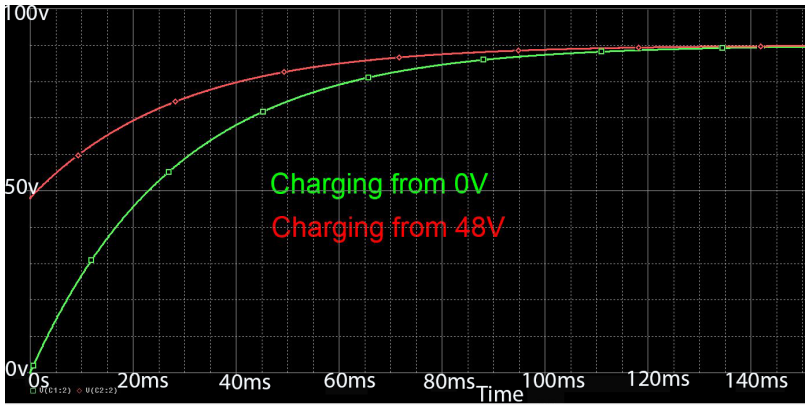

Figure 5.11: Simulation of capacitor charging.

5.4.1. SIMULATION

The validation of the proposed DC measurement technique was done with simulation on OrCAD and pSpice. We created an equivalent charging and discharging circuit of the proposed voltage measurement technique as shown in Figure 5.10. With this circuit, we validated (5.11) for different values of V_0. For example, we present our simulation for one case where the voltage to be measured $V_0 = 48\,V$. We consider two steps as explained earlier- (i) to measure t_0, V_0 was set to 0 V initially. This is a one-time calculation; (ii) V_0 was set to 48 V, and the capacitor was charged with $V = 90\,V$. R1 was set as 20 MΩ and capacitance to 1.42 nF as mentioned in Section 5.3.2. The pSpice simulation results are shown in Figure 5.11. According to simulation results, the time taken to charge the capacitor from 0 V to 90 V was 0.142 s, and the time taken to charge from 48V to 90V was 0.12035 s. Let us assume that V_0 is unknown. Now, using (5.11), we can calculate $V_0 = 48.007\,V$.

$$V_0 = 90\left(1 - e^{\frac{-(0.142-0.12035)}{20M\times 1.42n}}\right) = 48.007\,V$$

Thus, the simulation verifies our model.

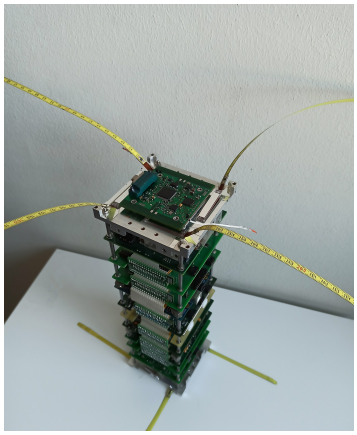

(a) Chirper on a nano-satellite

(b) Chirper tied to a helium balloon

Figure 5.12: Chirper on different evaluation systems

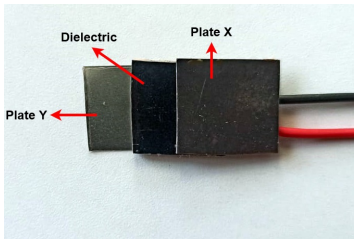

(a)

(b)

Figure 5.13: (a) Voltage probe (b) Current probe

The Chirper can be mounted on top of a space system, e.g., a nanosatellite as shown in Figure 5.12a. Chirper was powered by its own dedicated six solar cells (not shown in the figure). Multiple voltages and current measurement probes were connected across different subsystems of the satellite. A few thermistors - PS103J2 from LittleFuse placed at different locations (including the satellite body and a few critical chips on the PCBs) were connected to the ADC of the Chirper using wires to measure the temperature. Extensive tests were performed on the Chirper. Several table-top equipment, such as Tektronix DMM4020 digital multimeter, were used to validate the voltage and current measurements done by the Chirper. Figure 5.13a and Figure 5.13b shows our experimental voltage and current measurement probes, respectively. The capacitor plates of the voltage probe were covered with Kapton tape (which is not shown here) to ensure proper isolation and safety. The outer casing of the current probe was taken from Winson WCS1700 current measurement sensor. We replaced their hall-effect sensor with TLE4997E2 as it was not qualified for space. The wire-carrying current that had to be measured was passed through the centre hole of the probe.

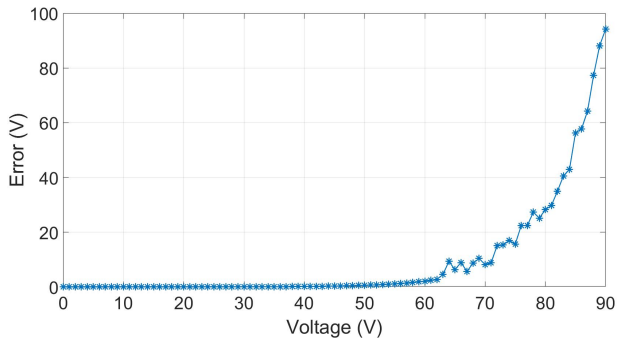

Figure 5.14: Error in measured voltage

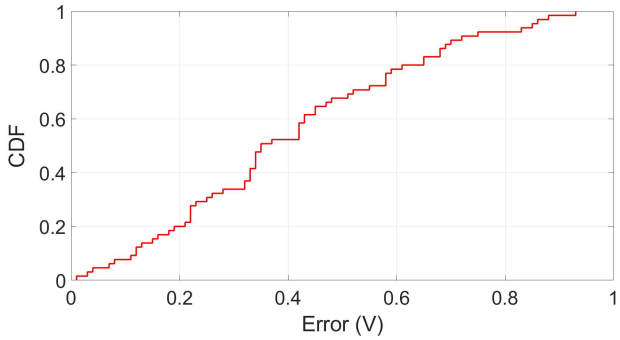

Figure 5.15: CDF of error in measured voltage for $V_0 = 0\,\text{V}$ to $50\,\text{V}$ while $V = 90\,\text{V}$

The tests performed were as follows.

LABORATORY TESTS

The accuracy of the proposed voltage measurement technique was tested using a function generator. Varying DC voltages from 0V to 90V in steps of 1V were applied on a resistor load with variable resistance up to $100\,\text{k}\Omega$. Using the measurement probes, the voltages and currents for different combinations were measured by the Chirper. Figure 5.14 shows the absolute values of error in voltage measurement for one channel. We observe from the figure that the error curve is exponential. This is because, when the difference between the charging voltage 'V' (see (5.11)) and the voltage to be measured V_0 is high, the capacitor takes more time to get charged. This time can be easily measured by the microcontroller. However, when V is very close to V_0, the capacitor will be quickly charged to full as one of the plates (plate Y in Figure 5.8a) of the probe is already at V_0. For example, in our setup, the measurement error was within $1\,\text{V}$, for voltage up to $V = 60\,\text{V}$. Beyond that, the error increases as the charge – discharge cycle of the capacitor is very short. Hence, depending on the measurement accuracy required and the maximum voltage that needs to be measured, the charging voltage V for the Chirper needs to be set. In our case, we choose $V = 90\text{V}$ as

(a) a 3-axis rotation mechanism shown here for clarity

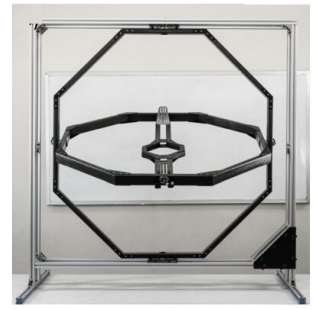

(b) A commercially available solar simulator

Figure 5.16: Solar simulator and rotating mechanism

most of the satellites have a bus voltage of 48V. The current measurement error was almost constant throughout the measurement range, irrespective of the current passing through the wire. The maximum error observed was 62 mA. For all the voltage/current channels used in measurement, the error plot for each channel is similar to the one shown in Figure 5.14. Moreover, each measurement channel is independent of the other and isolated.

Figure 5.15 shows the CDF of voltage measurement errors for $V_0 = 0\,\text{V}$ to $50\,\text{V}$ while $V = 90\,\text{V}$. We observe that 90% of the time the error is within 0.8 V, and the maximum error observed was 0.9 V.

ENERGY HARVESTING

The Chirper mounted on a 3-axis rotation mechanism was subjected to the solar simulator to test the amount of energy harvested. An example of a solar simulator is shown in Figure 5.16b. The simulator produces luminescence equivalent to 1 Sun luminosity. The Chirper mounted on a 3-axis rotating mechanism FFT Gyro-450 [121] (which is usually used to test drones) from Eureka Dynamics is shown in Figure 5.16a, and it was placed in front of the solar simulator. [8]. The 3-axis rotation of the satellite was facilitated by PC-based software and the emulated sunlight was made incident on the satellite. As solar cells were placed on all six sides of a test system to power the Chirper, the Chirper could harvest at least 145mW of power irrespective of the tumbling direction or speed. This almost falls in line with the theoretical value 155 mW, as mentioned in Sec 5.2.2. Voltage lines with different potentials - 3.3V, 5V, 7.2V, 8V, and 12V were emulated and were measured using the Chirper. The required current measurement range was 0A to 1.5A. The results obtained were similar to the ones during lab tests.

Apart from the above tests, the Chirper has undergone environmental tests required by the launch providers - high vibration level and thermo-vacuum cycles. Our Chirper passed all the tests.

[8] The photograph of the actual large-scale test setup is not permitted to be reproduced here

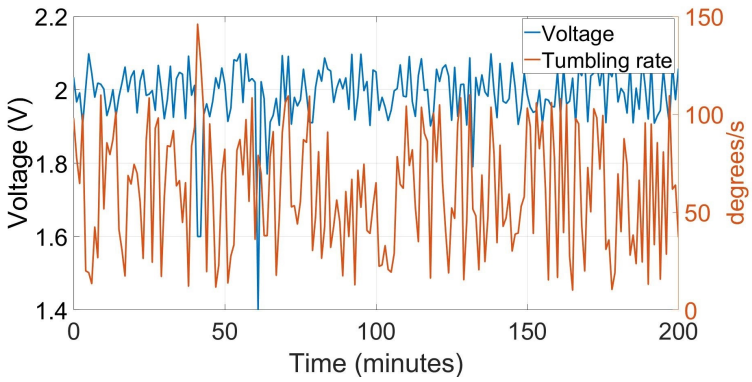

Figure 5.17: Voltage generated by the solar cell during tumbling

5.4.2. CHIRPER ON A HIGH ALTITUDE BALLOON

The Chirper was launched on a helium balloon up to 2 km from the ground station receiver to emulate the tumbling scenario and validate the communication range. The Chirper, along with a single CTJ30 solar cell from CESI was tied to the balloon and left hanging as shown in Figure 5.12b. As the balloon went up, it started tumbling and drifted due to the wind. The tumbling speed was calculated using IMU. The measured harvested voltage, current, and tumbling rate were sent to the ground on LoRa (SF7, 125kHz), as well as with FSK every five seconds. The transmission frequency was set to 436 MHz, and the transmission power on the Chirper was set to 22 dBm. A -2 dBi monopole antenna was used on the Chirper. The communication packet size was set as 14 bytes.

SOLAR CELL VOLTAGE VS TUMBLING

The voltage generated by the solar cell at different tumbling rates for 200 minutes of the flight is shown in Figure 5.17. The voltage is averaged over one-minute measurements. Irrespective of the tumbling direction/rate, the solar cell was incident on the sunrays most of the time. It generated sufficient power for the Chirper to operate even with a single solar panel. However, in some instances, e.g., around 60^{th} minute, the solar cell voltage dropped instantaneously. This is because the solar cell was under the shadow of the balloon and the sunlight was not incident on the cell at 90°. As there was no attitude control on the balloon, the tumbling rate was very high – as high as 146°/s as shown in Figure 5.17. However, in an actual satellite, the tumbling rate will be much less than 146°/s. Thus this experiment depicted the occurrence of the worst-case scenario. This evaluation also validates the Chirper to be functional even with a single solar cell; however, six solar panels would help if the orientation is not proper, as discussed earlier.

COMMUNICATION– LORA VS FSK

The data transmitted by the Chirper on the balloon was received on the ground using a custom-designed SX1268 board and 5 dBi yagi antenna. The RSSI obtained at different distances for both LoRa (SF7) and FSK is shown in Figure 5.18. It is known that at the same

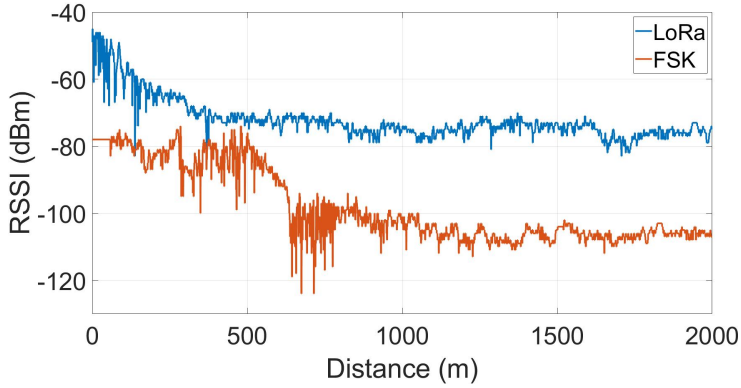

Figure 5.18: RSSI of the received signal from the balloon

transmission power, LoRa outperforms FSK over distance. This is evident from Figure 5.18. Though the distance between the receiver on the ground and the balloon went up to 2 km, we extrapolated the obtained RSSI results up to 2000 km - the outer edge of the Low Earth Orbit. As per the Friis transmission equation, we could get the extrapolation result as -129 dBm for 2000 km where LoRa chip (whose receiver sensitivity is -136 dBm) can decode the messages successfully. However, this is not feasible with FSK at the previously mentioned power and antenna gains. Indeed, the communication distance can be increased further by operating LoRa with higher spreading factors such as SF12 at the cost of huge bandwidth and longer airtime (more than 1.6 s to transmit 14 B at 125 kHz). However, the selection of physical layer, spreading factor, transmission bandwidth, and antenna gains is up to the satellite or parent space system manufacturer.

5.5. RELATED WORK

In this section, we list relevant works in the literature that are close to a fault monitoring system, such as Chirper.

Fault-monitoring systems in terrestrial applications are not new. There are ample works in the literature that concentrate on supervising the critical systems for failures [122–125]. Most of them are either software-based where failures are detected based on abnormal data from the sensor units, or they are contact-based where there will be an electrical contact between the measurement module and the target hardware. These solutions cannot be used on satellites as isolation is a requirement. Indeed there are a few isolated voltage measurement techniques where the voltage on a current carry line is measured without having any electrical contact. However, these target high-voltage AC measurements using capacitance technology, wherein the coupling capacitance formed between the current-carrying conductor and the cable insulation is measured. This capacitance is mapped to the voltage on the conductor [126–129]. TDK released a surface potential sensor to measure high voltage DC (0 - 1000 V) without any contact. The sensor can be placed as far as 10 cm from the surface of the conductor on which the voltage has to be measured [120]. The sensor has a

resolution of only 10 V, and the integration is complex because of the placement requirements.

Apart from software, the most common approach to fault detection and identification is hardware redundancy. If one of the subsystems fails, then its redundant part starts functioning. Having redundancy increases the reliability of the system but it may not identify the fault. Further, many satellites that failed in the last two decades had redundancy in their subsystems [32, 104]. In some cases, one of the subsystems is responsible for monitoring the health of the satellite and transmitting it to the ground station as housekeeping data. Traditionally, in the context of satellites, health monitoring was performed based on the limits of sensor values and power consumption. This method does not provide complete details on the failure as the monitoring results are binary. For instance, we can know if the temperature is above or below a threshold but not the actual value. T. Yairi et al., proposed a novel anomaly detection method for spacecraft systems based on data-mining techniques. [105]. Data mining provides a tighter bound to the limits. The solution does not include any additional hardware on the satellite but mining is done on the housekeeping data obtained from the satellite. The monitoring process is entirely data-driven. Similarly, S. Bottone et al. presented a novel technique to diagnose and predict the failure of a satellite subsystem using Bayesian network and probabilistic approaches [106]. The technique needs to have prior knowledge of the sensor data, and it is completely data-driven. A satellite health monitoring system that reduces the need for hardware redundancy is proposed by R. H. Chen et al [107]. The proposed technique uses a modelled dynamic relationship between system inputs and measured system outputs to form a residual process used to detect and identify faults. The monitoring algorithm resides on the On-Board Computer of the satellite and entirely relies on the data obtained from the satellite.

Health monitoring and fault detection in embedded systems have a lot of literature but they cannot be employed as is, for the following reasons.

(1) Most of the existing methods for monitoring the health of satellites are based on data analytics, which employs the historical data received from the satellite. There may be cases, such as in GSAT 6A, wherein specific commands have to be up-linked to the satellite immediately when the subsystems are in a particular state in case of issues [117]. The existing software and statistical data approaches may not be beneficial in this case. Alongside, conventional fault detection methods generally require a tremendous prior knowledge of each satellite's system behaviour, whereas that kind of knowledge is not always obtained easily beforehand. For example, a perfect dynamics model for simulating all the possible failure cases is too expensive to prepare for each satellite. To this end, we present a new independent and isolated system for monitoring the health of a satellite. Though the notion of Chirper is not new and fault monitoring systems do exist in the embedded systems domain, Chirper revisits it with a new, isolated, and reliable approach.

(2) Re-use of knowledge from past missions is also limited because each spacecraft is usually more or less different from the past ones. Another reason is that these methods can grasp only limited aspects of overall spacecraft system behaviour. For example, limit-sensing examines only the upper and lower bounds of individual sensor values; dynamics simulation can be performed on only several subsystems such as attitude control systems.

(3) The existing fault monitoring techniques need to be electrically connected to the

satellite, and they rely on the satellite's main power. Therefore, any failure in the satellite's primary power system affects the health monitoring module.

(4) High-resolution isolated voltage measurement is necessary to monitor the voltage levels on different subsystems of a satellite. For instance, the functional solar panel voltage or a battery can vary between 9V and 13.1V; hence a measurement resolution of 1V would suffice. To the best of our knowledge, there is no isolated DC voltage measurement that can provide a resolution of 1 V measuring low voltages in the range 0 to 48 V. Chirper provides the DC voltage measurement accuracy of 1V. However, the proposed measurement technique can be improvised to get accuracy in mV by choosing an appropriate capacitor plate material and dielectric medium.

5.6. CONCLUSION

In this chapter, we presented a novel and complete design of a space system called Chirper. Chirper is a low-power, independent, low-cost system that monitors a large space system (parent), such as satellites, when mounted on them. The name is Chirper symbolizes the sound a bird makes to communicate. We explicated the need, requirements, and challenges in designing and developing such systems. SpaceWorks estimates that up to thousands of small satellites (in the mass range of 1-50 kg) will be launched over the next few years, thus, a system like Chirper will be highly sought after. We also provided a new approach to measure the DC voltage in a completely isolated way. Further, Chirper measures the current flow, orientation, and tumbling rate of the parent. We built a Chirper, tested its suitability for space launch, and evaluated its capabilities to collect health parameters in state-of-the-art simulators. We also launched Chirper on a helium balloon to test it in a highly unstable environment. Additionally, Chirper is capable of receiving telecommands from the ground station and communicating with the subsystems (of course, if wireless connectivity between the parent and the Chirper is enabled). Chirper can be used not only in space applications but also in terrestrial applications to monitor the health of several embedded devices.

Future work. While the Chirper is reliable in terms of operation, it can also fail and provide inaccurate measurements like any other space-grade component. In this case, we can adapt existing software-based self-heal techniques onboard Chirper, or historical data-based solutions on ground stations for analysis [123]. Moreover, Chirper only monitors the health parameters and does not fix the faults on board the satellite. If Chirper is provided with the ability to power control the different subsystems or communicate with them wirelessly, then we can command the subsystems using Chirper. The future work includes the removal of the harness used for thermal and voltage measurements by introducing wireless systems.

6

CONCLUSION

6.1. LOOKING BACK

Progress in low-power miniaturized electronics and wireless technologies has promoted the growth of IoT immensely in the past decade. Consequently, the number of IoT devices deployed is increasing rapidly, and new requirements, problems, and solutions are emerging. Space can be a suitable platform to solve many of these problems concerning the applications of IoT on the ground. These solutions are yet to be explored thoroughly in the space environment. We see much enthusiasm in the IoT industry with respect to small satellites to provide global wireless connectivity for IoT devices by taking one step further in the form of Space-IoT. As we discussed in Chapter 1, there is a commercial race to place thousands of low-cost satellites around Earth to enable space-terrestrial communication. Most of the existing satellites are not designed with IoT in focus, yet new revolutionary ideas and research are necessary to accomplish Space-IoT. However, adapting the existing satellite technology from the perspective of Space-IoT comes with many challenges.

This thesis is one of the first attempts in tackling issues for Space-IoT in the academic domain. In this work, we portrayed the primary challenges concerning embedded and networked systems to realize Space-IoT. We started with the goal of addressing prominent challenges - miniaturization, energy minimization, resilience, communication, and localization (listed in Chapter 1). To this end, we considered three subsystems of a satellite: communication, attitude determination, and health monitoring. We provide innovative solutions that consider minimizing energy consumption or working with a low energy budget. In this chapter, we briefly discuss the accomplishments of this thesis in Section 6.2 and then we argue the positives of this thesis and discuss the big picture in Section 6.3. We conclude this chapter by listing the vistas for the future.

6.2. ACCOMPLISHMENTS

In this section, we present the major contributions of this thesis.

6.2.1. SPACE-IOT.

We began with defining the term Space Internet of Things (Space-IoT), and then we elucidated how Space-IoT can complement the existing terrestrial IoT. The concept of Space-IoT involves a network of satellites to address the main challenges in terrestrial IoT deployments, that is, global coverage, scalability, and connectivity. Space-IoT has multiple benefits and applications compared to terrestrial IoT networks. As one of the contributions to the research community, we have charted out the crucial challenges at a higher level and provided a broader picture of the problems that need to be tackled for realizing Space-IoT.

6.2.2. SWANS.

As discussed in 2, Space-IoT is not just limited to the communication between a satellite and terrestrial IoT nodes. A satellite is already a collection of different sensor and actuator systems, hence, it is a network of IoT devices in space, where different electronic subsystems are connected using the harness. In this work, we pushed the boundaries by avoiding harness with the vision of a Sensor Wireless Actuator Network in Space (SWANS). While Space-IoT imposes new requirements for space applications, such as mass production, miniaturization, low-cost solutions, innovative system designs, and reliable inter-networking, SWANS charts a new domain towards realizing Space-IoT. Realization of SWANS requires innovation, optimization of form factor and weight, and higher levels of reliability. With SWANS, we presented our vision of many future innovations, such as radio interferometry, that are expected to make it easy in space in the coming years, wielding the developments in Space-IoT. We provided a new outlook to the research community to chart new horizons for innovations in space-embedded systems in the near future. While looking at the possible new horizons, we also, subsequently, listed some of the essential challenges that are needed to be addressed concerning miniaturization, resource optimization, embedded software, algorithms, wireless communications, and networking en route to realizing SWANS.

We selected major three problems to realize our vision as we envisaged in SWANS. We specifically demonstrated novel communications for Space-IoT, positioning subsystem, and a diagnostic tool for any space system while being highly energy-efficient. We recapitulate them in the sequel below.

A. Revisiting Frequency Shift Keying.

The existing terrestrial-based IoT devices are configured to communicate with gateway(s) or a cellular tower(s), which can be a few kilometres away at the maximum. However, in Space-IoT, these devices are expected to communicate with satellites directly – over hundreds of kilometres. Therefore, the signal received at an IoT node and a satellite is influenced by high degradation in SNR. Factors such as Doppler shift, phase changes in the ionosphere, antenna disorientation, and miniaturized antennas further affect the SNR thus the communication reliability. In the context of Space-IoT, we presented an energy-efficient communication scheme, called the Teager Energy Decoder (TED), for small satel-

lites and low-power sensor/actuator nodes. TED is based on the Teager Energy Operator (TEO) and decodes noisy FSK signals with low SNRs. TED eliminates the need for Two Line Elements unlike in the existing satellite-ground station communication. TED does not need any Doppler correction mechanisms and can dynamically adapt to the changing frequency shifts. We evaluated the performance of TED by employing it on actual telemetry signals received from two nanosatellites. Through simulations and our microcontroller-based hardware, we demonstrated that TED can be used to communicate between a terrestrial IoT node and a satellite.

B. An energy-efficient GPS module.

Localization is an important tool for enabling many applications, not only on the ground but also in space; indeed much more important. Localization is a huge challenge in space, because of the vast space and also due to the fact that satellites are orbiting at enormous speeds. The Satellite Positioning System (SPS) is known to be one of the subsystems that consume a significant portion of the available energy in small satellites. Hence, reducing the energy consumption of SPS is necessary within the vision of SWANS. In our work, we chose GPS as a standard positioning system and demonstrated how several important challenges in energy minimization can be addressed. We demonstrated how widely accepted duty-cycle-based solutions are ineffective if the Time-To-First-Fix (TTFF) is longer, which is usually the case in space-borne GPS receivers. We proposed an energy optimization algorithm called $F^3$to improve the TTFF, which is the main energy consumption phase during the cold start. Thus, improvements in TTFF enable duty cycling to assist in minimizing the energy consumption of the receiver efficiently. To evaluate F^3, we designed a low-power, low-cost GPS receiver called μGPS and launched it on three nanosatellites to obtain in-orbit results. The outcome was promising, wherein our receiver could save significant energy (up to 90%) compared to the state-of-the-art receivers. Further, the performance of μGPS was exceptional even when the satellite was tumbling. μGPS showed in a nutshell that miniaturization and the energy constraint that comes along would not adversely affect the accuracy of the positioning subsystem.

C. An independent satellite health monitoring system.

Space-IoT relies on a constellation of hundreds of satellites to accomplish global coverage. Apart from having backup satellites, it is crucial to monitor the health of all the satellites in a constellation to revive them in case of any failures. Most of the existing solutions are based on software and hardware diagnostics embedded with different subsystems of a satellite and are not isolated. Any fault in the subsystem may adversely affect its onboard health monitoring modules as they are electrically connected. We presented a miniaturized, independent satellite health monitoring system called Chirper. The Chirper can provide a secondary channel for the health monitoring systems of satellites. Chirper is not only energy-efficient but also measures the different health parameters of a satellite reliably. These health parameters are transmitted at regular intervals to the ground stations over a low-power, long-range onboard communication channel such as TED. Chirper can identify even critical failures such as main power blackouts and communication module breakdowns of a satellite. Further, to enable electrical isolation between Chirper and the

rest of the satellite subsystems, we proposed a novel methodology to measure bus voltage based on induced capacitive technology. We conducted extensive performance evaluations of Chirper through circuit-level simulations and tested it by mounting it on an actual satellite. Since we could not launch it during the COVID-19 period, we tested it by launching it on a high-altitude balloon emulating almost similar conditions by reducing the transmission power. We demonstrated that the Chirper is functional even when it is tumbling. When a satellite is in distress, the information provided by the Chirper can aid in diagnosing the fault. We believe that Chirper can aid in saving satellites in the future. It is also a significant step in showcasing what IoT can accomplish in space.

6.3. DREAM BIG BE SMALL

IoT has revolutionized a plethora of applications and becomes the building block of smart-* systems because of its low-cost, flexible, miniaturized, and easily deployable nature. In contrast, space systems, hitherto, are usually huge, high-cost, long-term development, and ossified. However, the vision of Space-IoT is to bring the characteristics of terrestrial IoT to space and connect the world globally. In this thesis, we addressed some important aspects of our vision - Space-IoT. In the previous section, we presented our accomplishments through demonstrable applications that prove the possibility of bringing the vision to life. However, in this section, we want to take a step back and reflect on the important challenges we started with (in Chapter 1) concerning the vision of Space-IoT. We briefly look at them in the sequel and share our learning.

Cost: COTS - Access to space is affordable if planned well. COTS components are a suitable alternative for space-grade radiation-hardened components for satellites in Low Earth Orbits. Recent developments in nanotechnology have contributed to the space community with “high-reliability” COTS components that are better than consumer-grade electronics in terms of reliability and performance in harsh temperature environments. Such components help to improve the overall resilience of satellites. Since the high-reliability COTS are readily available in the market and their cost is almost the same as that of consumer-grade components, the lead time is significantly lower compared to space-grade radiation-hardened components. All the subsystems that we presented in this thesis are equipped with high-reliability components. All the components have survived the environment tests, such as temperature, radiation, and vacuum, required for a satellite to survive in space. Further, our COTS-based μGPS performed well on a satellite in space, as discussed in 4.

Miniaturization: Small satellites are catching the eyes of many new players in the space market and are closely followed by many space organizations. Decades ago, a single rocket used to carry only one big satellite to space. The case is different now. ISRO’s 104 satellite launch on PSLV C37, and SpaceX’s recent 143 satellite launch in a single mission exhibit how miniaturization has enabled us to accomplish great things in the space industry. Interest in the miniaturization of satellites has also led to the conception of small launch vehicles, such as ISRO’s Small Satellite Launch Vehicle (SSLV) to launch small satellites in LEO. Such launch vehicles will soon become operational, and the launch bottleneck is set to decrease, thus opening up more room for frequent small satellite launches.

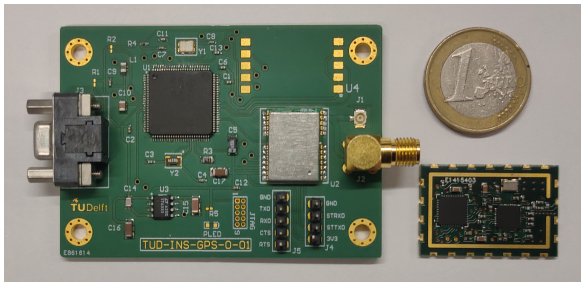

Figure 6.1: ηGPS (on the right) with dimension 30 mm x 20 mm, placed next to μGPS (on the left)

Miniaturization is a continuous process. Miniaturization continues to co-exist with advancements in nanotechnology. For instance, our μGPS having the size 60mm x 40mm, presented in Chapter 4, has now evolved into ηGPS, shown in Figure 6.1, with the dimension 30 mm x 20 mm as the next step of development. ηGPS has high-reliability COTS components, similar to μGPS but with better performance in terms of energy consumption and localization accuracy. Miniaturization is the gateway to sustained, quick, and inexpensive mass production and deployment of satellites. Since the cost is lower, small satellites can be replaced easily. Furthermore, miniaturization eases small-scale startup companies to develop small satellites swiftly and conduct missions that are difficult with large satellites.

Energy: Energy optimization in Space-IoT is necessary for every aspect of space technology. Reducing the energy requirement has a positive effect on miniaturization. For example, smaller solar panels and smaller power systems/modules lead to faster production and lower launch costs. In all three subsystems we built (Chapter 3, 4, and 5), we demonstrated how we could achieve energy minimization alongside miniaturization. These demonstrators certainly provide much more confidence in building more such energy-constrained, yet reliable, Space-IoT devices.

Resilience: In terrestrial applications, IoT is being used for making systems resilient, but to achieve this, IoT devices themselves need to be resilient. Taking this concept to space, we developed Chirper for monitoring the health of the satellites. Chirper can be mounted on any space subsystem.The system can even be adopted on terrestrial IoT applications. In the future, we expect Chirper to accompany every space system since it is low cost, and of a significantly small form factor. Space industries have already shown interest in this module. This may raise a question as to how resilient the Chirper is. The easy answer would be to deploy more Chirpers, e.g., on all sides of a satellite. This is possible because of the miniaturization, low cost, low weight, and capability to work with ultra-low-power.

Reliability vs Energy consumption: Reliability need not consume more energy. By designing systems and devices with reliability in mind, energy consumption can be optimized without compromising on reliability. This can be achieved by using energy-efficient components, reducing unnecessary features or functions, and optimizing software and hardware

design. Redundancy can be built into systems to increase reliability without consuming more energy. For example, redundant power supplies can be used to ensure that a system continues to function even if one power supply fails. Similarly, data can be stored redundantly to ensure that it is not lost if one storage device fails. Further, Predictive maintenance techniques can be used to identify potential problems in systems before they occur. By detecting and repairing issues early, system reliability can be improved without the need for excessive energy consumption. Optimizing systems to minimize energy consumption can also improve reliability. For example, reducing the number of unnecessary system checks or reducing the frequency of data transmission can reduce energy consumption without compromising system reliability.

Communication: Small satellites in LEO are expected to play a key role in 5G and 6G networks. Space industries are showing interest in using LoRa for Space-IoT applications in 5G, but this thesis proves that there is *ample space* to improve simple traditional communication protocols such as FSK. Communication in 5G and Space-IoT is a developing research field where optimizations for long-range, low-power, and high data rates are of key concern. Communication modules are pretty standardized however, Software Defined Radios (SDR) on a constellation of satellites will provide an appropriate platform to conduct innovative research by designing new communication techniques or optimizing the existing ones. The SDR platform must be made re-programmable over the air so that industries and academics can fine-tune their techniques without any need of launching a new satellite/payload. One of our future works includes developing a programmable SDR platform that allows space enthusiasts to easily deploy their satellite – terrestrial communication techniques for Space-IoT and test them.

Closing remarks. In this thesis, we have introduced Space-IoT as a new field of study. Space-IoT is an emerging field. While space technology itself is decades old, Space-IoT brings in a fresh breath of air and new dimensions, making it a hotbed for innovation. It is an interdisciplinary technology that combines space systems, structural, mechanical, electrical, communications, and importantly, embedded systems and software engineering. There are ample opportunities and challenges to address in accomplishing Space-IoT, and this thesis puts forth most of them under a single umbrella. We took a pragmatic and positive step to address the challenges by working on *what needs to be solved* rather than *what can be solved*. The challenges in realizing Space-IoT is something that *needs to be solved* and also *can be solved*! This work is foundational and provides the vision of Space-IoT. This thesis is the first step towards realizing Space-IoT. Within the *space* of these, we have demonstrated how we can proceed toward bringing the vision into reality. This field is vast, and we focused on embedded and networked systems in this dissertation. Space-IoT represents a new breed of mobile computing concept, that pushes us “beyond the clouds”.

6.4. WHERE NEXT?

The unique combination of challenges outlined in this thesis, along with their interdisciplinary nature, offers fertile ground for the mobile computing community to conceive new problems and their solutions, or to revisit existing solutions in a new context. Moreover, the

quest for efficiency within extremely limited resources does not forgive unnecessary complexity, and it eminently demands simple solutions to complex problems. The challenge lies in bringing together elegant and intuitive solutions.

The next step begins with addressing the challenges listed in Chapter 2, and SWANS must be fabricated. Miniaturization and energy minimization are of utmost importance in realizing SWANS. Though the frequency of launching small satellites has increased recently, their failure rate has also been significant (see Chapter 5). Hence, reliability is of great concern in the development of SWANS, which we have to consider prominently. While there is massive interest from the space industry in realizing Space-IoT, academics should also aid in fulfilling the needs of Space-IoT and address the challenges head-on.

The final step is to launch a constellation of SWANS in planned orbits. "Every eleph*ant* has an *ant* in it" – while a single ant cannot perform a major task, an army of them can accomplish elephantine tasks. Similarly, a cluster of small satellites can assist in connecting ground from space – linking anything, anywhere, and anytime. While there is a need to execute many tasks in different domains for realizing Space-IoT, we laid a foundation through this thesis in tackling the challenges. The list below provides a sneak peek into the near future.

Self-organization and self-coordination in satellites: As discussed in 2, Space-IoT is not just the communication between a satellite and terrestrial IoT nodes. Going one step ahead, Space-IoT also involves communication between sensors and actuators between satellites, and within a satellite. While satellites with artificial intelligence, self-healing, and/or repairing are becoming more prominent nowadays, multiple satellites must be enabled with the characteristics of self-developing, self-deploying, and self-coordinating as a swarm.

Removal of Debris: This is very crucial now because there are already more than 1 M space debris with the size >1 cm [130] orbiting the earth as of Aug 2022. Multiple small satellites in space coordinating with each other can help in identifying and cleaning space debris. In this context, we are working on Debrinet, which is a network of AI-based spacecraft that autonomously cleans space debris by attaching it to the debris and sending them back to Earth.

Radio Interferometry: Antenna design and deployment for sensing low-frequency radio (10 MHz or less) on a miniaturized satellite are extremely challenging because antennas for low frequencies tend to be large. Further, satellites need to be stable, deployment of huge antennas requires thorough design and expertise, and the coordination between multiple such satellites needs to be addressed. This will open up a new field of science, where experts from different fields need to come together. Some discussions on interferometry are presented in Chapter 2.

Remote sensing on low capability satellites: Huge satellites have significantly high resources to support, many applications, such as weather forecast, water resource mapping, and finding minerals. Mapping the earth accurately using fewer resources (and cost) from LEO satellites is a trade-off and it is further exacerbated by the high speed of small satellites. This requires agility among the payloads of the small satellites to operate under high resource constraints and also in challenging environments.

Epilogue

Billions of IoT devices will be deployed in the coming years and we need to be prepared to connect them to the Internet. Space-IoT is a game-changer for the future of IoT, and it opens a world of new possibilities by providing global network coverage, scalability, and connectivity. The future of IoT looks promising with *space* in fusion. We believe that space is largely an unconquered frontier where **even the sky is not the limit – literally and figuratively**.

BIBLIOGRAPHY

[1] J. Cañedo and A. Skjellum, "Using machine learning to secure iot systems," in *2016 14th Annual Conference on Privacy, Security and Trust (PST)*, pp. 219–222, 2016.

[2] N. M. Karie, N. M. Sahri, and P. Haskell-Dowland, "Iot threat detection advances, challenges and future directions," in *2020 Workshop on Emerging Technologies for Security in IoT (ETSecIoT)*, pp. 22–29, 2020.

[3] V. Galactic. `https://www.virgingalactic.com/`, 2021. [Online], last accessed - December 2022.

[4] B. Origin, "Blue origin." `https://www.blueorigin.com/news-archive/first-human-flight-updates`, 2021. [Online], last accessed - December 2022.

[5] ISRO, "University/academic institute satellites." `http://www.isro.gov.in/spacecraft/university-academic-institute-satellites`, 2017. [Online], last accessed - December 2022.

[6] m-cramer Satelliteenservices, "Iridium — satellite network." `https://m-cramer-satellitenservices.de/en/basics-solutions/iridium-satellite-network/`, 2023. [Online], last accessed - March 2023.

[7] Y. Yu, "The aftermath of the missing flight mh370: What can engineers do? [point of view]," *Proceedings of the IEEE*, vol. 103, no. 11, pp. 1948–1951, 2015.

[8] S. K. Routray and H. M. Hussein, "Satellite based iot networks for emerging applications," 2019.

[9] SpaceX, "Starlink." `https://www.starlink.com/`, 2021.

[10] L. space, "Lacuna - low-cost, simple and reliable global connections to sensors and mobile equipment." `https://lacuna.space/`, 2018. [Online], last accessed - December 2022.

[11] Y. Guan, F. Geng, and J. H. Saleh, "Review of high throughput satellites: Market disruptions, affordability-throughput map, and the cost per bit/second decision tree," *IEEE Aerospace and Electronic Systems Magazine*, vol. 34, no. 5, pp. 64–80, 2019.

[12] B. Foing, "Towards A Moon Village: Vision and Opportunities," in *EGU General Assembly Conference Abstracts*, EGU General Assembly Conference Abstracts, pp. EPSC2016–15695, Apr. 2016.

[13] Inmarsat, "Satellites - inmarsat." https://www.inmarsat.com/en/about/technology/satellites.html, 2021. [Online], last accessed - December 2022.

[14] S. Saleem, A. Bais, and R. Sablatnig, "Towards feature points based image matching between satellite imagery and aerial photographs of agriculture land," *Computers and Electronics in Agriculture*, pp. 12–20, 2016.

[15] M. Galli, S. Lardon, E. Marraccini, and E. Bonari, "Agricultural management in peri-urban areas," *Land Lab-Scuola Superiore Sant'Anna (Italy), INRA et AgroParisTech-ENGREF, UMR Métafort Clermont Ferrand (France)*, 01 2010.

[16] ORBCOMM, "Smart agriculture monitoring with iot and m2m | orbcomm." https://www.orbcomm.com/eu/industries/natural-resources/smart-agriculture-monitoring, 2021. [Online], last accessed - December 2022.

[17] eoPortal, "Dove-1 and dove-2 nanosatellites." https://directory.eoportal.org/web/eoportal/satellite-missions/d/dove, 2016.

[18] A. H. Stygar, Y. Gómez, G. V. Berteselli, E. Dalla Costa, E. Canali, J. K. Niemi, P. Llonch, and M. Pastell, "A systematic review on commercially available and validated sensor technologies for welfare assessment of dairy cattle," *Frontiers in Veterinary Science*, vol. 8, p. 177, 2021.

[19] B. G. Evans, "The role of satellites in 5g," in *2014 7th Advanced Satellite Multimedia Systems Conference and the 13th Signal Processing for Space Communications Workshop (ASMS/SPSC)*, pp. 197–202, 2014.

[20] Hiber, "Introducing hiberband." https://hiber.global/, 2018. [Online], last accessed - December 2022.

[21] Inmarsat, "Inmarsat to provide satellite connectivity to vodafone's internet of things platform." https://www.inmarsat.com/en/news/latest-news/enterprise/2016/inmarsat-provide-satellite-connectivity-vodafones-internet\-things-platform.html, 2021. [Online], last accessed - December 2022.

[22] S. Space, "Swarm - low cost, global satellite connectivity for iot." https://swarm.space, 2021. [Online], last accessed - December 2022.

[23] Semtech, "Semtech and swarm deliver satellite communications with lora." https://www.semtech.com/company/press/semtech-and-swarm-deliver-satellite-communications-with-lora, 2021. [Online], last accessed - December 2022.

[24] Astrocast, "Astrocast - taking iot further." https://www.astrocast.com/, 2021. [Online], last accessed - December 2022.

[25] J. Coopersmith, "Affordable access to space," *Issues in Science and Technology*, vol. 29, no. 1, 2012.

[26] D. Selva and D. Krejci, "A survey and assessment of the capabilities of cubesats for earth observation," *Acta Astronautica*, vol. 74, pp. 50 – 68, 2012.

[27] N. Saeed, A. Elzanaty, H. Almorad, H. Dahrouj, T. Y. Al-Naffouri, and M. S. Alouini, "Cubesat communications: Recent advances and future challenges," *IEEE Communications Surveys Tutorials*, vol. 22, no. 3, pp. 1839–1862, 2020.

[28] A. Campbell, P. McDonald, and K. Ray, "Single event upset rates in space," *IEEE Transactions on Nuclear Science*, vol. 39, no. 6, pp. 1828–1835, 1992.

[29] M. J. Bentum, C. Verhoeven, and A.-J. Boonstra, "Olfar-orbiting low frequency antennas for radio astronomy," in *Proceedings of the ProRISC 2009, Annual Workshop on Circuits, Systems and Signal Processing, Veldhoven*, pp. 1–6, 2009.

[30] P. Misra, W. Hu, Y. Jin, J. Liu, A. S. de Paula, N. Wirström, and T. Voigt, "Energy efficient gps acquisition with sparse-gps," in *IPSN-14 Proceedings of the 13th International Symposium on Information Processing in Sensor Networks*, pp. 155–166, April 2014.

[31] K. Chen, G. Tan, and M. Lu, "Improving the energy performance of gps receivers for location tracking applications," in *2017 IEEE Conference on Computer Communications Workshops (INFOCOM WKSHPS)*, pp. 85–90, May 2017.

[32] NASA, "Small-satellite mission failure rates." `https://ntrs.nasa.gov/archive/nasa/casi.ntrs.nasa.gov/20190002705.pdf`, 2019. [Online], last accessed - October 2022.

[33] Space.com, "Saving hubble: Astronauts recall 1st space telescope repair mission 20 years ago." `http://www.space.com/23640-hubble-space-telescope-repair-anniversary.html`, 2017. [Online], last accessed - December 2022.

[34] N. Ineke, C. Wangi, R. V. Prasad, M. Jacobsson, and I. Niemegeers, "Address autoconfiguration in wireless ad hoc networks: protocols and techniques," vol. 15, pp. 70–80, February 2008.

[35] C. Sarkar, A. U. S. N. Nambi, R. V. Prasad, and A. Rahim, "Diat: A scalable distributed architecture for iot," in *IEEE INTERNET OF THINGS JOURNAL*, vol. 2, June 2015.

[36] N. I. C. Wangi, R. V. Prasad, I. Niemegeers, and S. H. de Groot, "Ad hoc federation of networks (fednets) - mechanisms and requirements," in *2nd International Conference on Communication Systems Software and Middleware*, pp. 1–6, Jan 2007.

[37] N. Olsen, C. Stolle, R. Floberghagen, G. Hulot, and A. Kuvshinov, "Special issue "swarm science results after 2 years in space"," *Earth, Planets and Space*, vol. 68, no. 1, p. 172, 2016.

[38] J. Thangavelautham, M. Herreras Martinez, A. Warren, A. Chandra, and E. Asphaug, "The suncube femtosat platform: A pathway to low-cost interplanetary exploration," 05 2016.

[39] M. Uludag, V. Pallichadath, S. Speretta, and S. Radu et. al, "Design of a micro-propulsion subsystem for a pocketqube." https://repository.tudelft.nl/islandora/object/uuid%3Ac8ea432f-4e73-45b1-83d0-a65e1b61b492, 2019.

[40] G. S. Page, "Vermont lunar cubesat." https://space.skyrocket.de/doc_sdat/vermont-lunar-cubesat-1.htm, 2013.

[41] T. Delft, "Tu delft." http://www.delfispace.nl/delfi-c3, 2017. [Online], last accessed - December 2022.

[42] S. Gao, K. Clark, M. Unwin, J. Zackrisson, W. A. Shiroma, J. M. Akagi, K. Maynard, P. Garner, L. Boccia, G. Amendola, G. Massa, C. Underwood, M. Brenchley, M. Pointer, and M. N. Sweeting, "Antennas for modern small satellites," *IEEE Antennas and Propagation Magazine*, vol. 51, pp. 40–56, Aug 2009.

[43] EPFL, "Swiss cube." http://swisscube.epfl.ch/, 2017. [Online], last accessed - December 2022.

[44] S. S. T. Ltd., "Surrey satellite technology ltd." http://www.sstl.co.uk/Missions/STRaND-1--Launched-2013, 2017. [Online], last accessed - December 2022.

[45] B. Virgili and H. Krag, "Small satellites and the future space debris environment," *ResearchGate*, 07 2015.

[46] C. P. SLO, "Cubesat design specification." https://static1.squarespace.com/static/5418c831e4b0fa4ecac1bacd/t/56e9b62337013b6c063a655a/1458157095454/cds_rev13_final2.pdf, 2014.

[47] T. Villela, C. A. Costa, A. M. Brandão, F. T. Bueno, and R. Leonardi, "Towards the thousandth cubesat: A statistical overview," *International Journal of Aerospace Engineering*, pp. 1348–1361, January 2019.

[48] ISRO, "PSLV-C37 Successfully Launches 104 Satellites in a Single Flight." http://www.isro.gov.in/update/15-feb-2017/pslv-c37-successfully-launches-104-satellites-single-flight. [Online, accessed 01-Feb-2018].

[49] NASA, "Cube quest challenge." https://www.nasa.gov/cubequest/details, 2017. https://www.nasa.gov/cubequest/details [Online].

[50] MagnitudeSpace, "Magnitude space - insights of things." https://magnitudespace.com/, 2017. [Online], last accessed - December 2022.

[51] OneWeb, "Oneweb." http://oneweb.world/, 2017. [Online], last accessed - December 2022.

[52] M. P. Z. Manchester and A. Filo, "Kicksat: A crowd-funded mission to demonstrate the world's smallest spacecraft," 2013.

[53] R. L. Balthazor, M. G. McHarg, C. S. Godbold, D. J. Barnhart, and T. Vladimirova, "Distributed space-based ionospheric multiple plasma sensor networks," in *2009 IEEE Aerospace conference*, pp. 1–10, March 2009.

[54] S. American, "Inside the breakthrough starshot mission to alpha centauri." https://www.scientificamerican.com/article/inside-the-breakthrough-starshot-mission-to-alpha-centauri/, 2017. [Online], last accessed - December 2022.

[55] B. Warneke, M. Last, B. Liebowitz, and K. S. J. Pister, "Smart dust: communicating with a cubic-millimeter computer," *Computer*, vol. 34, pp. 44–51, Jan 2001.

[56] D. L. Jones, T. J. W. Lazio, and J. O. Burns, "Dark ages radio explorer mission: Probing the cosmic dawn," in *2015 IEEE Aerospace Conference*, pp. 1–8, March 2015.

[57] Phys.org, "China begins operating world's largest radio telescope." https://phys.org/news/2016-09-china-world-largest-radio-telescope.html, 2017. [Online], last accessed - December 2022.

[58] nature.com, "Astronomers grapple with new era of fast radio bursts." http://www.nature.com/news/astronomers-grapple-with-new-era-of-fast-radio-bursts-1.21557, 2017. [Online], last accessed - December 2022.

[59] L. Pederson, D. Kortencamp, D. Wettergreen, and I. Nourbakhsh, "A survey of space robotics," *7th International Symposium on Artificial Intelligence, Robotics, and Automation in Space, Munich, Germany*, 2003.

[60] engadgett.com, "Russia and the us will work together to build a moon base." https://www.engadget.com/2017/09/27/russia-us-cooperate-on-lunar-base/, 2017. [Online], last accessed - December 2022.

[61] R. Radhakrishnan, W. W. Edmonson, F. Afghah, R. M. Rodriguez-Osorio, F. Pinto, and S. C. Burleigh, "Survey of inter-satellite communication for small satellite systems: Physical layer to network layer view," *IEEE Communications Surveys Tutorials*, vol. 18, no. 4, pp. 2442–2473, 2016.

[62] P. Thomas, J. Veverka, and S. Dermott, "Small satellites," *IAU Colloq. 77: Some Background about Satellites*, pp. 802–835, 1986.

[63] S. Narayana, R. V. Prasad, V. S. Rao, and C. Verhoeven, "Swans: Sensor wireless actuator network in space," in *Proceedings of the 15th ACM Conference on Embedded Network Sensor Systems*, SenSys '17, (New York, NY, USA), pp. 23:1–23:6, ACM, 2017.

[64] D. Guimaraes and R. de Souza, "Exploring practical aspects of the fsk modulation with non-coherent matched filter detection," *Revista de Tecnologia da Informação e Comunicação (RTIC)*, vol. 5, pp. 22–28, May 2015.

[65] I. Ali, P. G. Bonanni, N. Al-Dhahir, and J. E. Hershey, *Doppler Applications in LEO Satellite Communication Systems*, vol. 656. Boston, MA: Springer US, 2002.

[66] S. M. Dilek, A. Ayranci, A. Şeker, O. Ceylan, and H. B. Yagci, "Ax.25 protocol compatible reconfigurable 2/4 fsk modulator design for nano/micro-satellites," in *2012 20th Telecommunications Forum (TELFOR)*, pp. 416–419, Nov 2012.

[67] J. Bouwmeester and J. Guo, "Survey of worldwide pico and nanosatellite missions, distributions and subsystem technology," in *Acta Astronautica, Volume 67*, pp. 854–862, Acta Astronautica, 2010.

[68] D. E. Booth, "A doppler compensation scheme for rf communications useable on dynamically retargeted projectiles," in *Proceedings for the 24th Army Science Conference*, December 2004.

[69] G. Boudouris, "A method for interpreting the doppler curves of artificial satellites," *Radio Engineers, Journal of the British Institution of*, vol. 20, pp. 933–935, December 1960.

[70] B. Sklar, "Digital communications." `http://userspages.uob.edu.bh/mangoud/mohab/Courses_files/sklar.pdf`, 2018. [Online], last accessed - December 2018.

[71] Airspy, "Sdr sharp." `https://airspy.com/download/`, 2018. [Online], last accessed - December 2022.

[72] J. F. Kaiser, "Some useful properties of teager's energy operators," in *Proceedings of the 1993 IEEE International Conference on Acoustics, Speech, and Signal Processing: Digital Speech Processing - Volume III*, ICASSP'93, (Washington, DC, USA), pp. 149–152, IEEE Computer Society, 1993.

[73] P. K. Banerjee and N. B. Chakrabarti, "Noise sensitivity of teager-kaiser energy operators and their ratios," in *2015 International Conference on Advances in Computing, Communications and Informatics (ICACCI)*, pp. 2265–2271, Aug 2015.

[74] A. Vahter, "cubehub." `https://github.com/cubehub/demod`, 2017. [Online], last accessed - December 2018.

[75] GPredict, "Gpredict:free, real-time satellite tracking and orbit prediction software." `http://gpredict.oz9aec.net/`, 2018. [Online], last accessed - December 2022.

[76] S. Hara, A. Wannasarnmaytha, Y. Tsuchida, and N. Morinaga, "A novel fsk demodulation method using short-time dft analysis for leo satellite communication systems," *IEEE Transactions on Vehicular Technology*, vol. 46, Aug 1997.

[77] R. Nivin, J. S. Rani, and P. Vidhya, "Design and hardware implementation of reconfigurable nano satellite communication system using fpga based sdr for fm/fsk demodulation and bpsk modulation," in *2016 International Conference on Communication Systems and Networks (ComNet)*, pp. 1–6, July 2016.

[78] K. S. Gomadam and S. A. Jafar, "Modulation and detection for simple receivers in rapidly time-varying channels," *IEEE Transactions on Communications*, vol. 55, pp. 529–539, March 2007.

[79] W. R. Remley, "Doppler dispersion effects in matched filter detection and resolution," *Proceedings of the IEEE*, vol. 54, pp. 33–39, Jan 1966.

[80] R. Lerner, "A matched filter detection system for complicated doppler shifted signals," *IRE Transactions on Information Theory*, vol. 6, pp. 373–385, June 1960.

[81] S. I. Corporation, "Dove (3m) | satellite imaging corp." `https://www.satimagingcorp.com/satellite-sensors/other-satellite-sensors/dove-3m/`, 2021. [Online], last accessed - December 2022.

[82] T. Ebinuma, M. Unwin, C. Underwood, and E. Imre, "A miniaturised gps receiver for space applications," *Elsevier*, vol. 37, pp. 1103–1106, 2017.

[83] P. Bissig, M. Eichelberger, and R. Wattenhofer, "Fast and robust gps fix using one millisecond of data," in *2017 16th ACM/IEEE International Conference on Information Processing in Sensor Networks (IPSN)*, pp. 223–234, April 2017.

[84] F. van Diggelen, *A-GPS: Assisted GPS, GNSS, and SBAS*. NavtechGPS, 2000.

[85] M. Anghileri, M. Paonni, E. Gkougkas, and B. Eissfeller, "Reduced navigation data for a fast first fix," in *2012 6th ESA Workshop on Satellite Navigation Technologies (Navitec 2012) European Workshop on GNSS Signals and Signal Processing*, pp. 1–7, Dec 2012.

[86] S. Y. F. Leung, O. Montenbruck, and B. Bruninga, "Hot start of gps receivers for leo microsatellites." `https://www.dlr.de/rb/en/Portaldata/38/Resources/dokumente/GSOC_dokumente/RB-RFT/NAV_0107.pdf`, 2001.

[87] O. Montenbruck and E. Gill, *Satellite Orbits - Models, Methods and Applications*. Berlin: Springer-Verlag, Edition:1, Pages: XI, 371, 2000.

[88] E. Kahr, O. Montenbruck, K. O'Keefe, S. Skone, J. Urbanek, L. Bradbury, and P. Fenton, "Gps tracking of a nanosatellite – the canx-2 flight experience," in *8th International ESA Conference on Guidance, Navigation and Control Systems*, pp. 5–10, June 2011.

[89] M. S. Grewal, L. R. Weill, and A. P. Andrews, *Global Positioning Systems, Inertial Navigation, and Integration*. New York, NY, USA: Wiley-Interscience, 2007.

[90] G. Xu and Y. Xu, *GPS - Theory, Algorithms and Applications*. Berlin: Springer-Verlag, Edition:2, Pages: XXII, 340, 2016.

[91] D. Orn, M. Szilassy, B. Dil, and F. Gustafsson, "A novel multi-step algorithm for low-energy positioning using gps," in *2016 19th International Conference on Information Fusion (FUSION)*, pp. 1469–1476, July 2016.

[92] H. Technologies, "Gnss200." `https://hyperiontechnologies.nl/products/gnss200/`, 2019. [Online], last accessed - December 2019.

[93] N. Systems, "Newspace gps receiver." `http://www.newspacesystems.com/wp-content/uploads/2018/10/NewSpace-GPS-Receiver_8b.pdf`, 2019. [Online], last accessed - December 2019.

[94] S. Labs, "Cubesat gps receiver/next generation." http://www.skyfoxlabs.com/pdf/piNAV-NG_Datasheet_rev_F.pdf, 2019. [Online], last accessed - December 2019.

[95] S. C. Spangelo, M. W. Bennett, D. C. Meinzer, A. T. Klesh, J. A. Arlas, and J. W. Cutler, "Design and implementation of the gps subsystem for the radio aurora explorer," *Acta Astronautica*, vol. 87, pp. 127 – 138, 2013.

[96] H. Leppinen, A. Kestilä, T. Tikka, and J. Praks, "The aalto-1 nanosatellite navigation subsystem: Development results and planned operations," in *2016 European Navigation Conference (ENC)*, pp. 1–8, May 2016.

[97] U. D. o. H. S. Navigation Center, "Navstar gps user equipment." https://www.navcen.uscg.gov/pubs/gps/gpsuser/gpsuser.pdf, 1996.

[98] T. Kelso, "Validation of sgp4 and is-gps-200d against gps precision ephemerides." https://celestrak.com/publications/AAS/07-127/AAS-07-127.pdf, 2007.

[99] F. R. Hoots and R. L. Roehrich, "Spacetrack report no. 3: Models for propagation of norad element sets." https://www.celestrak.com/NORAD/documentation/spacetrk.pdf, 1980.

[100] B. Patil, R. Patil, and A. Pittet, "Energy saving techniques for gps based tracking applications," in *2011 Integrated Communications, Navigation, and Surveillance Conference Proceedings*, pp. J8–1–J8–10, May 2011.

[101] J. Liu, B. Priyantha, T. Hart, Y. Jin, W. Lee, V. Raghunathan, H. S. Ramos, and Q. Wang, "Co-gps: Energy efficient gps sensing with cloud offloading," *IEEE Transactions on Mobile Computing*, vol. 15, pp. 1348–1361, June 2016.

[102] K. Chen and G. Tan, "Satprobe: Low-energy and fast indoor/outdoor detection based on raw gps processing," in *IEEE INFOCOM 2017 - IEEE Conference on Computer Communications*, pp. 1–9, May 2017.

[103] R. Hartmann, David, "Power savings through onboard orbit propagation for small satellites like npsat1." https://calhoun.nps.edu/handle/10945/48532, 2016. [Online], last accessed - December 2018.

[104] M. Tafazoli, "A study of on-orbit spacecraft failures," *Acta Astronautica*, vol. 64, no. 2, pp. 195 – 205, 2009.

[105] T. Yairi, Y. Kato, and K. Hori, "Fault detection by mining association rules from housekeeping data," in *In Proceedings of the 6th International Symposium on Artificial Intelligence, Robotics and Automation in Space*, 2001.

[106] S. Bottone, D. Lee, M. O'Sullivan, and M. Spivack, "Failure prediction and diagnosis for satellite monitoring systems using bayesian networks," in *MILCOM 2008 - 2008 IEEE Military Communications Conference*, pp. 1–7, Nov 2008.

[107] R. H. Chen, H. K. Ng, J. L. Speyer, L. S. Guntur, and R. Carpenter, "Health monitoring of a satellite system," *Journal of Guidance, Control, and Dynamics*, vol. 29, no. 3, pp. 593–605, 2006.

[108] L. A. Times, "The latest lost satellite is now space junk that could put other spacecraft at risk." https://www.theverge.com/2019/4/19/18507439/intelsat-29e-geostationary-orbit-satellite-failure-space-debris, 2019. [Online], last accessed - December 2022.

[109] NASA, "Cots components in spacecraft systems: Understanding the risk." https://www.nasa.gov/sites/default/files/atoms/files/cots.pdf, 2014. [Online], last accessed - December 2022.

[110] M. E. S. Sally Cole, "Small satellites increasingly tapping cots components." http://mil-embedded.com/articles/small-tapping-cots-components/, 2020. [Online], last accessed - December 2022.

[111] S. Narayana, R. Muralishankar, R. V. Prasad, and V. S. Rao, "Recovering bits from thin air: Demodulation of bandpass sampled noisy signals for space iot," in *Proceedings of the 18th International Conference on Information Processing in Sensor Networks*, IPSN '19, p. 1–12, Association for Computing Machinery, 2019.

[112] S. News, "Digitalglobe loses worldview-4 satellite to gyro failure." https://spacenews.com/digitalglobe-loses-worldview-4-satellite-to-\gyro-failure/, 2019. [Online], last accessed - November 2021.

[113] ESA, "Ers-2 goes gyro-less." https://www.esa.int/Enabling_Support/Operations/ERS-2_goes_gyro-less, 2001.

[114] L. Mittag, "Hardware-assisted debugging." https://m.eet.com/media/1170505/esc_1991_vol1_page355_mittag%20-%20hardware-assisted%20debugging.pdf, 2020. [Online], last accessed - December 2022.

[115] G. A. Landis, "Tabulation of power-related satellite failure causes," in *11th International Energy Conversion Engineering Conference*, 2013.

[116] L. A. Times, "Hughes satellite failure cause is still unknown." https://www.latimes.com/archives/la-xpm-1998-aug-12-fi-12289-story.html, 1998.

[117] Spaceflight-Now, "Isro loses contact with new communications satellite." https://spaceflightnow.com/2018/04/03/isro-loses-contact-with-new-communications-satellite/, 2018. [Online], last accessed - December 2019.

[118] M. Oredsson, "Electrical power system for the cubestar nanosatellite," University of Oslo, 2010.

[119] Y. Borthomieu, "14 - satellite lithium-ion batteries," in *Lithium-Ion Batteries* (G. Pistoia, ed.), (Amsterdam), pp. 311 – 344, Elsevier, 2014.

[120] TDK, "Surface potential sensors efs series." https://product.tdk.com/info/en/products/sensor/sensor/surface-potential/technote/tpo/index.html, 2020.

[121] E. Dynamics, "Fft gyro 600 pro." https://eurekadynamics.com/fft-gyro-600/, 2020. [Online], last accessed - December 2022.

[122] V. Chatzigiannakis and S. Papavassiliou, "Diagnosing anomalies and identifying faulty nodes in sensor networks," *IEEE Sensors Journal*, vol. 7, no. 5, pp. 637–645, 2007.

[123] T. Chakraborty, A. U. Nambi, R. Chandra, R. Sharma, M. Swaminathan, Z. Kapetanovic, and J. Appavoo, "Fall-curve: A novel primitive for iot fault detection and isolation," in *Proceedings of the 16th ACM Conference on Embedded Networked Sensor Systems*, SenSys '18, (New York, NY, USA), p. 95–107, Association for Computing Machinery, 2018.

[124] B. Sheng, Q. Li, W. Mao, and W. Jin, "Outlier detection in sensor networks," in *Proceedings of the 8th ACM International Symposium on Mobile Ad Hoc Networking and Computing*, MobiHoc '07, (New York, NY, USA), p. 219–228, Association for Computing Machinery, 2007.

[125] F. Koushanfar, M. Potkonjak, and A. Sangiovanni-Vincentelli, "On-line fault detection of sensor measurements," in *SENSORS, 2003 IEEE*, vol. 2, pp. 974–979 Vol.2, 2003.

[126] D. Lawrence, J. S. Donnal, S. Leeb, and Y. He, "Non-contact measurement of line voltage," *IEEE Sensors Journal*, vol. 16, no. 24, pp. 8990–8997, 2016.

[127] P. S. Shenil, R. Arjun, and B. George, "Feasibility study of a non-contact ac voltage measurement system," in *2015 IEEE International Instrumentation and Measurement Technology Conference (I2MTC) Proceedings*, pp. 399–404, 2015.

[128] S. Wei, L. Zhang, W. Gao, and Z. Cao, "Non-contact voltage measurement based on electric-field effect," *Procedia Engineering*, vol. 15, pp. 1973 – 1977, 2011. CEIS 2011.

[129] A. Delle Femine, D. Gallo, C. Landi, A. Lo Schiavo, and M. Luiso, "Low power contactless voltage sensor for low voltage power systems," *Sensors*, vol. 19, no. 16, 2019.

[130] ESA, "Space debris by the numbers." https://www.esa.int/Space_Safety/Space_Debris/Space_debris_by_the_numbers, 2022. [Online], last accessed - December 2022.

SUMMARY

The Internet of Things (IoT), a recent technology that has enabled many innovative applications, has dominated the world by creating smart systems and applications. It is predicted that the number of connected gadgets in IoT will double by 2030 compared to 2020. Thus, it is essential to address the key challenges, such as scalability, ubiquitous global coverage, and real-time connectivity, that arise due to this immense growth of IoT devices. However, extending the existing terrestrial networks such as mobile towers to under-served regions of the world including remote areas, oceans, and mountains, to achieve scalability and global coverage is not a cost-viable solution. Space, on the other hand, can be a suitable platform to solve the majority of these existing/upcoming problems in the IoT domain.

Space is the next frontier for innovations in IoT. The main idea is to employ space technologies for IoT applications. Space Internet of Things (Space-IoT), as we call, is a concept that involves a satellite, or a network of them, to address the main challenges in terrestrial IoT deployments – global coverage, scalability, and connectivity. Space-IoT is opening up a world of new possibilities for several applications.

Small satellites are the building blocks of Space-IoT. They represent a formidable mobile computing platform enabling large-scale space applications at a fraction of the cost of larger satellites. Space-IoT calls for hundreds or thousands of small satellites that can communicate directly with various IoT devices on Earth. However, access to space has been expensive due to the high satellite development and launch costs. Miniaturizing a satellite can reduce launch costs but presents a range of interdisciplinary challenges that must be tackled. Resources are severely constrained in terms of size, mass, and available power. Addressing these challenges requires different communities to push the envelope in the design and realization of miniaturized subsystems of a small satellite.

In this dissertation, we chart out a vision for Space-IoT and innovations in embedded and wireless systems for Space-IoT applications. We enlist several important challenges that need to be addressed immediately to bring the vision of Space-IoT to reality. This thesis targets one of the most significant tradeoffs – miniaturization leading to constrained energy while not compromising the reliability of operations of subsystems. We consider three subsystems of a satellite: communication, attitude determination, and health monitoring, to demonstrate the inter-dependencies and novel ways to tackle them. Further, we explain with examples what we envision for the next decade to facilitate Space-IoT.

In Space-IoT, the IoT nodes on Earth are expected to communicate with (small) satellites directly over hundreds of kilometres. Both these terrestrial nodes and the satellites in space are energy-constrained. Hence, the communications must not only be energy-efficient but also support long range. Moreover, the received signal strength and the Signal to Noise Ratio (SNR) on the receiver decrease as the communication distance increases. Further, Doppler shift is inevitable in Low Earth Orbit bound satellite communication. Boosting the transmission power and adopting high-gain large antennas are obvious solutions for reli-

able communication, however, not feasible with miniaturization and energy minimization as our objectives. One of the solutions to support low-power, long-range communication is to improve the demodulation technique to decode signals with low SNR.

In this dissertation, we revisit the demodulation approach of a widely used modulation technique - Frequency Shift Keying (FSK). We propose a scheme to demodulate bandpass sampled FSK signals that are influenced by Doppler shift and low SNR. Unlike the state-of-the-art techniques, our approach does not compensate for the Doppler shift but lives with it. To suppress the Doppler effect and improve the SNR of the received signal, we employ a matched filter and the Teager Energy Operator, respectively. With extensive evaluations using actual telemetry signals from two satellites, we demonstrate how our proposed technique outsmarts the state-of-the-art FSK demodulation schemes.

Besides the communication subsystem, Global Positioning System (GPS) is one of the essential but significantly energy-guzzling subsystems in a satellite. While big satellites typically do not have any constraints on energy consumption for GPS subsystem, such is not the case in miniaturized satellites. Unlike terrestrial GPS systems, several challenges are imposed on obtaining a position fix in space-borne GPS receivers. The high orbital velocities of a satellite (up to 7.8 km/s) result in a significant Doppler shift in the received signals by the receiver when compared to their terrestrial counterparts. Consequently, the receiver has to search for the GPS signals in a larger Doppler frequency range, thus increasing the signal acquisition duration. Further, the visibility of the GPS satellites to the receiver changes frequently due to high orbital speeds and orbital periods of satellites on which the receiver is mounted. As a result, the receiver needs to search for GPS satellites more often to get a position fix. Likewise, the visibility of GPS satellites is affected adversely if the satellite is tumbling. Due to these constraints, energy conservation techniques such as duty-cycling are not efficient; the receiver is ON most of the time, searching for GPS satellites to obtain a position fix.

To this end, we design a low-power, space-qualified GPS receiver for small satellite applications. We propose an algorithm to significantly improve the ability of the receiver to acquire GPS signals as quickly as possible, thus reducing the ON time when it is duty-cycled. We perform long-duration simulations and real-time in-orbit tests on our GPS receiver to evaluate its performance. Further, we demonstrate that up to 96% of energy savings can be achieved on our GPS receiver compared to the state-of-the-art receivers.

Space-IoT relies on a constellation of hundreds of satellites to accomplish global coverage. Disruption in services can occur if one of the satellites malfunctions or ceases to work. Certain applications may not endure such risks, especially where satellites are typically employed as secondary communication channels. Hence, it is crucial to monitor the health of satellites regularly.

Existing satellites are generally equipped with onboard health monitoring units as a part of the subsystems. However, they are tightly coupled in terms of hardware and software. Any fault in the subsystem may affect its onboard health monitoring modules as they are electrically connected. Hence, we propose a system called Chirper, which is an electrically isolated and independent module that monitors the health of critical subsystems. The Chirper is equipped with multiple sensors that can measure several parameters, such as temperature, bus voltage, current, and rotation rate, of a satellite at specified intervals

and transmits them to ground stations through an independent communication module.

The proposed system is not only energy-efficient but also measures the different health parameters of a satellite reliably. This work mainly addresses the resilience and energy issues of a satellite. In this dissertation, we present the overall design of the Chirper. We also provide a novel approach to measuring the DC voltage at different locations of a satellite in a completely isolated way. Further, we subject Chirper to different tests in state-of-the-art simulators and a helium balloon to evaluate its capabilities.

This thesis advocates that Space-IoT is an ideal complement to terrestrial IoT networks and deployments. Small satellites can bring the vision of Space-IoT into existence. However, several technical breakthroughs need to emerge in small satellites to realize Space-IoT. We tackled some of the primary challenges through theory, experimentation and demonstration on satellites in orbit. With the results obtained, we are convinced that revolutionary transformations can be brought in small satellites to enable Space-IoT and will significantly influence the space related-activities, both in research and development.

Propositions

accompanying the dissertation

SPACE INTERNET OF THINGS (SPACE-IOT)

by

Sujay Narayana

1. Only Space IoT fulfils the definition of IoT as *connecting anything, anywhere, anytime* (Chapter 1).
2. The future is not far, where the satellites are mounted on the payloads and not the other way around (Chapter 2).
3. Aim big, be SMALL (Chapter 2).
4. Reliability need not consume more energy (Chapter 4, 5).
5. The Internet of Things can not exist without wireless technology.
6. Natural intelligence is required to select the best artificial intelligence.
7. Researchers are abnormal; while everyone tends to stray away from problems, researchers go after them.
8. Once upon a time, necessity was the mother of inventions. This is no longer true.
9. Nature does not waste anything, not even the waste.
10. If you want to forget something deliberately, you need to remember it.

These propositions are regarded as opposable and defendable, and have been approved as such by the promotors prof. dr. K.G. Langendoen, and Dr. R.R. Venkatesha Prasad.

ACKNOWLEDGMENTS

This thesis would not have been possible without the support of many people who are like the stars in the night sky – they guided me to success and provided a brilliant light that illuminated my path. I would take this opportunity to thank them for their helping hand, and guidance and for walking with me on this exciting journey.

Foremost, I would like to express my deepest gratitude to my promotors Dr. Koen Langendoen (Koen), and Dr. R. Venkatesha Prasad (VP) for their invaluable guidance, motivation, and feedback throughout Ph.D. Their expertise and insights have been instrumental in shaping this thesis, and I am deeply grateful for their support. Koen's constructive criticism and encouragement have always helped me to improve the quality of my work and to publish them at top-notch conferences. I always admire his problem-solving skills and critical comments on my work, the quality of my writing, including flow and presentation.

I still remember Koen's words to me before I started my Ph.D. - "It is very important to have good chemistry between you and your supervisor for a successful Ph.D.". Without any hesitation, this has been the case for me with VP as my daily supervisor during Ph.D. VP had also been my co-supervisor from TU Delft for my Master's thesis executed at ETH Zurich. VP has backed me at every stage and provided me with the freedom, which is unconditional and unforgettable, have helped me achieve bigger targets than initially planned. I would need another book to acknowledge his role in my Ph.D. and personal development. Moreover, our rapport now is beyond saying thanks. So, let me stop here.

Apart from my promotors, there are several others who supported me substantially in my research. I would like to express my sincere gratitude to Dr. Kiran Kumar (former chairman, ISRO) and Dr. Mylswamy Annadurai (former director, URSC, ISRO) for their encouragement and support during my internship days at ISRO. I extend my appreciation to Prof.dr.ir. Rob Fastenau (former dean, EEMCS, TU Delft), and Prof.dr. John Schmitz (former dean, EEMCS, TU Delft) for providing me with the necessary resources and facilities to conduct this research. Their support has been crucial in completing this thesis.

I had the privilege of working with many erudite collaborators. When working with Dr. T. V. Prabhakar (TVP) (principal research scientist, Indian Institute of Science) during my internship, I picked up a thing or two from his unfading passion for research, attack mode when solving a problem, and novel approaches/ideas through systems thinking. There is still a lot to learn from him and I am always indebted to him for the opportunity. Further, I would like to extend my heartfelt thanks to Dr. Muralishankar from CMR Institute of Technology, India, and Dr. Luca Mottola from Politecnico di Milano, Italy for their collaboration, guidance, and feedback. I gained a wealth of knowledge from them, especially in communicating the research outcomes.

If there is someone who deserves special thanks, then it is my brother, my colleague, and well-wisher, Dr.ir. Vijay Rao. He has always been with me during the course of my Ph.D. and helped me in various ways. In fact, VP and Vijay have become part of my family.

I express my sincere gratitude to several key people at ISRO for supporting me at various stages. First, I would like to extend my sincere thanks to Dr. S. V. Sharma (former deputy director, URSC, ISRO) and my supervisor at ISRO - Dr. Sudhakar (deputy director, URSC, ISRO) for their guidance and support. At ISRO, I interacted with many researchers, scientists and experts. Dr. Muthuvel, Dr. Udupa, Prashanth, Navneet, Naveen, Prakhar, Vijaypal, Nandeesh, Das, Partha, Srividya madam, Dr. C.S. Madhusudhana, Kiran, Ashvij, and Sham-Rao are the key people I am thankful to. These people never treated me as an outsider but always looked like a friend to me.

I am also thankful to ir.dr. Chris Verhoeven from TU Delft for backing me in many of the projects and trusting me for timely delivery. I would like to acknowledge all my colleagues from the Embedded and Networked Software group - Fernando, Marco, Przemek, Qing Wang, Chayan, Kishor, Vineet, Ashutosh, Eric, Nikos, Kees, Anup, Ioannis, and Minaksie with whom I have interacted during my Ph.D. Many thanks to Niels, Nikos, and Ashvij for their hard work as a team that bagged us the first prize at the prestigious Airbus Fly Your Ideas 2019.

I had the pleasure of starting up a high-tech company, called ZED, with TU Delft and my colleagues, Niels, Suryansh, Prof.dr. John Schmitz, Kiran Muthal, and VP. I am currently enjoying working with this team and thankful for the efforts that they have put into this endeavour. I am also grateful to Mrs. Vasanthi Prasad (VP's wife), Kruthika (Vijay's wife), and Srividya (VP's daughter, my younger sister) for their warmth whenever I met them. I have greatly enjoyed (enjoying) the time we have spent together, especially, making VP's legs longer by pulling his legs!

Lastly, I would like to express my sincere gratitude to my family and friends for being beside me in every step that I took. It would be a remiss if I don't recollect Ajay Keshava, my younger brother, who has always been my right hand in many projects and has also taken the responsibility to manage my family in India. Though the relationship between a father, mother, and son is beyond any acknowledgement, I am deeply grateful to my father (Dr. Subramanya Bhat) and my mother (Vijayalaxmi) for their sacrifices, understanding, and patience that led me to what I am today. Also, letting me go wild with all my so-called creativity! I have also been receiving an enormous amount of support from my father-in-law (M V Krishna), and mother-in-law (Jyothi) during the course of my Ph.D. From the bottom of my heart, I thank my wife, Krithika, for her unwavering care and love. I am truly blessed to have her by my side. Last, but not least, I'm happy and thankful to have my teeny-tiny daughter, Dyuthi, the bundle of joy in our lives.

- Singing off...

Sujay Narayana
10-04-2023

LIST OF PUBLICATIONS

The list of publications accomplished during PhD.

1. **S. Narayana**, R. Venkatesha Prasad, V. Rao, and Chris Verhoeven, *"SWANS: Sensor Wireless Actuator Network in Space"*, In Proceedings of the 15th ACM Conference on Embedded Network Sensor Systems **(SenSys '17)**, art. 23, pp. 1-6, 2017.

2. **S. Narayana**, R. Muralishankar, R. Venkatesha Prasad, and V. Rao, *"Recovering bits from thin air: demodulation of bandpass sampled noisy signals for space IoT"*, In Proceedings of the 18th International Conference on Information Processing in Sensor Networks **(IPSN '19)**, pp. 1–12, 2019.

3. **S. Narayana**, R. Venkatesha Prasad, V. Rao, L. Mottola, and T. V. Prabhakar, *"Hummingbird: energy efficient GPS receiver for small satellites"*, In Proceedings of the 26th Annual International Conference on Mobile Computing and Networking **(MobiCom '20)**, art. 9, pp. 1–13, 2020, ***- the best paper award***.

4. **S. Narayana**, R. Venkatesha Prasad, V. Rao, L. Mottola, and T.V. Prabhakar, *"A Hummingbird in Space: An energy-efficient GPS receiver for small satellites"*, In **GetMobile**: Mobile Comp. and Comm. 25, pp. 24–29, 2021.

5. **S. Narayana**, R. Venkatesha Prasad, V. Rao, L. Mottola, and T.V. Prabhakar, *"Hummingbird: Energy Efficient GPS Receiver for Small Satellites"*, In Communications of the ACM **CACM**, Volume 65, Issue 11, November 2022.

6. **S. Narayana**, R. Venkatesha Prasad, and T. V. Prabhakar, *"SOS: isolated health monitoring system to Save Our Satellites"*, In Proceedings of the 19th Annual International Conference on Mobile Systems, Applications, and Services **(MobiSys '21)**, pp. 283–295, 2021.

7. **S. Narayana**, and R. Venkatesha Prasad, *"Space, the Final "Communications" Frontier?"*, In ComSoc Technology News (CTN), November 2022, [Online Access - https://www.comsoc.org/publications/ctn/space-final-communications-frontier].

—

8. **S. Narayana**, V. Rao, R. Venkatesha Prasad, A. Keshava Kanthila, K. Managundi, L. Mottola, and T. V. Prabhakar, *"LOCI: Privacy-aware, Device-free, Low-power Localization of Multiple Persons using IR Sensors"*, In Proceedings of the 19th ACM/IEEE International Conference on Information Processing in Sensor Networks **(IPSN '20)**, pp. 121-132, 2020.

9. **S. Narayana**, R. Venkatesha Prasad, and K. Warmerdam, *"Mind your thoughts: BCI using single EEG electrode"*, In IET Cyber-Physical Systems: Theory and Applications, vol. 4, Issue 2, pp. 164-172, 2019.

10. C. Sarkar, J. J. Treurniet, **S. Narayana**, R. V. Prasad, and W. de Boer, *"SEAT: Secure Energy-Efficient Automated Public Transport Ticketing System"*, In IEEE Transactions on Green Communications and Networking **(TGCN)**, vol. 2, no. 1, pp. 222-233, 2018

11. N. Kouvelas, A. K. Keshava, **S. Narayana** and R. V. Prasad, *"Pushing the Boundaries of IoT: Building and Testing Self-powered Batteryless Switch"*, In IEEE 5th World Forum on Internet of Things **(WFIoT '19)**, pp. 231-236, 2019.